PROCEEDINGS OF THE KECK GEOLOGY CONSORTIUM

Volume 34
2021-2022 Projects

Dr. Cameron Davidson and Dr. Karl Wirth, Editors
Co-Directors, Keck Geology Consortium

Theresa Klauer
Keck Geology Consortium Administrative Assistant
Macalester College

Keck Geology Consortium
Macalester College
1600 Grand Ave, St. Paul, MN 55105
(651) 696-6108, Info@KeckGeology.org

ISSN# 1528-7491
doi: 10.18277/AKRSG.2022.34

Funding Provided by:
Keck Geology Consortium Member Institutions
The National Science Foundation Grant NSF-REU 1659322

PROCEEDINGS OF THE KECK GEOLOGY CONSORTIUM

2021-2022 Projects

Cameron Davidson Editor and Co-Director Carleton College	Keck Geology Consortium Macalester College 1600 Grand Ave. St Paul, MN 55105	Karl Wirth Editor and Co-Director Macalester College

Keck Geology Consortium Member Institutions:

Amherst College, Beloit College, Carleton College, Colgate University, The College of Wooster, The Colorado College, Franklin & Marshall College, Macalester College, Oberlin College, Pomona College, Trinity University, Union College, Washington & Lee University, Wesleyan University, Whitman College

2021-2022 GATEWAY PROJECTS

USING THE GEOCHEMISTRY OF SEDIMENTS (AND METASEDIMENTS) AS WINDOWS INTO THE EVOLUTION OF ANCIENT AND MODERN MOUNTAIN RANGES
Faculty: ZEB PAGE and REBECCA A. VANDERLEEST, Oberlin College
Students: SOFIA T. BARTH, Union College; EMILY I. BENGSTON, Oberlin College; AMELIA S. G. BRONFMAN, Oberlin College; SARAH E. BROWN, Scripps College; ELISE BOUCHER, Pitzer College; MATTEA HORNE, Peer Mentor, Pomona College; JOSIPHINE LISSET, Oberlin College; CONNER MINKOWITZ, Franklin & Marshall College; BEN ROCHE, Colorado College

BIOGEOCHEMICAL CONTROLS ON NATURAL AND ANTHROPOGENIC GROUNDWATER CONTAMINANTS IN CALIFORNIA'S CENTRAL VALLEY
Faculty: ARIC MINE, California State University-Fresno, and BRADY ZIEGLER, Trinity University
Students: AMALIA CULPEPPER-WEHR, Williams College; JOHN GOODMAN, Union College; MIA GOUDY, California State University-Fresno; JACKSON KOHN, Colorado College; MARK NICKELS, Trinity University LAUREN O'ROURKE, Whitman College; TIA PETERSON, Colorado College; RICHARD STEINER-OTOO, Montclair State University

CARBON SEQUESTRATION BY ENHANCED SILICATE WEATHERING IN AGRICULTURAL SOILS
Faculty: DANIEL P. MAXBAUER, Carleton College
Students: JAHMAINE RENZO YAMBING, Peer Mentor, Carleton College; FIONA ANTSEY, Amherst College; DEMETRIUS BLACKMON-JIMENEZ, Carleton College; SARAH LEIBOVITZ, Amherst College; SOPHIE NAYLOR, Colgate University

GEOCHEMICAL PROPERTIES OF SEEPAGE-FILTRATION AND FRACTURE SPRINGS IN WISCONSIN
Faculty: SUSAN SWANSON, Beloit College
Students: OCEAN CLEVETTE, Peer Mentor, Beloit College; ISABELLA ERGH, College of Wooster; MARGARET MORGAN, Macalester College; WILLOW TEIPEL, Beloit College; PHILLIP TELGEN, Whitman College

2021-2022 GATEWAY PROJECTS – Continued

RISING WATERS, SHRINKING HABITATS: THE INFLUENCE OF FLUCTUATING WATER LEVELS ON THE GEOLOGY AND ECOLOGY OF A GREAT LAKES ARCHIPELAGO
Faculty: KIM C. DIVER, Wesleyan University
Students: ARIEL ALEXANDER, Carleton College; RYANN BUSILLO, Wesleyan University; ADALIA RODRIGUEZ, Bryn Mawr College; VERONICA SEIXAS, Hamilton College; JENNA OTAOLA, Peer Mentor, Wesleyan University

---

2021-2022 ADVANCED PROJECTS

ASSESSING GROUND AND SURFACE WATER QUALITY AT REDOX INTERFACES ACROSS THE SHENANDOAH VALLEY, VIRGINIA
Faculty: MARGARET A. G. HINKLE and EVA LYON, Washington & Lee University
Students: ANI CROY, Washington and Lee University; HALEY CULBERTSON, Washington and Lee University; CHRIS GOLDMANN, Trinity University; MIA GROFF, Whitman College; MADDIE HOLICKY, Beloit College; KATIE LARKIN, Washington and Lee University; MARTINA PULIDO, Beloit College; KALLAN WILDE, St. Norbert College; NOAH WILLIS, Whitman College

Short Contributions and Conference Presentations – Oberlin Gateway Project

USING THE GEOCHEMISTRY OF SEDIMENTS (AND METASEDIMENTS) AS WINDOWS INTO THE EVOLUTION OF ANCIENT AND MODERN MOUNTAIN RANGES
ZEB PAGE and REBECCA A. VANDERLEEST, Oberlin College

SURVEY OF ADIRONDACK METAMORPHIC TEMPERATURES USING QUANTITATIVE EDS MAPPING
BOUCHER, E., HORNE, M., LEON, A., LISSIT, J., MINKOWITZ, C., ROCHE, B., and PAGE, F.Z.
Presented at 2021 Fall Meeting, AGU, 13-17 Dec. [V45D-0173]

SEDIMENT PROVENANCE OF THE MAGALLANES-AUSTRAL BASIN 51 S USING KERNEL DENSITY ESTIMATES FROM DETRITAL ZIRCON U-PB AGES AND SANDSTONE COMPOSITION TO ANALYZE TECTONICS AND EROSION ACTIVITY
BROWN, S., BARTH, S., BENGSTON, E., BRONFMAN, A., VANDERLEEST, R., and FOSDICK, J.
Presented at 2021 Fall Meeting, AGU, 13-17 Dec. [EP55A-1096]

Short Contributions and Conference Presentations – California Gateway Project

BIOGEOCHEMICAL CONTROLS ON NATURAL AND ANTHROPOGENIC GROUNDWATER CONTAMINANTS IN CALIFORNIA'S CENTRAL VALLEY
ARIC MINE, California State University-Fresno, and BRADY ZIEGLER, Trinity University

MOBILIZATION OF TRACE ELEMENTS FROM SEDIMENTS INTO GROUNDWATER IN CALIFORNIAS CENTRAL VALLEY
CULPEPPER-WEHR, A., STEINER-OTOO, R., KOHN, J., GOUDY, M., NICKELS, M., PETERSON, T., GOODMAN, J., O'ROURKE, L., ZIEGLER, B., and MINE, A.
Presented at 2021 Fall Meeting, AGU, 13-17 Dec. [H45F-1231]

GEOSPATIAL AND STATISTICAL ANALYSES OF GROUNDWATER CONTAMINANTS IN THE SAN JOAQUIN RIVER VALLEY DURING DROUGHT AND NON-DROUGHT PERIODS
NICKELS, M., GOUDY, M., GOODMAN, J., KOHN, J., O'ROURKE, L., PETERSON, T., STEINER-OTOO, R., CULPEPPER-WEHR, A., ZIEGLER, B., and MINE, A.
Presented at 2021 Fall Meeting, AGU, 13-17 Dec. [H15V-1294]

MICROBIAL COMMUNITY RESPONSE TO CHANGING GROUNDWATER CHEMISTRY IN THE SAN JOAQUIN VALLEY
PETERSON, T., KRON, E., O'ROURKE, L., GOODMAN, J., CULPEPPER-WEHR, A., STEINER-OTOO, R., KOHN, J., GOUDY, M., NICKELS, M., MINE, A., and ZIEGLER, B.
Presented at 2021 Fall Meeting, AGU, 13-17 Dec. [H55O-0902]

Short Contributions and Conference Presentations – Carleton Gateway Project

CARBON SEQUESTRATION BY ENHANCED SILICATE WEATHERING IN AGRICULTURAL SOILS
DANIEL P. MAXBAUER, Carleton College

FIELD TRIALS TESTING CARBON SEQUESTRATION AND AGRICULTURAL CO-BENEFITS OF ENHANCED SILICATE WEATHERING WITH BASALTIC SOIL AMENDMENTS IN A CORN-SOYBEAN AGRICULTURAL FIELD IN NORTHFIELD, MINNESOTA
MILLIKEN, E., YAMBING, J.R., LEIBOVITZ, S., NAYLOR, S., ANSTEY, F., BLACKMON-JIMENEZ, D., and MAXBAUER, D.
Presented at 2021 Fall Meeting, AGU, 13-17 Dec. [B35L-1558]

GREENHOUSE CONSTRAINTS ON THE INORGANIC CARBON SEQUESTRATION POTENTIAL OF ENHANCED SILICATE WEATHERING IN AGRICULTURE
YAMBING, J.R., MILLIKEN, E., ANSTEY, F., BLACKMON-JIMENEZ, D., NAYLOR, S., LEIBOVITZ, S., and MAXBAUER, D.
Presented at 2021 Fall Meeting, AGU, 13-17 Dec. [B35L-1560]

Short Contributions and Conference Presentations – Wisconsin Gateway Project

GEOCHEMICAL PROPERTIES OF SEEPAGE-FILTRATION AND FRACTURE SPRINGS IN WISCONSIN
SUSAN SWANSON, Beloit College

GEOCHEMICAL PROPERTIES OF SEEPAGE-FILTRATION AND FRACTURE SPRINGS IN WISCONSIN
ERGH, I., MORGAN, M., TEIPEL, W., TELGEN, P., CLEVETTE, O., and SWANSON, S.
Geological Society of America Abstracts with Programs. Vol 53, No. 6
doi: 10.1130/abs/2021AM-370439

Short Contributions and Conference Presentations – Great Lakes Gateway Project

RISING WATERS, SHRINKING HABITATS: THE INFLUENCE OF FLUCTUATING WATER LEVELS ON THE GEOLOGY AND ECOLOGY OF A GREAT LAKES ARCHIPELAGO
KIM DIVER, Wesleyan University

THE INFLUENCE OF FLUCTUATING WATER LEVELS ON THE ECOLOGY AND MORPHOLOGY OF A GREAT LAKES ARCHIPELAGO
DIVER, K.; OTAOLA, J.; ALEXANDER, A.; BUSILLO, R.; RODRIGUEZ, A.; and SEIXAS V.
Virtual paper presentation, 2022 Annual Meeting of the Association of American Geographers, New York, NY, United States.

ISLAND SHAPE, SOIL DEPTH, AND PLANT BIOGEOGRAPHY IN A GREAT LAKE ARCHIPELAGO
ALEXANDER, A.; and DIVER, K.
Virtual poster presentation, 2022 Annual Meeting of the Association of American Geographers, New York, NY, United States.

CHANGES IN ISLAND AREA AND WATER LEVELS BETWEEN 2001 AND 2020 IN THE MASSASAUGA PROVINCIAL PARK, LAKE MICHIGAN-HURON, ONTARIO
SEIXAS, V.; and DIVER, K.
Virtual poster presentation, 2022 Annual Meeting of the Association of American Geographers, New York, NY, United States.

Short Contributions – Virginia Advanced Project

ASSESSING GROUND AND SURFACE WATER QUALITY AT REDOX INTERFACES ACROSS THE SHENANDOAH VALLEY, VIRGINIA
MARGARET A. G. HINKLE and EVA LYON, Washington & Lee University

ANALYZING THE RELATIONSHIPS BETWEEN AQUEOUS MANGANESE AND GEOLOGICAL FACTORS IN GROUNDWATER IN THE SHENANDOAH VALLEY
MARINA CROY, Washington and Lee University
Research Advisor: Margaret A. G. Hinkle

ASSESSING THE IMPACT OF SOIL ON MANGANESE CONTAMINATION IN SPRINGS AND GROUNDWATER IN THE SHENANDOAH VALLEY, VIRGINIA
HALEY CULBERTSON, Washington & Lee University
Research Advisor: Margaret A. G. Hinkle

ASSESSING MANGANESE CONCENTRATIONS IN GROUNDWATER ACROSS THE SHENANDOAH VALLEY, VA
CHRISTOPHER GOLDMANN, Trinity University
Research Advisor: Brady Ziegler

ASSESSING THE GRAIN SIZE OF LEGACY SEDIMENTS AND POTENTIAL FOR HEAVY METAL CONTAMINATION IN ROCKBRIDGE COUNTY, VA
MIA GROFF, Whitman College
Research Advisor: Kirsten Nicolaysen

ASSESSING LAND USE CHANGES USING THE LEGACY SEDIMENTS IN THE SHENANDOAH VALLEY OF VIRGINIA
MADELINE HOLICKY, Beloit College
Research Advisor: James Rougvie

MEASURING CHANGES IN CHANNEL MORPHOLOGY AND VOLUME OF MOBILIZED SEDIMENT FOLLOWING THE REMOVAL OF A LOWHEAD DAM IN ROCKBRIDGE COUNTY, VA
KATIE LARKIN, Washington and Lee University
Research Advisor: Eva Lyon

THE GEOCHEMISTRY OF RELICT MILL POND WATERS AND STRATIFIED RESERVOIRS IN THE SHENANDOAH VALLEY, VA
MARTINA PULIDO, Beloit College
Research Advisor: James Rougvie

ANALYSIS OF LAND USE IN ROCKBRIDGE COUNTY, VA, FROM PRECOLONIAL TIMES TO CURRENT DAY AND CONSEQUENCES FOR RIPARIAN ECOSYSTEMS
KALLAN R. WILDE, Saint Norbert College
Research Advisor: Nelson Ham

ANALYSIS OF SOIL GEOCHEMISTRY TO BETTER UNDERSTAND GEOGENIC MANGANESE CONTAMINATION IN THE SHENANDOAH VALLEY
NOAH WILLIS, Whitman College
Research Advisor: Nick Bader

KECK Geology Consortium
Learning Science Through Research
Published by the Keck Geology Consortium
Short Contributions
Keck Geology Consortium
Volume 34
May 2022
doi: 10.18277/AKRSG.2022.34.01

GEOCHEMICAL PROPERTIES OF SEEPAGE-FILTRATION AND FRACTURE SPRINGS IN WISCONSIN

ZEB PAGE, Oberlin College
REBECCA A. VANDERLEEST, Oberlin College

INTRODUCTION

Young Mountains: The Patagonian Andes

Mountains are modified over time via exhumation, erosion, and climate. Archives of past orogenic modification are recorded in the adjacent foreland basin. Provenance studies of the foreland basin examine these archives to recognize where sediment is being derived and what the origin reveals about past tectonic and magmatic activity. The Magallanes-Austral Basin, located at the southern tip of South America (Fig. 1), provides an excellent example of continuous stratigraphic section (e.g., Biddle et al., 1986; Romans et al., 2010; Daniels et al., 2018; Fosdick et al., 2020) from which provenance studies can be conducted to study past tectonic and magmatic activity. Further, this basin underwent several tectonic changes including episodes of ridge subduction (Ramos and Kay, 1992; Ramos, 2005), thrust belt advancement (Fosdick et al., 2011), and opening of oceanic passageways (Eagles and Jokat, 2014), which may be recorded in the sediment archives.

Detrital zircon ages have proven diagnostic when determining sediment sources for the southern Patagonian Andes (Fig. 2) (e.g., Schwartz et al., 2016; Leonard et al., 2020; Fosdick et al., 2020). Currently, Cenozoic-based provenance studies using modal sandstone analysis, clast counts, and detrital

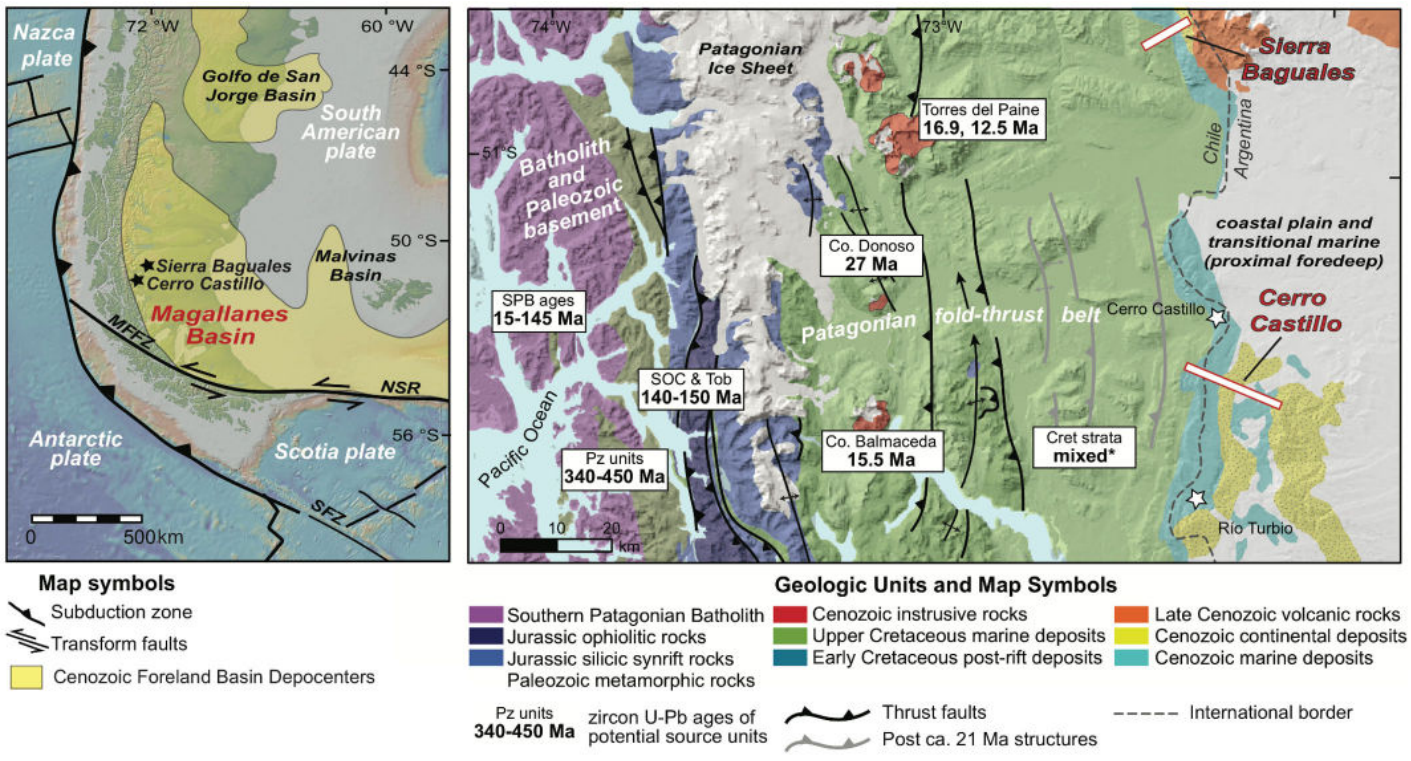

Figure 1 (Left). Tectonic setting of the Magallanes-Austral Basin.

Figure 2 (Right). Geologic map of the study area in the Patagonian Andes. Modified from Fosdick et al. (2020).

zircon ages reveal that Oligocene-Miocene fluvial sediment is dominantly sourced from the volcanic arc despite increased fold and thrust belt activity during this time in the Cerro Castillo area (Leonard et al., 2020; VanderLeest et al., 2020). Comprehensive detrital zircon ages from Cenozoic stratigraphy within Cerro Castillo reveal loss of Paleozoic and Jurassic sources throughout the Cenozoic due to Paleogene orogenesis and rise of Cretaceous sources due to fold and thrust belt activity (Fosdick et al., 2020). North of Cerro Castillo in Sierra Baguales, comprehensive provenance analysis has not been conducted. Further, the stratigraphy of the Sierra Baguales displays differences in grain size and fossil content (Ugalde et al., 2018) when compared to Cerro Castillo, and basin subsidence histories reveal slight differences in patterns of tectonic uplift (VanderLeest, 2020). These differences could signal changes in basin geometry which may reflect tectonic and magmatic differences within the Patagonian Andes between these study areas. A provenance study that captures how Cenozoic tectonics has influenced Sierra Baguales and Cerro Castillo areas would provide a more holistic view of the Ultima Esperanza region.

In 2017, detrital zircon U-Pb ages, modal sandstone and clast counts were completed for the Sierra Baguales and Cerro Castillo study areas. A total of 10 detrital zircon samples were collected from the Paleogene to Miocene section at Sierra Baguales and 10 detrital zircon samples collected from Paleogene to Miocene sections at Cerro Castillo and Cancha Carrera. Along with a total of 40 sandstone petrographic thin section samples and clast counts between the two study areas. We will analyze the detrital zircon age populations and geochemistry along with the modal sandstone and clast count datasets to determine origin of the sediment and unravel tectonic and magmatic phases within the Ultima Esperanza region of the Patagonian Andes to understand differences between these two study areas.

Ancient Mountains: The Adirondacks

The Adirondack Mountains of New York are a fragment of the exposed core of a massive, worldwide mountain-building event known as the Grenville Orogeny. The geology of the Adirondacks is notoriously complex and records multiple episodes of subduction, collision and igneous intrusion from 1.3 to 1.05 Ga (e.g., Heumann et al., 2006). Sedimentary basins formed along the margin of the Laurentian continent, including detrital zircons similar to those being studied in the "Young Mountains" project (e.g., Chiarenzelli et al., 2015), which were heated to the point of partial melting during the collisional episodes, growing new zircon that dates the metamorphism (e.g., Heumann et al., 2006; Bickford et al., 2008). In addition to growing new zircon, metamorphic minerals such as biotite and garnet formed, the chemistry of which can be used to determine the conditions of metamorphism.

The study of metamorphism in the Adirondacks has been ongoing for more than a century. The first widespread application of a modern thermodynamic approach to the study of metamorphism established high temperatures (>700˚C) across the Adirondack Highlands, with the highest temperatures found in the center of the region (Bohlen et al., 1985). More recent work focused on metamorphosed igneous rocks has established peak temperatures of up to 850˚C (Spear and Markussen, 1997). Oxygen isotope studies in the Adirondacks have likewise confirmed high regional temperatures (e.g., Peck and Valley, 2004; Quinn et al., 2016), as well as the sedimentary origin of the partially-melted rocks known as migmatites (Lancaster et al., 2008). Recent work on a small number of these partially-melted metasediments has also resulted in extremely high-temperature estimates (Storm and Spear, 2005; 2009).

Approaches to extracting temperatures and pressures from metamorphic rocks have evolved with changing technologies, and the previous paragraph cites studies using a variety of techniques. A fairly recent development in metamorphic petrology has been the use of internally calibrated X-ray composition maps to generate clouds of P-T (Pressure-Temperature) data to better evaluate the information preserved in the chemistry of zoned minerals. This approach is typically applied to quantify X-ray maps generated using Wavelength Dispersive Spectrometry. We applied this technique (with the free software package XMap Tools, Lanari et al., 2014) using Energy Dispersive Spectrometry (EDS) on predominantly un-zoned minerals from the Adirondack Highlands.

We simultaneously contribute to the P-T dataset that can be used to reconstruct the geometry of this ancient mountain range, and evaluate the use of quantitative EDS mapping for this purpose.

RESEARCH AND RESULTS

This research involved eight rising sophomore students, a rising senior peer mentor, and two faculty from Oberlin College. Students worked in two groups on their research projects. Together we had daily check-in meetings and split time collecting data on the SEM at Oberlin College for the respective projects.

STUDENT PROJECTS

Young Mountains

Sediment Provenance of the Magallanes-Austral Basin ~ 51° S Using Kernel Density Estimates from Detrital Zircon U-Pb Ages and Sandstone Composition to Analyze Tectonics and Erosional Activity

SOFIA T. BARTH, Union College; **EMILY I. BENGSTON**, Oberlin College; **AMELIA S. G. BRONFMAN**, Oberlin College; **SARAH E. BROWN**, Scripps College

We used the Scanning Electron Microscope (SEM) at Oberlin College to evaluate tectonic provenance of sandstones. Polished sandstone thin sections were carbon coated and placed in the SEM to produce Backscatter Electron (BSE) images and Energy-dispersive X-ray Spectroscopy (EDS) maps for petrographic point counting (Fig. 3). We conducted point counts using these maps and images. Point counts were complete after a total of 400 counts. We plotted the results on ternary diagrams after Dickinson and Susek (1979) in R (R Core Team, 2020).

Detrital zircon U-Pb ages were compiled from VanderLeest et al. (2018); Leonard et al. (2020); Fosdick et al. (2020); and Fosdick et al. (2015). We generated and analyzed KDEs and bar graphs in detritalPy (Sharman et al., 2018). This team explored how sediment provenance, including detrital zircon U-Pb ages and petrographic point counts, reflects tectonic influence over time using two study sites along strike within the Magallanes-Austral retroarc foreland basin. The Magallanes-Austral retroarc foreland basin has undergone tectonic changes due to its location inboard of the Chilean trench and Southern Patagonian Andes.

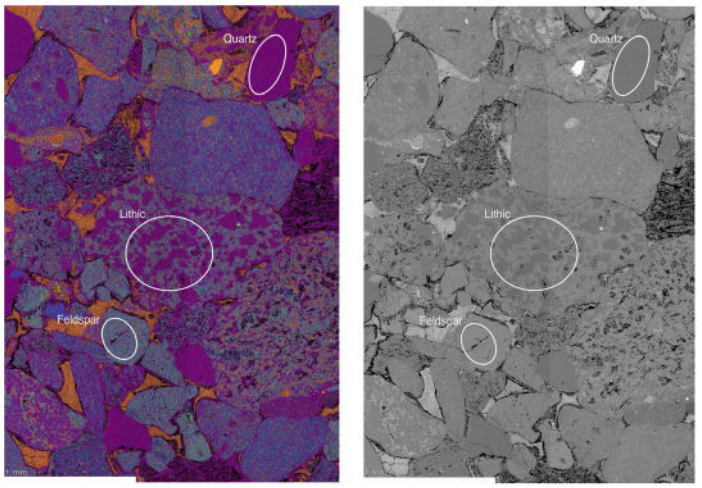

Figure 3. Left: Portion of Energy-dispersive X-ray Spectroscopy (EDS) image of thin section sample 15LDC-02 from the Cerro Dorotea formation at Cerro Castillo. We overlaid grids while counting to provide clear boundaries when point counting (not shown in figure). Elements are color coded to help identify minerals. Magenta-Si; Cyan-Na; Organge-Fe and Mg; Green-Ca; Blue-K; Yellow-Al. Right: Portion of backscatter electron image (BSE) of thin section sample 15LDC02 from the Cerro Dorotea formation at Cerro Castillo. Image includes quartz, lithic, feldspar, and calcite grains. Distinguishing textures aided in the process of identifying minerals.

The team examined Paleocene to Miocene formations at two study sites, Sierra Baguales and Cerro Castillo (Fig. 4). From west to east, the Jurassic to Miocene Patagonian Batholith and Paleozoic metamorphic basement complexes, the Jurassic hinterland fold-and-thrust belt, and the Cretaceous fold-and-thrust belt contributed sediment to these formations (Fig. 2).

The team quantified sediment provenance using KDEs (Fig. 5; Sharman et al., 2018) and ternary diagrams after Dickinson and Suscek (1979) (Fig. 6). They discovered that pronounced zircon U-Pb age clusters from Sierra Baguales include 25-0 Ma, 40-25 Ma, 65-40 Ma, 136-80 Ma, and 175-136 Ma. Pronounced zircon U-Pb age clusters from Cerro Castillo include: 25-0 Ma, 40-24 Ma, 65-40 Ma, 80-65 Ma, 136-80 Ma, and 175-136 Ma. The KDE shows younger zircon ages upsection with the appearance of 65-40 Ma, 40-25 Ma, and 25-0 Ma in the Lower Río Turbio Formation. A decrease in 420-250 Ma and 175-136 Ma age peaks occurs upsection at both study sites. Ternary diagrams

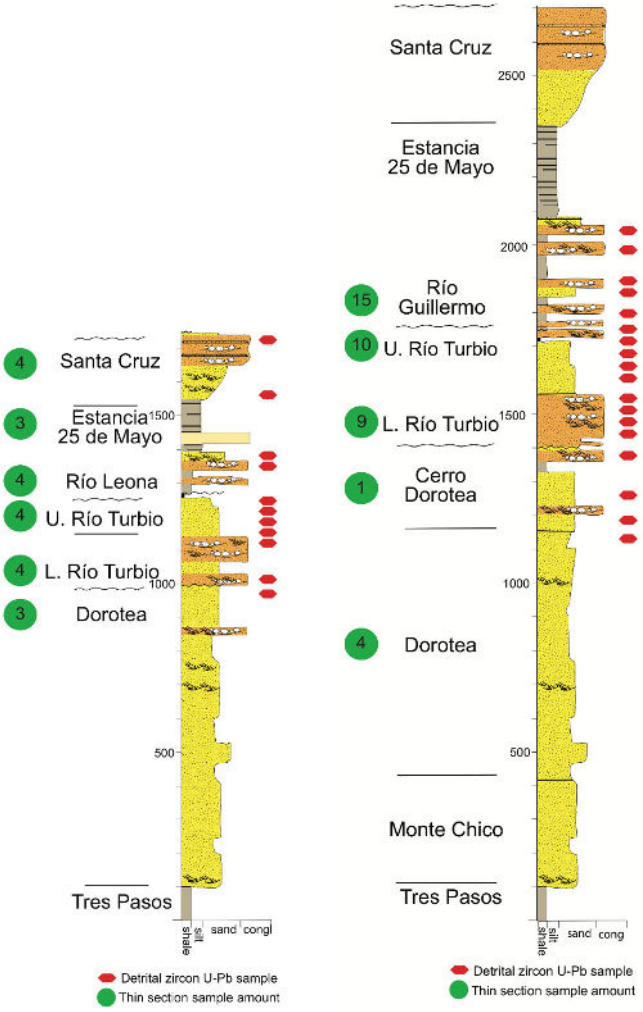

Figure 4. Left: Sierra Baguales lithostratigraphy after Fosdick et al. (2015). Right: Cerro Castillo lithostratigraphy after Fosdick et al. (2020).

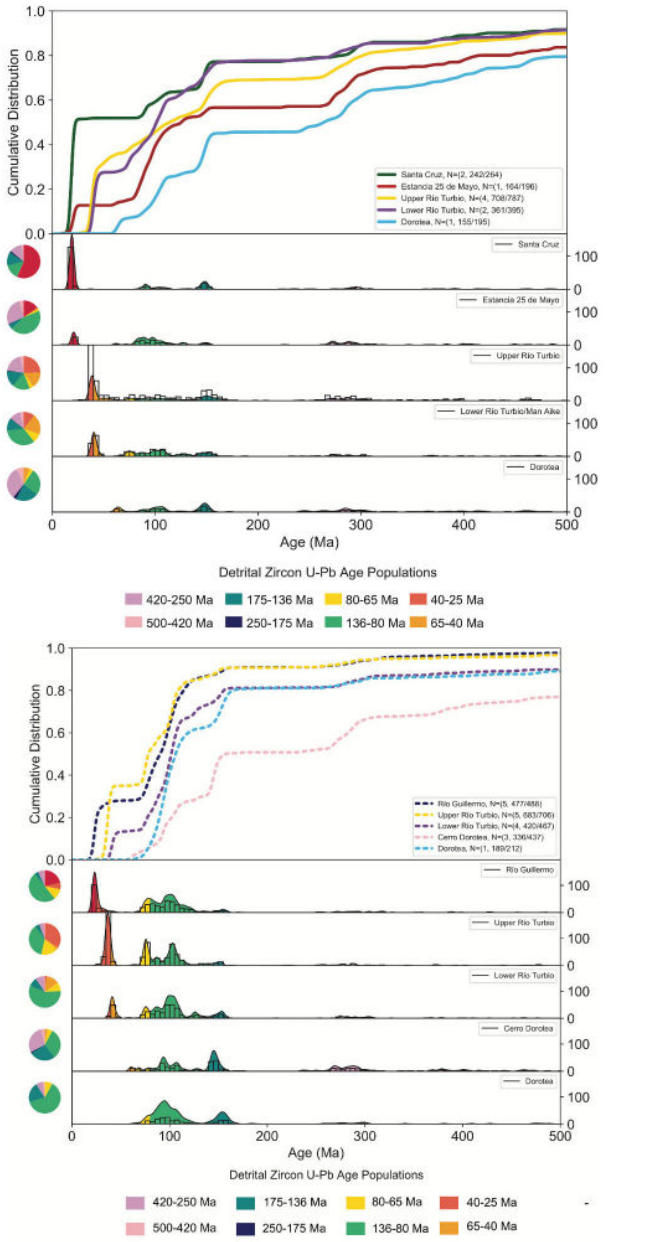

Figure 5. Left: Kernel Density Estimates (KDEs) graph of detrital zircon U-Pb data from Sierra Baguales. Detrital zircon dataset compiled from Fosdick et al. (2015) and VanderLeest et al. (2018). Right: Kernel Density Estimates (KDEs) graph of detrital zircon U-Pb data from Cerro Castillo. Detrital zircon dataset compiled from VanderLeest et al. (2018); Fosdick et al (2020); Leonard et al. (2020). KDEs generated in detritalPy (Sharman et al., 2018).

with data from both study sites show that Paleocene to mid-Eocene formations (Dorotea, Cerro Dorotea, Lower Río Turbio formations) tend to be more quartz-rich and lithic-poor than the upper Oligocene to mid-Miocene formations (Río Leona, Río Guillermo, Estancia 25 de Mayo, Santa Cruz formations).

Sediment provenance reveals that Paleocene units contain more quartz and higher proportions of zircons aged 420-250 Ma. Therefore, we suggest this sediment originated from the East Andean Metamorphic Complex, Metasedimentary Basement Complex and Patagonian Batholith. Ternary diagrams indicate Paleocene formations have a primarily mixed and dissected arc provenance consistent with the interpretation that the Patagonian Batholith was exposed during the Paleocene to mid Eocene due to erosion of the volcanic cap and/or less volcanic activity. Differences in sandstone composition and concentration of zircon age populations indicate a significant tectonic event occurred between the Paleocene units and Eocene-Miocene units. This change in provenance aligns well with the passage of the Aluk-Farallon slab window and that could be the reason for the zircon age population and sandstone composition changes. Differences in proportion of Permian, Jurassic, and Cretaceous aged zircon

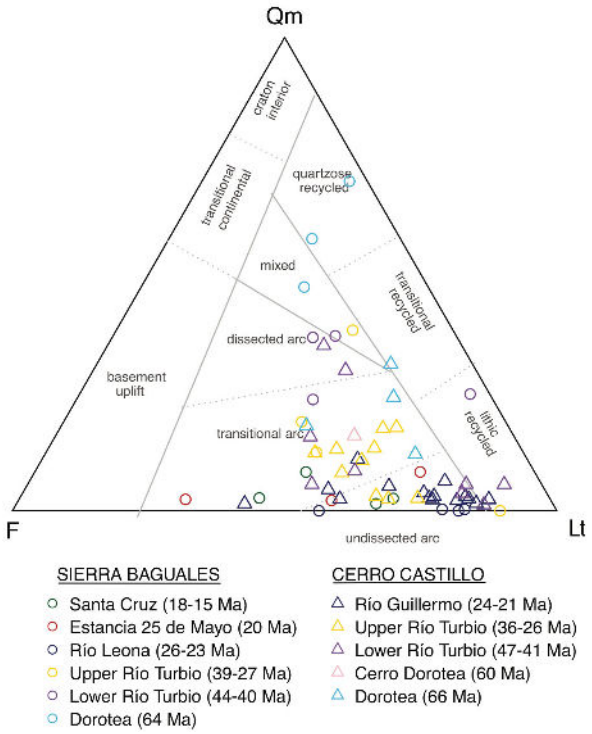

Figure 6. QmFLt ternary diagram showing tectonic provenance for Sierra Baguales and Cerro Castillo in the Magallanes-Austral Basin after Dickinson and Suczek (1979). Qm-monocrystalline quartz; F-feldspar; Lt-total lithics.

between Cerro Castillo and Sierra Baguales reveal the fold and thrust belt was more active to the south than to the north. These observations signal that hinterland orogenic growth may have been more prominent at Sierra Baguales than at Cerro Castillo.

Ancient Mountains

Survey of Adirondack Metamorphic Temperatures Using Quantitative EDS Mapping

ELISE BOUCHER, Pitzer College; **MATTEA HORNE**, Peer Mentor, Pomona College; **JOSIPHINE LISSET**, Oberlin College; **CONNER MINKOWITZ**, Franklin & Marshall College; **BEN ROCHE**, Colorado College

During the summer of 2021, the Ancient Mountains team prepared polished rock chips for EDS mapping from three classic Adirondack localities with differing lithologies. The samples studied were lecosome and melanosome from migmatitic gneiss from Treadway Mountain (08ADK-01; Heumann et al., 2006; Lancaster et al, 2008) and a coronitic olivine metagabbro (08ADK-04) at the southern margin of the Marcy Anorthosite (Johnson and Essene, 1982). Samples were carbon coated and long term (6-18 hour duration) EDS maps were collected guided by Back-Scattered Electron (BSE) imaging using a TescanVega 3 electron microscope and Oxford XMax80 large area Silicon Drift Detector. After analysis, ~15 spot analyses were collected per mineral within the 500-1000 µm field of view. Internal virtual standards were used. Careful attention was paid to a consistent working distance and samples were well-polished and flat. EDS maps were processed in XMapTools (Lanari et al., 2014), using the drift correction to compensate for variable detector sensitivity across the field of view. Temperature estimates were made using calibrations of cation exchange thermometers built into the XMapTools software.

Thermometry results from the two samples were consistent with existing estimates using conventional methods. Application of the Ti in biotite thermometer of Henry (2003) to the Treadway Mountain migmatite sample shown in Figure 7 yields 748±18˚C. The uncertainty in this result is due to the minor variability in Ti in the biotite pixels of Fig. 7. Garnet-biotite thermometry based on X-ray maps of Figure 7 results in a much lower temperature of 651±19˚C. The low reported uncertainty indicates homogeneous composition across the pixels in the maps, and the lower temperature is expected from retrograde diffusion of Fe and Mg between garnet and biotite in contact in a granulite-facies sample.

The metagabbro sample 08ADK-04 preserves variable textures at the thin section scale from multi-phase coronas of metamorphic minerals surrounding relict igneous olivine, no more equant textures as reported by Johnson and Essene (1992) consisting of garnet, clinopyroxene, and hornblende in a plagioclase matrix (Fig. 8). Garnet-hornblende (Grt-Hbl) (Ravna, 2000a) and Garnet-clinopyroxene (Grt-CPX) exchange thermometry applied to the corresponding pixels in Figure 8 result in identical temperatures 712±44˚C (Grt-Hbl) and 712 ±35˚C (Grt-CPX). The 712˚C result is consistent with previous thermometry of these rocks (e.g., Bohlen et al., 1985); however, the increased uncertainty when compared with the previous sample suggests more heterogeneity in the map pixels, although this could be due to true sample heterogeneity or errors in the EDS map.

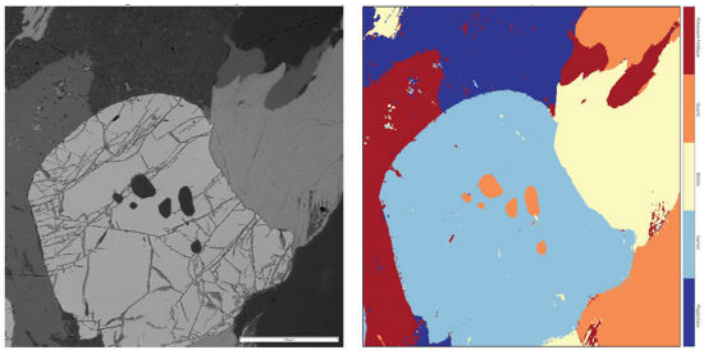

Figure 7. Left. Back-Scattered Electron (BSE) image of migmatite leucosome sample 08ADK-01 with a central garnet surrounded by potassium and plagioclase feldspars, biotite, and quartz. Right. Phase-map of the same image showing different minerals classified from X-ray maps.

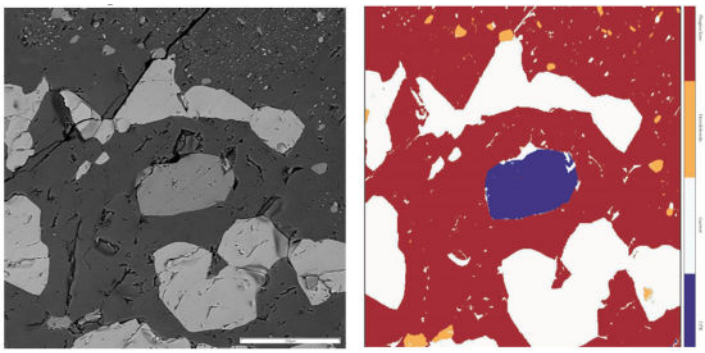

Figure 8. Left: BSE image of metagabbro 08ADK-04 with equant textures. Right: Phase map of the same field of view: garnet, plagioclase, clinopyroxene, and hornblende are present.

In order to better evaluate the precision and accuracy of this approach, we analyzed garnets from both samples using WDS point analyses by electron microprobe at the University of Michigan. The results of this comparison are presented in Figure 9. Although at first inspection, there appears to be significant scatter in the mapped compositions, these are primarily due to a small number of map pixels occurring in or along cracks or boundaries between phases. When all pixels are averaged from the full map, garnet compositions differ by less than 5% between WDS point analysis and the EDS mapping approach we used.

Thermobarometry based on quantified X-ray maps offers a new and exciting direction for metamorphic petrology. Our results suggest that careful attention to sample geometry and long counting times allow for this approach to be used with SEM-EDS. Furthermore, the use of calibrated EDS maps offers a powerful teaching tool for both mineralogical and petrological concepts such as solid solution and thermobarometry,

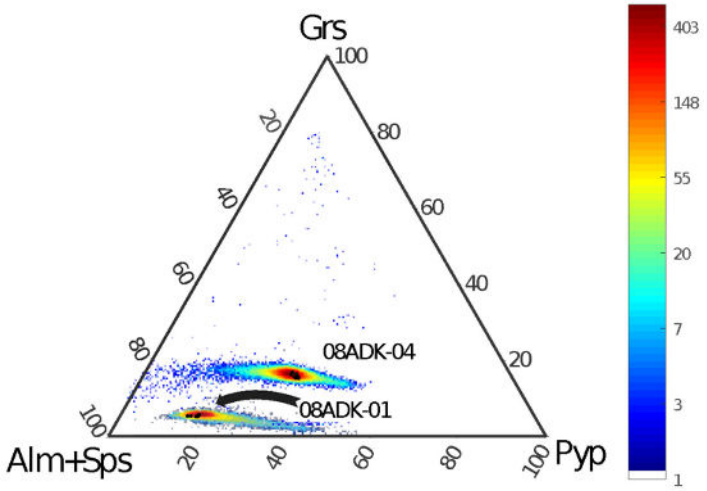

Figure 9. Ternary diagram of the composition of garnets in Adirondack migmatite (08ADK-01) and metagabbro (08ADK-04). Black points are WDS point analyses, colored points are pixels from Figs. 7 and 8 classified as garnet, the color scale is in number of pixels at a given composition. Average garnet compositions differ by less than 5% between techniques. (Grs – Grossular, Alm – Almandine, Sps – Spessartine, Pyp – Pyrope).

as well as more general skills such as multi-spectral imaging, data processing, and analysis.

ACKNOWLEDGEMENTS

This research is supported by the Keck Geology Consortium and the National Science Foundation under Grant EAR-1659322. The purchase of the SEM-EDS system used in this work was supported by NSF Grant EAR-1626271. Owen Neill is gratefully acknowledged for assistance with microprobe analyses. Additional funding for this project was generously provided by the Oberlin College Department of Geosciences.

REFERENCES

Young Mountains

Biddle, K.T., Uliana, M.A., Mitchum, R.M., Fitzgerald, M.G., Wright, R.C., 1986, The stratigraphic and structural evolution of the central and eastern Magallanes Basin, southern South America. In: In: Allen, P.A., Homewood, P. (Eds.), Foreland Basins 8. Blackwell Publishing Ltd, Oxford, UK, pp. 41–61. https://doi.org/10.1002/ 9781444303810.

Fosdick, J.C., Grove, M., Graham, S.A., Hourigan, J.K., Lovera, O., Romans, B.W., 2015, Detrital

thermochronologic record of foreland burial heating, sedimentary provenance, and orogenesis in Patagonia: Basin Res. 27, 546–572, https://doi.org/10. 1111/bre.12088.

Daniels, B.G., Auchter, N.C., Hubbard, S., Romans, B.W., Matthews, W.A., Stright, L., 2018, Timing of deep-water slope-evolution constrained by large-n detrital and volcanic ash zircon geochronology, Cretaceous Magallanes Basin, Chile: Geol. Soc. Am. Bull 130, 438–454.

Dickinson, W.R., and Suczek, C.A., 1979, Plate tectonics and sandstone compositions: Am. Assoc. Petrol. Geol. Bull. 63, 2164-2182.

Fosdick, J.C., VanderLeest, R.A., Bostelmann T., J.E., Leonard, J.S., Ugalde, R., Oyarzún, and Griffin, M., 2020, Revised timing of Cenozoic Atlantic incursions and changing hinterland sediment sources during southern Patagonian orogenesis: Lithosphere.

Leonard, J.S., Fosdick, J.C., VanderLeest, R.A., 2020, Dynamics of coupled surface and tectonic evolution of a retroarc orogenic wedge as revealed by sedimentary provenance: Front. Earth Sci. 7, 1–20. https://doi.org/10.3389/feart.2019.00353.

R Core Team, 2020, R: A language and environment for statistical computing. R Foundation for Statistical Computing, Vienna, Austria. URL https://www.R-project.org/

Ramos, V.A., Kay, S.M., 1992, Southern Patagonian plateau basalts and deformation: Backarc testimony of ridge collisions: Tectonophysics 205, 261–282.

Ramos, V.A., 2005, Seismic ridge subduction and topography: Foreland deformation in the Patagonian Andes: Tectonophysics 399, 73-86.

Romans, B.W., Fildani, A., Graham, S.A., Hubbard, S.M., Covault, J.A., 2010, Importance of predecessor basin history on the sedimentary fill or a retroarc foreland basin: Provenance analysis of the Cretaceous Magallanes basin, Chile (50-52 °S): Basin Res. 22, 640–658. https://doi.org/10.1111/j.1365-2117.2009.00443.x.

Schwartz, T.M., Fosdick, J.C., Graham, S.A., 2016, Using detrital zircon U-Pb ages to calculate Late Cretaceous sedimentation rates in the Magallanes-Austral basin, Patagonia: Basin Res. 29, 725–746. https://doi.org/10.1111/bre.12198.

Ugalde, R., Bostelmann, E., Fosdick, J., Alarcón, M., Oyarzún, J.L., 2018, Lithostratigraphy of the Cenozoic sedimentary series of Sierra Baguales, Magallanes, Chile: Actas digitales XV Congreso Geológico Chileno, Concepción, Chile.

VanderLeest, R.A., 2020, Detrital geothermochronology, geochemistry, and subsidence analysis of tectonics and sedimentation in the Magallanes-Austral Basin, Patagonian Andes [PhD Dissertation], 276 p.

VanderLeest, R.A., Fosdick, J.C., Leonard, J.S., Morgan, L.E., 2020, Detrital record of the late Oligocene - early Miocene mafic volcanic arc in the southern Patagonian Andes (~51°S) from single-clast geochronology and trace element geochemistry: Journal of Geodynamics 138, doi: 10.1016/j.jog.2020.101751.

Ancient Mountains

Bickford, M.E., Mclelland, J.M., Selleck, B.W., Hill, B.M., and Heumann, M.J., 2008, Timing of anatexis in the eastern Adirondack Highlands: Implications for tectonic evolution during ca. 1050 Ma Ottawan orogenesis: Bulletin of the Geological Society of America v. 120, p, 950.

Bohlen, S., Valley, J.W., and Essene, E.J., 1985, Metamorphism in the Adirondacks. I. Petrology, Pressure and Temperature: Journal of Petrology

Chiarenzelli, J., Kratzmann, D., Selleck, B.W., and Delorraine, W., 2015, Age and provenance of Grenville supergroup rocks, Trans-Adirondack Basin, constrained by detrital zircons: Geology v. 43, p, 183–186.

Heumann, M.J., Bickford, M.E., Hill, B.M., Mclelland, J.M., Selleck, B.W., and Jercinovic, M.J., 2006, Timing of anatexis in metapelites from the Adirondack lowlands and southern highlands: A manifestation of the Shawinigan orogeny and subsequent anorthosite-mangerite-charnockite-granite magmatism: Bulletin of the Geological Society of America v. 118, p, 1283.

Johnson, C.A., and Essene, E.J., 1982. The formation of garnet in olivine-bearing metagabbros from the Adirondacks. Contributions to Mineralogy and Petrology 81, 240–251.

Lanari, P., Vidal, O., De Andrade, V., Dubacq, B., Lewin, E., Grosch, E.G., and Schwartz, S., 2014,

XMapTools: A MATLAB©-based program for electron microprobe X-ray image processing and geothermobarometry: Computers & Geosciences v. 62, p, 227–240.

Lancaster, P.J., Fu, B., Page, F.Z., Kita, N.T., Bickford, M.E., Hill, B.M., Mclelland, J.M., and Valley, J.W., 2008, Genesis of metapelitic migmatites in the Adirondack Mountains, New York: Journal of Metamorphic Geology v. 27, p, 41–54.

Peck, W.H., and Valley, J.W., 2004, Quartz-garnet isotope thermometry in the southern Adirondack Highlands (Grenville Province, New York): Journal of Metamorphic Geology v. 22, p, 763–773.

Quinn, R.J., Kitajima, K., Nakashima, D., Spicuzza, M.J., and Valley, J.W., 2016, Oxygen isotope thermometry using quartz inclusions in garnet: Journal of Metamorphic Geology v. 35, p, 231–252.

Ravna, E.K., 2000a. Distribution of Fe2+ and Mg between coexisting garnet and hornblende in synthetic and natural systems: an empirical calibration of the garnet-hornblende Fe-Mg geothermometer. Lithos 53, 265–277.

Ravna, E.K., 2000b. The garnet-clinopyroxene Fe2+-Mg geothermometer: an updated calibration. Journal of Metamorphic Geology 18, 211–219.

Spear, F.S., and Markussen, J.C., 1997, Mineral zoning, PTXM phase relations, and metamorphic evolution of some Adirondack granulites, New York: Journal of Petrology v. 38, p, 757.

Storm, L.C., and Spear, F.S., 2005, Pressure, temperature and cooling rates of granulite facies migmatitic pelites from the southern Adirondack Highlands, New York: Journal of Metamorphic Geology v. 23, p, 107–130.

Storm, L.C., and Spear, F.S., 2009, Application of the titanium-in-quartz thermometer to pelitic migmatites from the Adirondack Highlands, New York: Journal of Metamorphic Geology v. 27, p, 479–494.

KECK Geology Consortium
Learning Science Through Research
Published by the Keck Geology Consortium
Short Contributions
Keck Geology Consortium
Volume 34
May 2022
doi: 10.18277/AKRSG.2022.34.02

BIOGEOCHEMICAL CONTROLS ON NATURAL AND ANTHROPOGENIC GROUNDWATER CONTAMINANTS IN CALIFORNIA'S CENTRAL VALLEY

ARIC MINE, California State University-Fresno
BRADY ZIEGLER, Trinity University

INTRODUCTION

The Central Valley of California is one of the most agriculturally productive regions of the world, relying on groundwater to support its domestic, municipal, and agricultural water needs. More than one million people in the region rely on groundwater as their primary drinking water source, and the highly productive agricultural region relies heavily on groundwater pumping for crop irrigation (DeSimone et al., 2009). Groundwater contamination is a pervasive concern in the Central Valley as a result of anthropogenic, abiotic, and biotic processes. Elevated concentrations of trace elements in groundwater such as As, U, and Cr occur in Central Valley sediments, but are mobilized by both geologic and anthropogenic forcings (Rosen et al. 2019; McClain et al., 2019).

Recently, attention has been raised regarding groundwater quality in the Central Valley due to impacts from agricultural development. Nitrate (NO^{3-}) is commonly applied to the land surface in the Central Valley to fertilize crop growth in agricultural regions (Nolan et al., 2014). Elevated concentrations of nitrates in groundwater have raised local concerns regarding human and ecological health as well as municipal water treatments costs (Burow et al., 2013). Additionally, the introduction of NO^{3-} can have unforeseen consequences by changing aquifer biogeochemistry to promote the mobilization of some redox-sensitive trace elements that naturally exist in sediments derived from the igneous parent material (Davis et al., 1959), often leading trace metal concentrations in groundwater exceeding safe drinking water thresholds (He et al, 2010). In this study, we sought to elucidate geologic and anthropogenic influences on the biogeochemical mechanisms that mobilize natural contaminants (e.g., arsenic, uranium, and hexavalent chromium) into groundwater in the Kings Groundwater Basin in the broader Central Valley of California.

METHODS

This study used a multifaceted approach of groundwater, sediment and microbiologic analyses in order to make a holistic assessment of the biogeochemical processes impacting trace elements in groundwater in the Central Valley. Publicly available groundwater chemistry data were accessed from the Groundwater Ambient Monitoring and Assessment Program (GAMA: https://www.waterboards.ca.gov/gama/) . Data was downloaded for the Kings Groundwater Basin, a part of the greater Central Valley. Multiple chemical constituents, including arsenic, uranium, nitrate, iron, manganese, calcium, dissolved oxygen, total organic carbon, pH and alkalinity were compiled in both shallow and deep groundwater to evaluate the geospatial extent of groundwater contamination. Correlations of multiple groundwater chemicals were analyzed to infer geochemical mechanisms that mobilize groundwater contaminants from native sediments.

Sediments from the saturated and unsaturated zones collected by previous researchers were analyzed to characterize the geochemical and physical properties of sediment in the Central Valley. Analyses included sequential chemical extractions to target ion exchangeable, carbonate-bound, oxide-bound, and sulfide-bound fractions of major, minor, and trace elements. Bulk elemental abundances were also

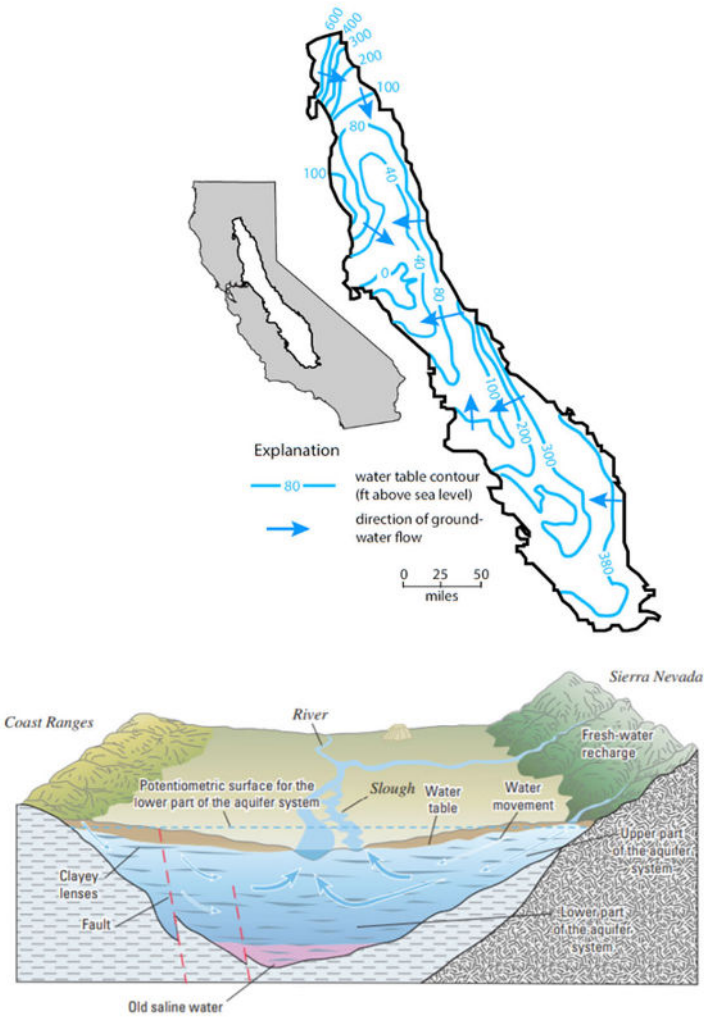

Figure 1. Water table contour map (top) showing the elevation of the water table and direction of groundwater flow in the Central Valley. The regional flow across the valley is shown in cross section (bottom); modified from Williamson et al., (1989) and DeSimone et al. (2009).

quantified using x-ray fluorescence. Particle size distributions were used to quantify the permeability of sediments. Fe(III)/Fe(II) extractions were performed to infer the redox state of the sediment.

We sampled both monitoring and pumping wells multiple times in summer 2021 to collect water for bacterial DNA analyses. Samples were filtered through a 0.2 µm Sterivex filter to concentrate microbial cells from a water sample. DNA extractions and purification was then performed using Qiagen DNeasy PowerWater Kit and a phenol-chloroform extraction method. Extracted DNA was amplified using PCR with 16s rDNA primers and analyzed using a MinIon benchtop sequencer to quantify bacterial community composition and relative abundances. These community compositions were then compared to current and historic well concentrations of groundwater contaminants to evaluate the bacterial influence on water quality.

RESEARCH

Three projects were crafted to address questions related to the mobilization of elements in groundwater as a means to assess how these processes impact groundwater contamination. The different projects focused on expanding our process-based understanding to contaminants via biological, chemical, and observational/statistical tools. Each project was spearheaded by two to three nascent, second-year student scientists with our guidance. The project investigation took place over a five-week immersive summer research experience. The data and information gathered during the summer experience was compiled and synthesized into presentations at the Fall 2021 American Geophysical Union conference in New Orleans.

PROJECT SUMMARIES

Basin-wide Geospatial and Geostatistical Assessment

Geospatial and Statistical Analyses of Groundwater Contaminants in the San Joaquin River Valley During Drought and Non-Drought Periods

Nickels, M., Goudy, M., Ziegler, B.A., Mine, A.H.

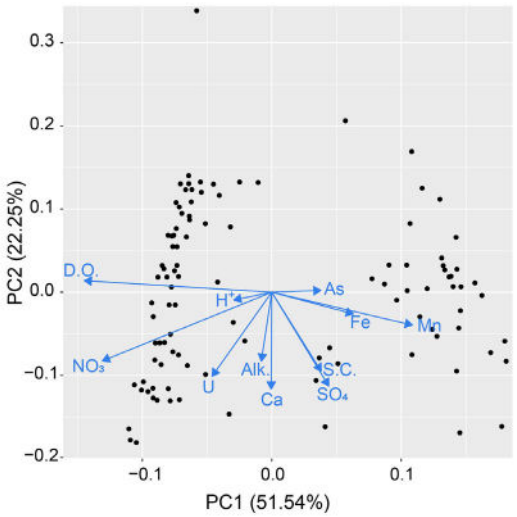

Figure 2. Principal component analysis for wells sampled in the Kings Groundwater Basin.

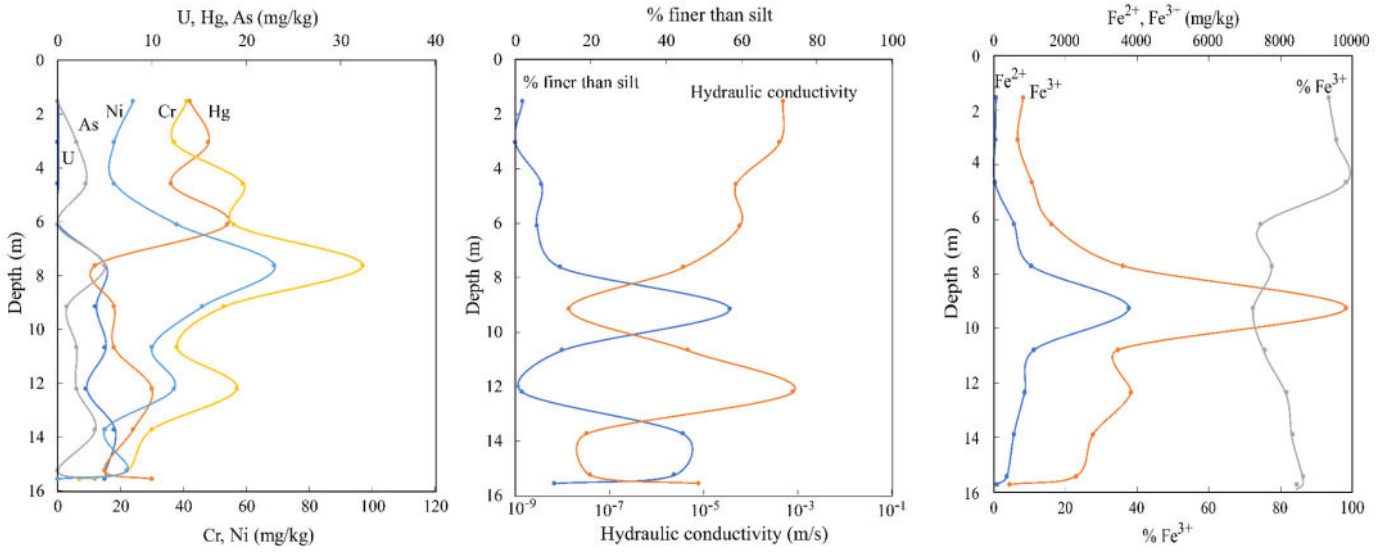

Figure 3. Unsaturated zone depth profiles for bulk concentrations of some trace elements (left), the percent finer than silt and calculated hydraulic conductivity (middle), and the iron redox speciation (right).

Groundwater analyses from the GAMA database show that there are regions in the Kings Groundwater Basin that contain unsafe levels of arsenic and uranium. In particular, shallow groundwater has elevated uranium. Using a principal component analysis (Figure 2), we show that the majority of the variation in the groundwater dataset (51.54% for principal component 1) appears to be related to redox, with dissolved oxygen and nitrate juxtaposed against Fe and Mn in the principal component 1 dimension. Elevated uranium in shallow groundwater was attributed to the more oxidizing conditions associated with nitrate and dissolved oxygen from groundwater recharging from the surface. These electron acceptors can oxidize reduced U(IV) in minerals that comprise the aquifer matrix to U(VI), which is soluble in groundwater as the UO^{2+} ion. Elevated U concentrations were concomitant with elevated alkalinity levels, likely due to the formation of uranium-carbonate complexes, which can inhibit the ability of dissolved uranium species to interact with mineral surfaces and be removed from groundwater.

Sedimentary Geochemistry

Mobilization of Trace Elements from Sediments into Groundwater in California's Central Valley

Culpepper-Wehr, A., Steiner-Otoo, R., Kohn, J., Ziegler, B.A., Mine, A.H.

Comparisons of sediments collected from the saturated and unsaturated zones show that most elements with statistically significant differences were higher in the saturated zone than the unsaturated zone. These elements included Ti, V, Mn, Cu, Zn, As, Rb, Sr, Ba, Th, and U. Only Au was statistically higher in the unsaturated zone than the saturated zone. However, Hg, W, and Co were also highly enriched in surface sediments, and decreased rapidly in concentration. We hypothesize that the elevated levels of Hg and Au in surface sediments might stem from the California Gold Rush, where Au-rich rocks in the Sierra Nevada experienced enhanced weathering during mining operations, and Hg was commonly used to amalgamate Au.

Depth profiles (Figure 3) in the unsaturated zone sediment show that near-surface sediments (zero to six m below land surface) have non-detectable levels of U (<1 mg/kg). Below six m, U concentrations increase to a consistent concentration of ~6 mg/kg to a depth of 16 m. Analyses of Fe(III)/Fe(II) show that near-surface sediments are highly oxidized (>95% Fe(III)) and have a high permeability. These findings, coupled with elevated U in shallow groundwater and nitrate from agricultural runoff, suggest that U from surface sediments are likely oxidatively dissolved and transported downward through the unsaturated zone and recharge into shallow groundwater.

Microbiological Characterization

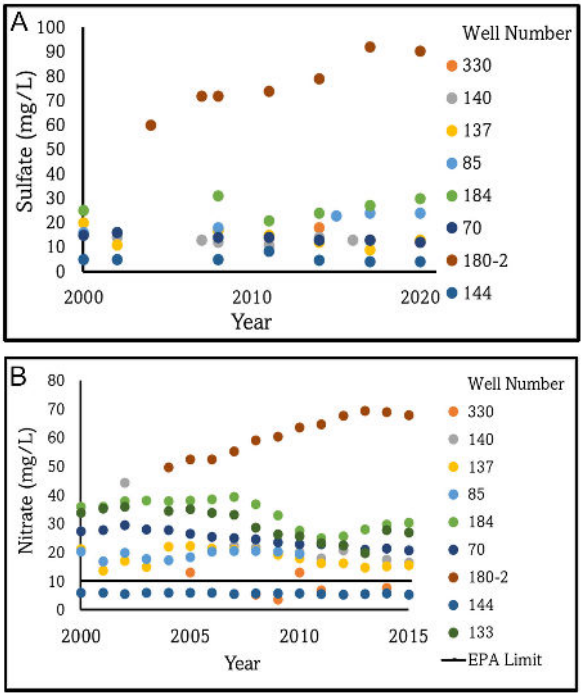

Figure 4. Sulfate (a) and nitrate (b) concentrations over a fifteen year period are shown for the array of wells sampled.

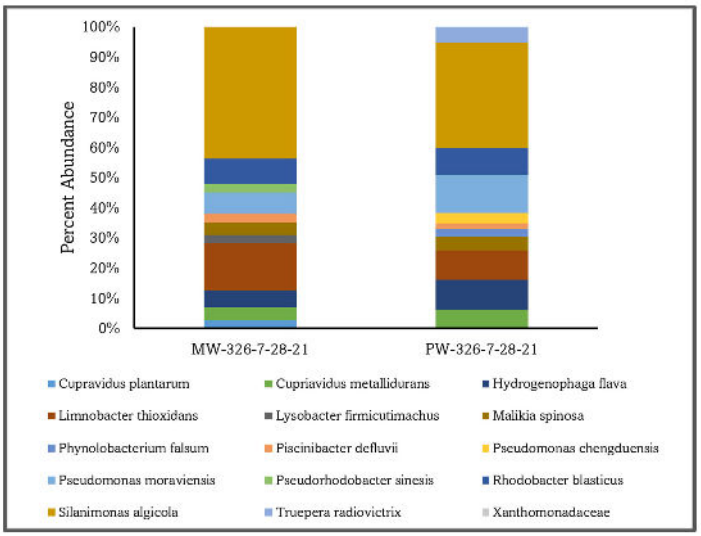

Figure 5. Relative abundance of bacterial groups in production well 326 (PW326) compared against its associated monitoring well (MW326).

Microbial Community Response to Changing Groundwater Chemistry in The San Joaquin Valley

Peterson, T.M., Kron, E.J., O'Rourke, L.E., Goodman, J.D., Mine, A.H., Ziegler, B.A.

Heterogeneous trends were observed in well contaminants in the City of Fresno, which lies within the Kings Groundwater Basin, and more broadly in the city municipal well network. This suggests that the aquifer environment is a dynamic system where sediment, water, and biological interactions are highly variable in space and time. Trends in contaminants at specific wells appear to be a result of aquifer sediment geochemistry, anthropogenic forcing, and microbial activity. As an example, Well 180-2, has both increasing sulfate and nitrate (Figure 4), likely due to fertilizer and gypsum applications in farming activities. Microbiological community analyses completed at a hydrogen sulfide producing well were not coupled to elevated levels of redox sensitive elements (e.g. Fe, Mn, Cr), although microbes capable of redox metabolisms coupled to those elements were observed (Figure 5). This suggests sulfate reduction occurring in the aquifer is not tied to microbially-mediated reduction and mobilization of sediment-derived redox-sensitive elements, or that this coupling varies in time and wasn't captured in our snapshot time sampling. The most abundant bacterial groups in both the monitoring and production wells tested, metabolize either sulfates or nitrates highlighting the significance of redox in well contamination. Differences in community composition between the monitoring and production well highlight the subsurface complexity; these wells are only 25ft apart.

IMPLICATIONS

More recent attention has been raised regarding groundwater quality in the Central Valley due to the impact of agricultural development. However, the introduction of NO^{3-} can have unforeseen consequences by changing aquifer biogeochemistry promoting the mobilization of some redox-sensitive trace elements that naturally exist in sediments derived from the igneous parent material. Elevated concentrations of nitrates and organic contaminants from industrial and agricultural activity appear to be important controls on groundwater contamination and likely biological community in the subsurface. Sustaining and providing clean drinking water will require a multi-faceted approach to water purification and groundwater pumping. Current observations of changes in the Central Valley include: groundwater level declines, subsidence, and the pervasiveness of groundwater contamination.

ACKNOWLEDGMENTS

This material is based upon work supported by the Keck Geology Consortium and the National Science Foundation under Grant No. 2050697.

REFERENCES

Burow, K. R., Jurgens, B. C., Belitz, K., Dubrovsky, N. M. (2013). Assessment of regional change in nitrate concentrations in groundwater in the Central Valley, California, USA, 1950s-2000s. Environmental Earth Sciences, 69(8), 2609–2621. https://doi.org/10.1007/s12665-012-2082-4

Davis, G. H., Green, J. H., Olmsted, F. H., Brown, D. W. (1959). Ground-water conditions and storage capacity in the San Joaquin Valley, California. USGS Water Supply Paper 1469. US Geological Survey. https://doi.org/10.3133/wsp1469

DeSimone, Leslie A., Pixie A. Hamilton. (2009) Quality of water from domestic wells in principal aquifers of the United States, 1991-2004. USGS Scientific Investigation 2009-1332. US Geological Survey.

He, Y. T., Fitzmaurice, A. G., Bilgin, A., Choi, S., O'Day, P., Horst, J., … Hering, J. G. (2010). Geochemical processes controlling arsenic mobility in groundwater: A case study of arsenic mobilization and natural attenuation. Applied Geochemistry, 25(1), 69–80. https://doi.org/10.1016/j.apgeochem.2009.10.002

Jurgens, B. C., Fram, M. S., Belitz, K., Burow, K. R., Landon, M. K. (2010). Effects of Groundwater Development on Uranium: Central Valley, California, USA. Ground Water, 48(6), 913–928. https://doi.org/10.1111/j.1745-6584.2009.00635.x

McClain, C., Fendorf, S., Johnson, S., Menendez, A., Maher, K. (2019). Lithologic and redox controls on hexavalent chromium in vadose zone sediments of California's Central Valley. Geochimica et Cosmochimica Acta, 265, 478–494. https://doi.org/10.1016/j.gca.2019.07.044

Nolan, B. T., Gronberg, J. M., Faunt, C. C., Eberts, S. M., Belitz, K. (2014). Modeling nitrate at domestic and public-supply well depths in the Central Valley, California. Environmental Science & Technology, 48(10), 5643-5651. https://doi.org/10.1021/es405452q

Nolan, J., Weber, K. A. (2015). Natural uranium contamination in major US aquifers linked to nitrate. Environmental Science & Technology Letters, 2(8), 215-220. https://doi.org/10.1021/acs.estlett.5b00174

Rosen, M. R., Burow, K. R., Fram, M. S. (2019). Anthropogenic and geologic causes of anomalously high uranium concentrations in groundwater used for drinking water supply in the southeastern San Joaquin Valley, CA. Journal of Hydrology, 577, 124009. https://doi.org/10.1016/j.jhydrol.2019.124009

Weber, K. A., Thrash, J. C., Van Trump, J. I., Achenbach, L. A., Coates, J. D. (2011). Environmental and taxonomic bacterial diversity of anaerobic uranium (IV) bio-oxidation. Applied Environmental Microbiology, 77(13), 4693-4696. https://doi.org/10.1128/AEM.02539-10.

KECK Geology Consortium
Learning Science Through Research
Published by the Keck Geology Consortium
Short Contributions
Keck Geology Consortium
Volume 34
May 2022
doi: 10.18277/AKRSG.2022.34.03

CARBON SEQUESTRATION BY ENHANCED SILICATE WEATHERING IN AGRICULTURAL SOILS

DANIEL P. MAXBAUER, Carleton College
JAHMAINE RENZO YAMBING, Carleton College, Peer Mentor

INTRODUCTION

Enhanced silicate weathering is a carbon dioxide removal technology that could be applied at scale on croplands to reduce greenhouse gas emissions associated with agriculture, one of the largest sources of emissions globally (Schuiling and Krugsman, 2006; Renforth, 2012; Hartmann et al., 2013; Beerling et al., 2018; Andrews and Taylor, 2019). Agricultural applications of enhanced weathering leverage existing infrastructure used to spread crushed rocks on soil for nutrient and pH management (Figure 1; Gillman, 1980; van Straaten, 2006; Anda et al., 2015). In place of more traditional materials (like carbonate rocks used for liming), silicate rocks rich in Ca and Mg (e.g., basalt) are attractive because their dissolution consumes atmospheric carbon dioxide (CO_2) and ultimately stores that carbon as alkalinity in the oceans (Renforth, 2012; Hartmann et al., 2013). Through applications of crushed silicate rocks, then, rates of mineral dissolution and carbon sequestration could be accelerated through increasing the available mineral surface area for weathering.

Recent international reports (IPCC, 2018; IPCC, 2021) include enhanced weathering in the mix of emerging carbon dioxide removal technologies needed to limit global temperature increase below the internationally established threshold of 2°C. However, the vast majority of available literature on enhanced weathering is based on modeling or theoretical frameworks that constrain potential rates of carbon sequestration (e.g., Wilson et al., 2009; Renforth, 2012; Hartmann, 2013; Beerling et al., 2018; Beerling et al., 2020). Observational data directly testing enhanced weathering are limited. Several studies evaluate enhanced weathering in controlled systems where crops are grown in a greenhouse or garden (ten Berge et al., 2012; Haque et al., 2019; Haque et al., 2020a; Amann et al., 2020; Kellend et al., 2020) but only one study is currently available with published data from a field trial (Haque et al., 2020b).

Figure 1. Example of crushed basalt being applied to croplands in this study using spreading equipment designed for lime.

This research project contributed to establishing a three-year field experiment on an agricultural field at Carleton College to test the carbon sequestration potential of enhanced silicate weathering along with associated impacts on soils and crops. A team of four students participated through the Keck Gateway program. Gateway students worked to help collect and analyze important baseline data for soils in the study area, and contributed to a pilot greenhouse study.

FIELD TRIAL

This Gateway project is part of a longer-term research effort aimed at evaluating enhanced silicate weathering in agriculture over a three-year experimental period. The field trial utilizes a randomized block design that distributes control and treatment plots across the study area (Figure 3). The initial round of treatments were

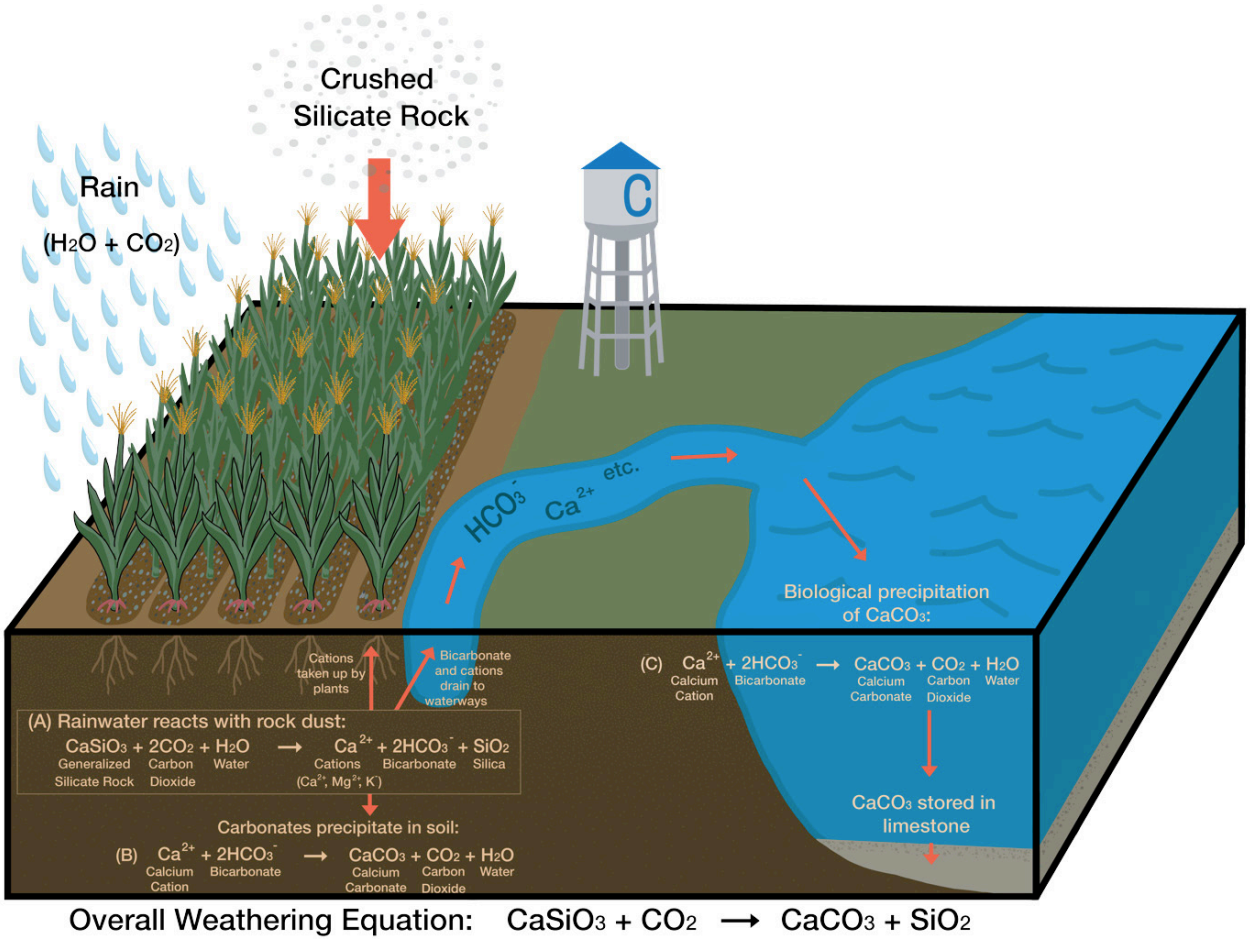

Figure 2. Schematic overview of enhanced silicate weathering in agriculture. (A) Initial reaction of silicate minerals with carbon dioxide in soils leads to the release and transport of cations and bicarbonate in soils and the local watershed. The ultimate fate of bicarbonate is to be precipitated as a carbonate mineral (B) or to contribute to carbonate mineral formation in the oceans (C). Figure and schematic adapted from Andrews and Taylor (2019).

applied during November of 2021 and monitoring of soil greenhouse gas flux and water chemistry is currently ongoing.

Baseline soil data collected during the summer of 2021 as part of the Gateway project described here is shown in Figure 4. Annual soil sampling and analysis will be conducted and compared against baseline data to compare the impacts of silicate treatments on soil properties and soil carbon storage. Soil pH ranges from ~5-8 and generally pH increases with depth in the soil profile (Figure 4). Soil in blocks A and B have notably elevated pH in comparison to blocks C and D, with the exception of the slag treatment plot in block A (Figure 3 and 4).

Based on personal communication with our cooperating farmer, dredged lake sediments from a man-made lake on campus at Carleton College were spread on the northern half of this field in the early 2000's. Based on the preliminary data collected here it is fairly clear that this impacts blocks A and B. Trends in soil organic matter, carbonate, and cation exchange capacity (CEC) mimic soil pH. The slag treatment plot in block A does not follow these trends, and more closely reflects soil properties in blocks C and D, indicating that the dredged material was not spread on this portion of block A. The observed gradient in soil pH across treatment plots should provide a good opportunity to determine how soil pH interacts with the efficacy of enhanced weathering for carbon sequestration (rate of dissolution) and co-benefits to growers (improving crop yield and soil properties).

GREENHOUSE EXPERIMENT

Students in this Gateway project initiated a greenhouse experiment aimed to test the impacts of enhanced silicate weathering in a more controlled setting compared with the field study. This report provides a

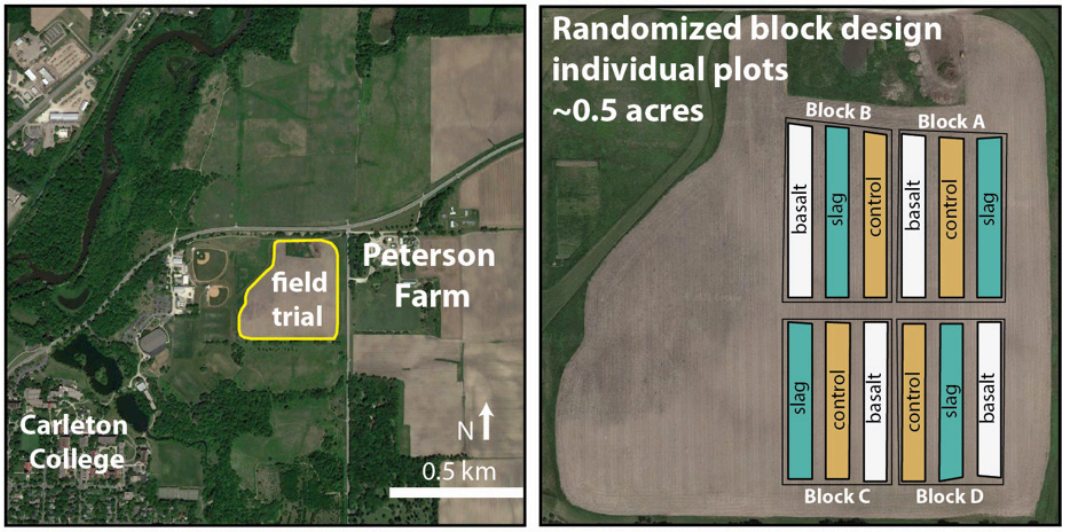

Figure 3. Location of field trial relative to Carleton College in Northfield, MN. Peterson Farms is the cooperating farmer partnering in this research. Location of field trials is only a ~10-minute walk from science center on campus at Carleton.

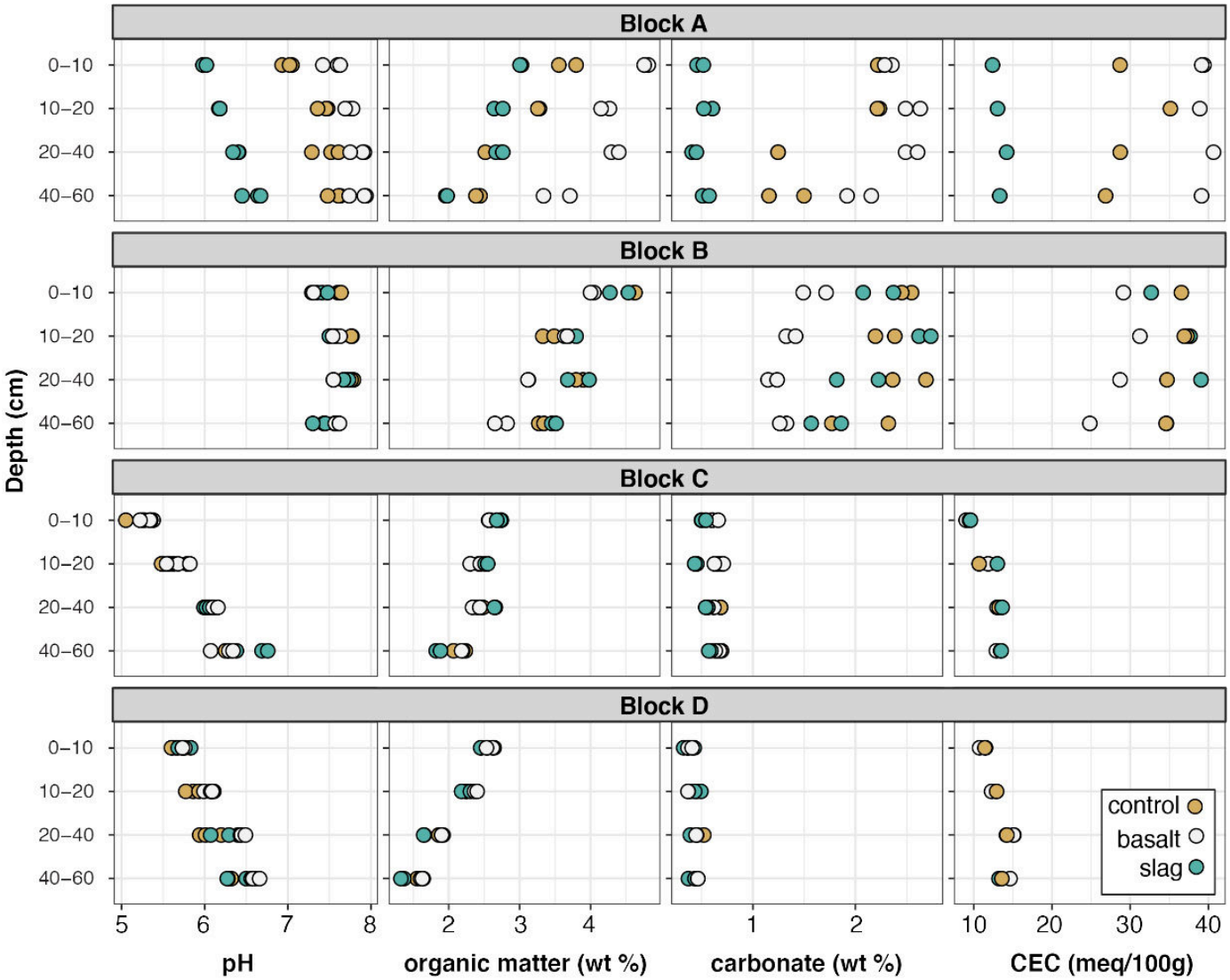

Figure 4. Preliminary soils data for field trials. Panels from left to right show soil pH, weight percentage organic matter and carbonate mineral, and cation exchange capacity (CEC) at various depths for homogenized plot samples. Data are organized by block (grey header blocks) and treatment (colored circles, see key in lower right corner).

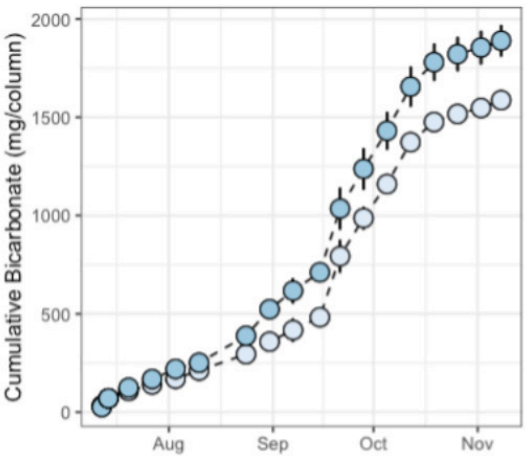

Figure 5. Cumulative bicarbonate leached from treatment (dark blue) and control (light blue) soil columns. Bicarbonate was calculated from measurements of total alkalinity. Error bars represent one standard deviation.

brief overview of our experimental design and a key result of the project.

A set of 12 soil reactors were packed to an approximate bulk density of 1.3 g cm-3 with sieved and homogenized topsoil (upper 20 cm) and subsoil (below 20 cm) collected from native silty loam soil from the agricultural field described in the previous section (see Figure 3; soils from NW corner of field used in field trial). Basalt was mixed into the upper 10 cm of topsoil in 6 of the reactors at a rate equivalent to 20 tonnes acre-1 prior to planting. Our application rate for our initial greenhouse experiment exceeds what we intend to apply in the field, but remains on the low end of rates applied in most previous greenhouse or pot studies (~60-200 tonnes acre-1; Haque et al., 2019; Haque et al., 2020a; Kellend et al., 2020; Amann et al., 2020). Despite the unlikely case that farming partners would adopt such high dosages, we evaluate a higher rate in our preliminary greenhouse study to ensure we are able to observe a signal with our methods for carbon sequestration accounting, if one exists at high loads.

A total of 48 corn seeds were germinated in small starter trays and kept moist for 2 weeks while seedlings developed. The 12 healthiest seedlings were transplanted into the soil reactors after 2 weeks marking the start of the experiment. The sample size for corn plants here follows other recent pot studies. Our irrigation scheme intended to match local rainfall during the growing season, with each reactor receiving 500 mL of water per week. However, beginning with week 6 of the experiment, additional water was added as the corn plants grew and increased their water use. This was done to ensure that enough drainage water could be collected for analysis – limited drainage water has impacted the ability of previous greenhouse studies to consistently evaluate carbon sequestration rates using bicarbonate concentrations (ten Berge et al., 2012; Kellend et al., 2020; Amann et al., 2020).

We harvested corn after an 18-week (~126 days) experiment, in line with the duration from other studies (Kellend et al., 2020). Trends in total bicarbonate in leachate water are shown in Figure 5. Basalt treated soil columns in our experiment have a significantly higher amount of total bicarbonate produced in leachate waters collected and analyzed from each soil column ($p < 0.05$ for simple t-test). These results suggest an increased rate of silicate weathering due to basalt amendments which corresponds to an increase in carbon removal.

The greenhouse study described here provides exciting data that suggests carbon removal through enhanced weathering is detectable through simple measurements of water chemistry, although ongoing work is continuing to evaluate these results and better clarify actual rates of carbon removal along with associated impacts to crops and soil.

ACKNOWLEDGMENTS

This work was supported by the Keck Geology Consortium and the National Science Foundation under grant no. 2050697. Additional funding was provided by Carleton College. We are grateful for helpful discussions and assistance provided by staff and faculty in the Geology Department at Carleton College, local farming partner Mike Peterson, David Legvold, and Clean River Partners. Ella Milliken worked closely with our research group during the summer of 2021 and contributed significantly to the work described here.

REFERENCES

Amann, T., Hartmann, J., Struyf, E., de Oliveira Garcia, W., Fischer, E.K., Janssens, I., Meire, P.,

and Schoelynck, J., 2020, Enhanced Weathering and related element fluxes – a cropland mesocosm approach: Biogeosciences, v. 17, p. 103–119, doi:10.5194/bg-17-103-2020.

Anda, M., Shamshuddin, J., and Fauziah, C.I., 2015, Improving chemical properties of a highly weathered soil using finely ground basalt rocks: Catena, v. 124, p. 147–161, doi:10.1016/j.catena.2014.09.012.

Andrews, M.G., and Taylor, L.L., 2019, Combating climate change through enhanced weathering of agricultural soils: Elements, v. 15, p. 253–258, doi:10.2138/gselements.15.4.253.

Beerling, D.J. et al., 2018, Farming with crops and rocks to address global climate, food and soil security: Nature Plants, v. 4, p. 138–147, doi:10.1038/s41477-018-0108-y.

Beerling, D.J. et al., 2020, Potential for large-scale CO_2 removal via enhanced rock weathering with croplands: Nature, v. 583, p. 242–248, doi:10.1038/s41586-020-2448-9.

Gillman, G.P., 1980, The effect of crushed basalt scoria on the cation exchange properties of a highly weathered soil: Soil Science Society of America Journal, v. 44, p. 465–468, doi:10.2136/sssaj1980.03615995004400030005x.

Hartmann, J., West, A.J., Renforth, P., Köhler, P., De La Rocha, C.L., Wolf-Gladrow, D.A., Dürr, H.H., and Scheffran, J., 2013, Enhanced chemical weathering as a geoengineering strategy to reduce atmospheric carbon dioxide, supply nutrients, and mitigate ocean acidification: Enhanced Weathering: Reviews of Geophysics, v. 51, p. 113–149, doi:10.1002/rog.20004.

Haque, F., Santos, R.M., and Chiang, Y.W., 2020a, Optimizing inorganic carbon sequestration and crop yield with wollastonite soil amendment in a microplot study: Frontiers in Plant Science, v. 11, p. 1012, doi:10.3389/fpls.2020.01012.

Haque, F., Santos, R.M., and Chiang, Y.W., 2020b, CO_2 sequestration by wollastonite-amended agricultural soils – An Ontario field study: International Journal of Greenhouse Gas Control, v. 97, p. 103017, doi:10.1016/j.ijggc.2020.103017.

Haque, F., Santos, R.M., Dutta, A., Thimmanagari, M., and Chiang, Y.W., 2019, Co-benefits of wollastonite weathering in agriculture: CO_2 sequestration and promoted plant growth: ACS Omega, v. 4, p. 1425–1433, doi:10.1021/acsomega.8b02477.

Kelland, M.E. et al., 2020, Increased yield and CO_2 sequestration potential with the C4 cereal Sorghum bicolor cultivated in basaltic rock dust-amended agricultural soil: Global Change Biology, v. 26, p. 3658–3676, doi:10.1111/gcb.15089.

Renforth, P., 2012, The potential of enhanced weathering in the UK: International Journal of Greenhouse Gas Control, v. 10, p. 229–243, doi:10.1016/j.ijggc.2012.06.011.

Schuiling, R.D., and Krijgsman, P., 2006, Enhanced Weathering: An effective and cheap tool to sequester CO_2: Climatic Change, v. 74, p. 349–354, doi:10.1007/s10584-005-3485-y.

ten Berge, H.F.M., van der Meer, H.G., Steenhuizen, J.W., Goedhart, P.W., Knops, P., and Verhagen, J., 2012, Olivine weathering in soil, and its effects on growth and nutrient uptake in ryegrass (Lolium perenne L.): a pot experiment: PLoS ONE, v. 7, p. e42098, doi:10.1371/journal.pone.0042098.

Van Straaten, P., 2006, Farming with rocks and minerals: challenges and opportunities: Anais da Academia Brasileira de Ciências, v. 78, p. 731–747, doi:10.1590/S0001-37652006000400009.

Wilson, S.A., Dipple, G.M., Power, I.M., Thom, J.M., Anderson, R.G., Raudsepp, M., Gabites, J.E., and Southam, G., 2009, Carbon dioxide fixation within mine wastes of ultramafic-hosted ore deposits: examples from the Clinton Creek and Cassiar Chrysotile Deposits, Canada: Economic Geology, v. 104, p. 95–112, doi:10.2113/gsecongeo.104.1.95.

KECK Geology Consortium
Learning Science Through Research
Published by the Keck Geology Consortium
Short Contributions
Keck Geology Consortium
Volume 34
May 2022
doi: 10.18277/AKRSG.2022.34.04

GEOCHEMICAL PROPERTIES OF SEEPAGE-FILTRATION AND FRACTURE SPRINGS IN WISCONSIN

SUSAN SWANSON, Beloit College
OCEAN CLEVETTE, Beloit College, Peer Mentor

INTRODUCTION

A wide variety of geologic and topographic settings, flow mechanisms, discharge rates, and physicochemical conditions have been documented for springs (Stevens et al., 2021). For any given spring, conditions within the spring environment may also be spatially variable, contributing to the diversity of spring biota. For example, macroinvertebrates can be very diverse in springs with microhabitats and heterogeneous substrates (Glazier, 2009). Yet, studies of spring water temperature and geochemistry often rely on sensors installed at the spring orifice or samples collected at a single position, and values are assumed to be representative of the entire spring environment (e.g., Luhman et al., 2011; Swanson et al., 2020). The spatial variability of temperature in the immediate spring environment has recently been shown to vary by spring source geomorphology. At fracture springs, groundwater flows from discrete sources and the distribution of temperature is spatially consistent, whereas at seepage-filtration springs, groundwater flows in a more diffuse manner from numerous openings in permeable material and the distribution of temperature is more spatially variable (Fig. 1) (Swanson and Graham, 2022).

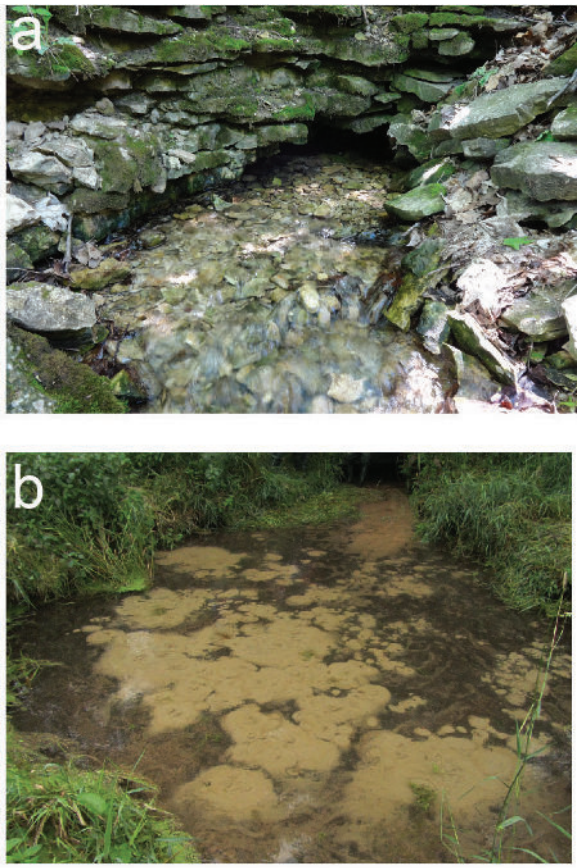

Figure 1. A typical fracture spring (a.), where groundwater flows from a discrete fracture and a typical seepage-filtration spring (b.), where groundwater flows from numerous openings in permeable, unlithified material.

In the summer of 2021, we undertook a four-student Keck Gateway project to evaluate relationships between the spatial variation of geochemical conditions and spring source geomorphology. Students selected six springs from over 400 springs inventoried in Wisconsin (Swanson et al., 2019). Some springs in Wisconsin exhibit more than one type of source geomorphology. Those selected for this study are exclusively fracture or exclusively seepage-filtration springs, the two most common spring source geomorphologies in the region and those which have distinct differences in spatial distribution of temperature (Fig. 2).

Most fracture springs in Wisconsin are found in the Driftless Area of southwestern Wisconsin. They form as a result of preferential groundwater flow through bedding-plane fractures in exposed or shallowly buried and mostly horizontal Paleozoic sedimentary strata composed of sandstone, shale, limestone, and dolomite. Seepage-filtration springs in Wisconsin

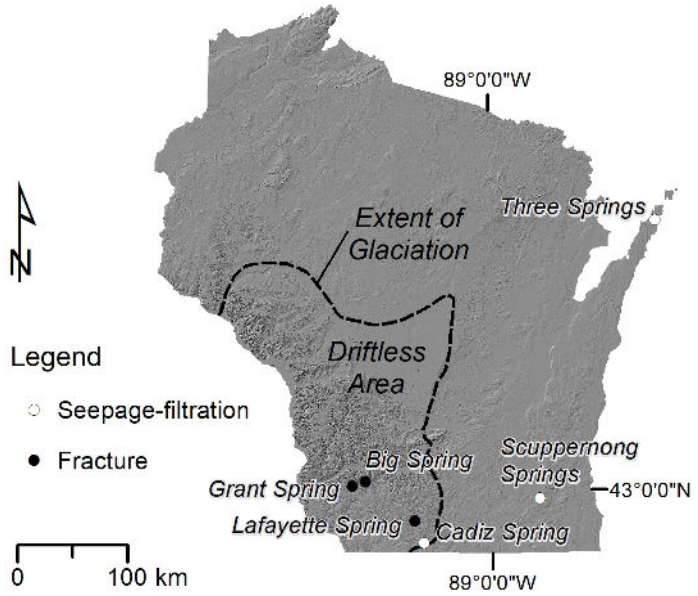

Figure 2. The three fracture springs and three seep-filtration springs utilized in this study.

are a result of variations in topography and lithology of surficial unlithified materials. They commonly form where groundwater emerges at the base of glacial moraines or near the margins of former glacial lakebeds (Swanson et al. 2019).

METHODS

Students worked as a team to document site environmental conditions, measure geochemical concentrations across the spring pool, collect water samples for laboratory analysis, image the water surface for temperature conditions, and measure spring flow (Fig. 3). They carefully drafted to-scale site maps by making measurements of the dimensions of the spring pool and noting physical features, such as the spring orifice, exposed bedrock, boulders, or vegetation. Photo points are noted on the maps, as well as GPS and discharge measurement positions and water quality sampling locations.

Once the students were familiar with the immediate spring environment, they could assess and design an optimal sampling array for the site. Sampling arrays were positioned as close to each spring orifice as possible. All sites used a sample grid spacing of 30 cm; however, the total length and width of each sampling array depended on the dimensions of the spring pool. At each sampling grid point, students measured water depth using a meter stick and

Figure 3. Students worked as a team to (a.) measure geochemical properties along a transect within a sampling array, (b.) measure spring discharge using a wading rod and flow meter, and (c.) sample groundwater after field-filtering.

measured water pH, specific conductance (µmhos/cm, 25°C), and temperature (°C) using a YSI 600 XLM Multiparameter Water Quality Sonde. They also collected water samples at each grid point using a small hand pump. The samples were kept on ice during transport and then analyzed within 24 hours for Chloride (Cl) and Nitrate (NO_3-N) concentrations using Vernier ion-specific electrodes. Because spring water samples are most commonly collected at a single position as close to emerging groundwater as possible, students also collected a water sample in a position such as this at each spring. This approach allowed for comparisons between the single sample and the sampling array concentrations. Water for the single sample was filtered using a handheld vacuum pump with a 0.45 µm filter and shipped on ice to the University of Wisconsin-Stevens Point Water and Environmental Analysis Lab for analysis of major ions and alkalinity.

After water quality sampling was completed, students used a FLIR Vue Pro 640 camera to capture thermal images in the vicinity of the sampling array and spring orifice. This process allowed students to

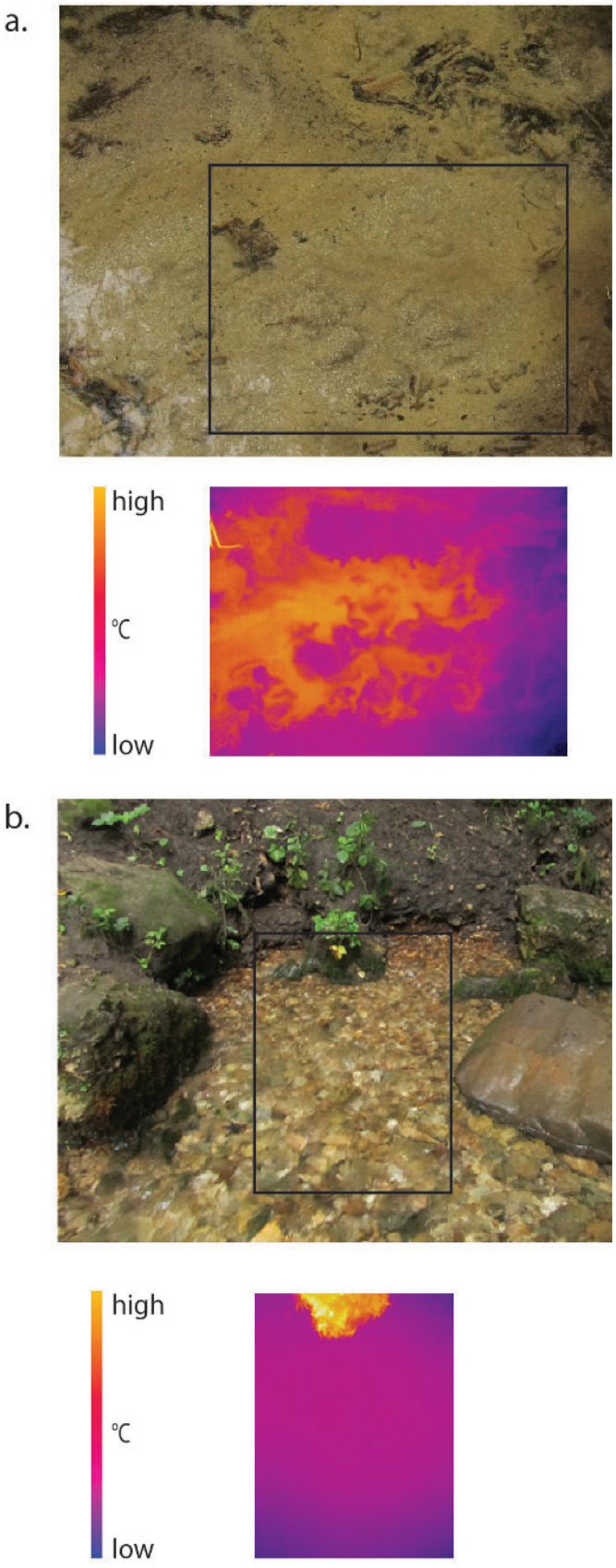

Figure 4. Examples of digital and thermal images for (a.) a seepage-filtration spring (Three Springs) and (b.) a fracture spring (Big Spring). The black rectangles show the approximate positions of the thermal images. Each thermal image is approximately 0.6 m by 1 m.

confirm the results of Swanson et al. (2022) for their own field sites. Fieldwork was conducted in July, so differences between spring pool surface water and emerging groundwater temperatures are likely to be at a maximum. A range pole, tripod, and overhead camera boom positioned the thermal camera 90° from and 1.2 m above the water surface. The camera has a 45° field of view (FOV), which results in a lateral distance across the bottom of the thermal images of about 1 m. Images are composed of 640 x 512 pixels, so the effective pixel size of each image is 2.4 mm^2. Students shaded the spring pool with a large tarp to minimize reflected radiation from clouds and tree canopy.

Finally, spring discharge was measured and calculated using a flow meter and the velocity area method or measured directly using a cutthroat flume. The measurement approach depended on the width of the spring channel and the depth of water.

As in the field, students worked as a team to catalog and analyze their field and laboratory results. They tabulated measurements and uploaded them to ArcGIS where the spatial distribution of geochemical characteristics (pH, specific conductance, Chloride, Nitrate-N) could be mapped for each site using the Inverse Distance Weighted method.

FINDINGS

All six springs under study are rheocrenes, or stream-forming springs. Three are fracture springs and three are seepage-filtration springs. The immediate spring environments, or spring pool areas, for all of the springs are relatively small (less than 70 m^2) and water depths are shallow (less than 50 cm). Discharge for the springs ranged from 6.3 x 10^{-3} to 4.6 x 10^{-1} m^3/sec with an average of 1.5 x 10^{-1} m^3/sec. All six springs have experienced disturbance from agriculture, recreation, or roads.

Thermal images support the previous work by Swanson and Graham (2022) by showing that the spatial distribution of temperature differs between spring types, with greater variation at seepage-filtration springs (Fig. 4). Temperature varied by up to 6.5°C across the surface of the seepage-filtration springs, whereas it varied by no more than 2°C across

the surface of the fracture springs.

Specific conductance (25ºC) was very consistent at the fracture springs, varying by only 2 to 3 µmhos/cm across the sampling arrays. Specific conductance at the seepage-filtration springs varied by 14 to 20 µmhos/cm across the sampling arrays (Fig. 5a., Table 1). Students noted less distinct differences between fracture springs and seepage-filtration for pH and Chloride concentrations, but patterns may still exist. The pH at the fracture springs varied by 0 to 0.1 pH across the sampling arrays, whereas it varied by 0.1 to 0.7 pH units across the sampling arrays at the seepage-filtration springs (Fig. 5b., Table 1). Similarly, Chloride concentrations were somewhat more consistent at the fracture springs. The ranges in concentrations were 0.2 to 2.9 mg/L at the fracture springs and 0.4 to 8.5 mg/L at the seepage-filtration springs (Fig. 5c., Table 1). Ranges in Nitrate-N concentrations were similar across all six sites (Fig. 5d., Table 1). However, due to instability during measurements, students suspected that the Nitrate-N electrode may have been less accurate.

In light of the field results for Chloride and Nitrate-N, the results of the lab-analyzed single position samples for each site were compared to average field Chloride and Nitrate-N concentrations. In both cases, field values were somewhat higher than lab values, but there was a stronger linear relationship between lab and field values for Chloride samples ($R^2 = 0.8$) versus Nitrate-N samples ($R^2 = 0.6$), further suggesting that the Nitrate-N ion-specific electrode may have been less reliable.

On the basis of their results, the students concluded that their results were promising and that they supported the idea that a single sampling point is unlikely to capture the range of geochemical and habitat characteristics in springs, especially for seepage-filtration springs. However, they also agreed on the need for further investigation. Additional fracture and seepage-filtration springs should be investigated, resulting in an ability to calculate more robust summary statistics. If spring pool area and time permit, the extent of the sampling arrays should be increased and the grid-spacing should be decreased. Repeating the same measurements in different seasons may also capture important temporal, as well as spatial, variations in geochemical characteristics.

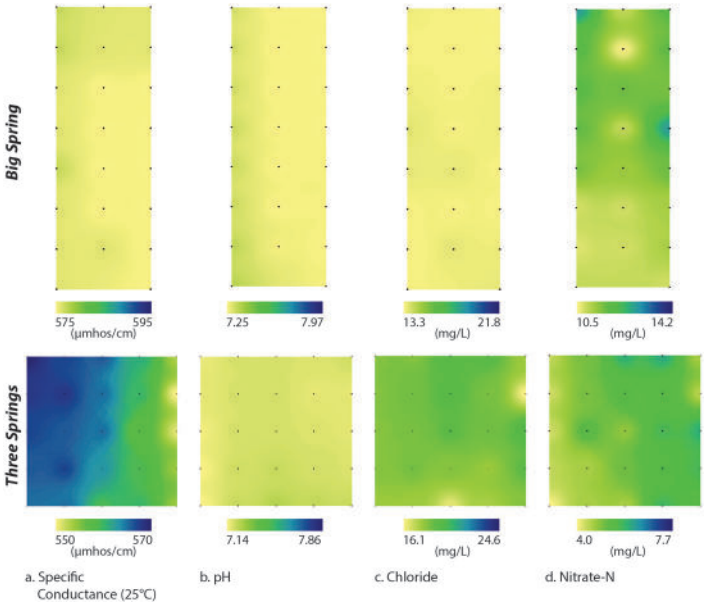

Figure 5. Examples of geochemical maps for a fracture spring (Big Spring) and a seepage-filtration spring (Three Springs). Sampling points, represented by small black dots, are spaced every 30 cm. Minimum and maximum values for each parameter differ between Big Spring and Three Springs, but ranges in values are the same, making comparisons of spatial variation possible.

Table 1. Geochemical results for three seepage-filtration and three fracture springs.

Spring		Specific Conductance (µmhos/cm, 25ºC)		pH		Chloride (mg/L)		Nitrate-N (mg/L)	
		Mean	Range	Mean	Range	Mean	Range	Mean	Range
Seepage-filtration	Cadiz	553	16	7.3	0.3	24.6	8.5	7.8	0.8
	Scuppernong	576	14	7.5	0.7	32.4	3.0	7.1	0.6
	Three Springs	562	20	7.2	0.1	18.2	0.4	5.1	0.6
Fracture	Grant	534	2	7.2	0.1	9.7	2.9	8.3	0.7
	Big Spring	576	2	7.3	0.1	13.5	0.4	11.4	0.6
	Lafayette	472	3	7.2	0	15.0	1.2	8.4	0.6

ACKNOWLEDGEMENTS

This material is based upon work supported by the Keck Geology Consortium and the National Science Foundation under Grant No. 2050697. Additional funding for this project was generously provided by the Beloit College Geology Department. We thank the private landowners and public land managers who allowed access to the springs.

REFERENCES

Glazier, D.S., 2009, Springs. In Likens GE (ed.) Encyclopedia of Inland Waters., Volume 1: Elsevier, Oxford, UK. p. 734–755.

Luhmann, A.J., Covington, M.D., Peters, A.J., Alexander, S.C., Anger, C.T., Green, J.A., Runkel, A.C., Alexander, E.C. Jr., 2011, Classification of thermal patterns at karst springs and cave streams: Groundwater v. 49, no. 3, p. 324–335. https://doi.org/10.1111/j.1745-6584.2010.00737.x

Stevens, L.E., Schenk, E.R., Springer, A.E., 2021, Springs ecosystem classification: Ecol Appl v. 31, no. 1, p. 1–28. https://doi.org/10.1002/eap.2218

Swanson, S.K., Graham, G.E., 2022. Spring flux as an indicator of source geomorphology, substrata, and temperature conditions in springs, Hydrogeology Journal 30(1), 221-229, https://doi.org/10.1007/s10040-021-02412-1.

Swanson, S.K., Graham, G.E., and Hart, D.J., 2019, An inventory of springs in Wisconsin: Wisconsin Geological and Natural History Survey Bulletin 113, 24p.

Swanson, S.K., Graham, G.E., and Hart, D.J., 2020, Using reference springs to describe expected flow, temperature, and chemistry conditions for geologically related groups of springs: Environmental & Engineering Geoscience v. 26, no. 3, p. 331-344, https://doi.org/10.2113/EEG-2312R.

KECK Geology Consortium
Learning Science Through Research
Published by the Keck Geology Consortium
Short Contributions
Keck Geology Consortium
Volume 34
May 2022
doi: 10.18277/AKRSG.2022.34.05

RISING WATERS, SHRINKING HABITATS: THE INFLUENCE OF FLUCTUATING WATER LEVELS ON THE GEOLOGY AND ECOLOGY OF A GREAT LAKES ARCHIPELAGO

KIM C. DIVER, Wesleyan University
JENNA OTAOLA, Peer Mentor, Wesleyan University

INTRODUCTION

Global and regional environmental change has resulted in water-level changes in the world's oceans and large lakes. The Great Lakes have a history of water-level fluctuations (Figure 1). A prolonged low water stage in the Huron-Michigan basin occurred from 1999-2014, with a record low in January 2013 (175.57 meters above sea level). Subsequent years showed a rapid climb above the long-term average, with near-record high levels in 2020 (177.45 m asl). (Note: the record high of 177.50 m asl occurred in 1986.) In this project, we used field data and satellite/aerial imagery spread over twenty years to analyze the spatiotemporal interplay of water-level fluctuations, shoreline configuration, and island characteristics affecting plant communities on islands in the Georgian Bay of Lake Huron.

Little is known regarding the role of feedbacks between climate patterns, coastline geomorphology, and shoreline vegetation on species richness patterns on islands. The Great Lakes contain the world's largest collection of freshwater islands (Vigmostad, 1999). Many of these islands form dense archipelagos in Lake Huron's Georgian Bay (Ontario, Canada).

We investigated spatiotemporal changes in island shoreline configuration and plant biogeography within the Ontario Ministry of Natural Resources' The Massasauga Provincial Park (Figure 2) on the eastern shore of the Georgian Bay and within the UNESCO Georgian Bay Littoral Biosphere Reserve. We hypothesized that the fluctuating water levels influence the area and shoreline configuration of the islands as shorelines and low elevation islands emerge and submerge with these fluctuations. The project had two main research objectives: (1) create accurate island shoreline data for years with field data and the existing low- and high-water years within the 2001-2021 study period and (2) analyze the influence of water level changes on shorelines (e.g., island area, shape), island characteristics (e.g., soil properties, shoreline types), and island ecosystems (plant species richness). The overall objective was to shed light on the applicability of the prevailing model of island biogeography in areas with fluctuating water levels.

STUDENT PROJECTS

This research involved four rising sophomore students, a rising senior near-peer mentor, and one faculty member. The 2001-2021 study period included four

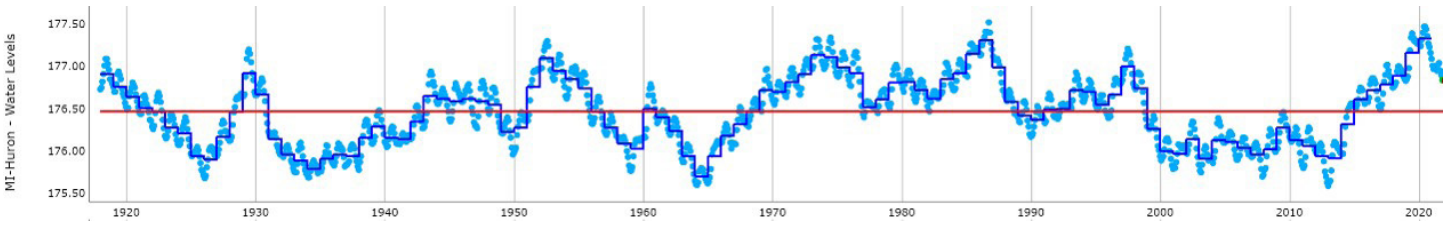

Figure 1. Historical monthly (light blue dots) and yearly (dark blue line) mean water level for the Lake Michigan – Huron Basin, 1918-2021. Note the prolonged low water period of 1999-2014. The vertical axis denotes lake level in meters above sea level (m asl). The red line indicates the average level (176.44 m asl) across the time period. Image source: Great Lakes Dashboard Project (https://www.glerl.noaa.gov/data/dashboard/GLD_HTML5.html).

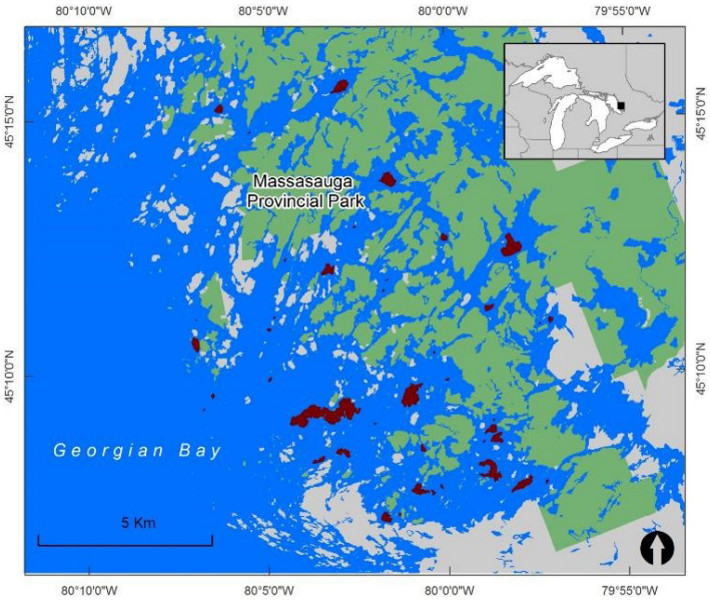

Figure 2. Map of The Massasauga Provincial Park, Ontario, Canada. The park (green and red) consists of mainland and approximately 200 islands. Red islands are park islands sampled during 2001 (n = 34), 2006 (n = 19), 2011 (n = 17), and 2016 (n = 16), for a total of 45 islands.

years of previously collected field data (2001, 2006, 2011, and 2016) and two additional years of solely remotely sensed data (the 2013 low-water year and 2018, which was the highest water level imagery we could obtain). Average annual lake levels for the study periods were 175.95 m asl (above sea level) in 2001, 176.02 m asl in 2006, 176.04 m asl in 2011, 175.90 m asl in 2013, 176.70 m asl in 2016, 176.87 m asl in 2018, and 177.31 m asl in 2020. Field data included plant species richness, shoreline Global Positioning System (GPS) waypoints, and soils data. Imagery included orthophotos (West Parry Sound Geographic Network) and WorldView-2 (Digital Globe) satellite imagery. Imagery and field data were obtained during the July of their respective year. Together, we created an island shoreline database consisting of island shoreline polygons for each year in the study period (Figure 3). We created the shoreline polygons in ArcGIS Pro v2.8 (Esri) by referencing the GPS waypoints and the aerial/satellite imagery. Individual student projects revolved around issues of global environmental change at a local level.

Relationships between island area and water levels

Veronica Seixas (Hamilton College)

Island area is an important predictor of plant species

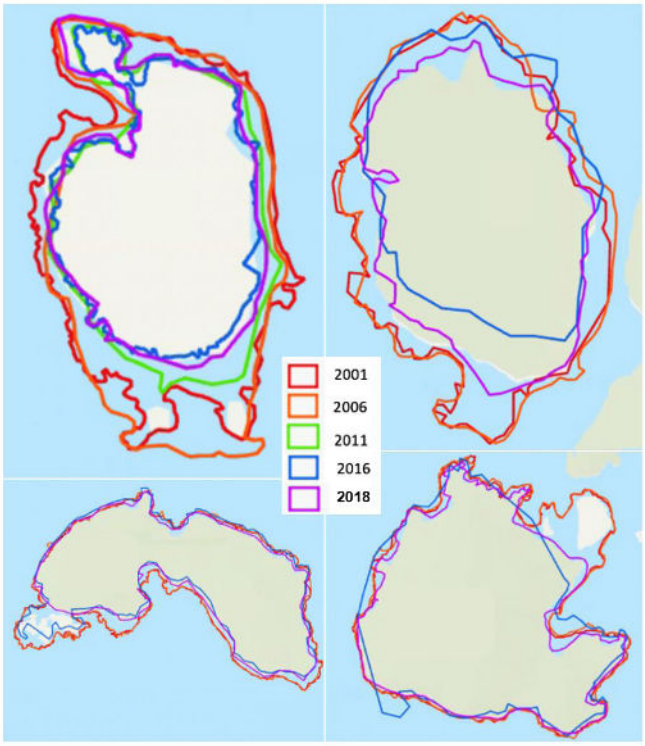

Figure 3. Visual depiction of the island shoreline database for five years and four islands in the database. Note: Islands are depicted at different scales.

richness (MacArthur & Wilson, 1967). Fluctuating water levels alter the morphology and area of the islands. Veronica performed t-tests, ANOVA tests, and correlations to analyze statistical relationships between island shape and water level. The percent change in island area was moderately correlated ($r = 0.608$, $p < 0.0001$) with the percent change in water level. A significant difference in island area existed between most of the years, thus indicating that island area does change with water level changes. The results have implications for island biogeography theory, which postulates that island area is a major influence on species occurrence on islands. Islands that decrease in size with high water levels should correlate with less plant species presence. A particular group of plant species, the Atlantic Coastal Plain disjunct species, appear on sandy shores in the region only during low water years and survive as underwater buried seed banks during high water years (Reznicek, 1994). More of these regionally rare species are expected on islands with emerging sandy shorelines. Future research should include additional years of imagery as well as additional islands from other archipelagoes in the lake.

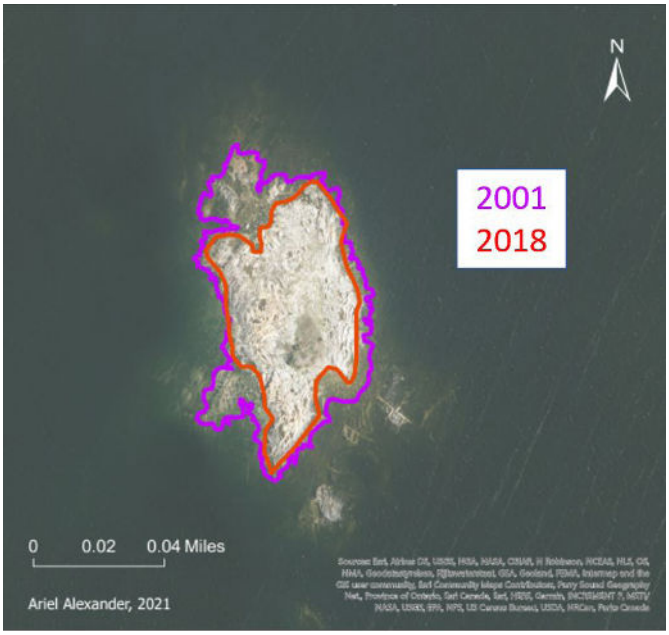

Figure 4. Shorelines for Matches Island in 2001 (purple) and 2018 (red). Results indicate that lower water levels correspond to irregular shoreline shapes and greater diversity of plant species.

Relationships between island shape, soil depth, non-native plant species, and water levels

Ariel Alexander (Carleton College)

Ariel's project had three aims: (1) to determine if island shape and soil characteristics fluctuate based on the water year; (2) to determine if native and non-native plant species richness varies in response to changing island shape and soil depth for the islands of interest; and (3) to determine if certain non-native plant species are recurring due to outcompetition of native species. Island shape was calculated as a function of island perimeter to the perimeter of a circle with area equal to the island. Shoreline shapes did change depending on the water year: shapes were more irregular in low water years than in high water years (Figure 4). Native and non-native plant species were located on islands with a more irregular shoreline. Irregular shorelines might better capture water dispersing plants such as the non-native mossy stonecrop (Sedum acre L.). Soil depth was positively correlated to native plant species richness. With soil depth serving as a proxy for habitat diversity, the results show that islands with deeper soils allow for the presence of both shallow- and deep-rooting plants. The results of the study have implications for park management, especially as related to non-native plant species presence along island shorelines with fluctuating water levels.

Relationships between island elevation, non-native plant species, and water levels

Ryann Busillo (Wesleyan University)

Monitoring the role of fluctuating conditions such as water levels on non-native species is important not only for understanding the complex ecology of the region but also to assist park authorities in managing native plant populations. Ryann used island morphology data (e.g., area, perimeter, maximum elevation) in conjunction with species presence/absence data from the four field years to analyze spatiotemporal trends in non-native plant species over the twenty-year study period. Four non-native plant species not encountered in 2001 were present in 2006. A handful of non-native plant species previously undocumented in the park were encountered in 2011. The non-native plant sheep sorrel (Rumex acetosella L.) was less abundant in 2016 than during previous field seasons. Mossy stonecrop continues to be a prevalent non-native invader of newly emerged bedrock habitats. Species-perimeter, species-area, and species-elevation relationships were not statistically significant for the 2011 field year. Species-perimeter relationships were statistically significant ($p < 0.01$) for the three other field years, with little difference between the strength of correlations for native and non-native plant species for the 2001 and 2006 field years. However, for field year 2016, relationships for native plant species ($r = 0.853$) were considerably stronger than for non-native plant species ($r = 0.674$). Species-area relationships showed a similar pattern to species-perimeter relationships, with the exception of a non-significant correlation for non-native species in 2016. For species-elevation relationships, there was a considerable difference between native ($r = 0.827$) and non-native plant species ($r = 0.687$) during the 2006 field year. The results suggest that non-native plant species might respond differently to water level changes than native plant species. However, further investigation is necessary.

Relationships between shoreline character and water levels

Adalia Rodriguez (Bryn Mawr College)

Shorelines in The Massasauga are varied (e.g., steep cliff, sandy beach, cobble shore) and therefore affect the colonization and persistence ability of plants differently. Adalia used the island shoreline database to quantify the shoreline character and identify any shoreline sections that changed significantly with differing water levels. Of the islands surveyed during field excursions, ten islands were sampled each year. These ten islands were used to compare changes in shorelines. Generally, visual analysis of the shorelines indicated that shoreline change is occurring. For example, qualitative evaluation showed more marshy shorelines in higher water level years than low water level years. However, the results of the statistical analyses were insignificant. This suggests that a combination of higher resolution imagery and more precise measures of shoreline change are necessary to sufficiently examine the degree of shoreline change and any relationship of those changes with fluctuating water levels.

IMPLICATIONS OF THE WORK

A longitudinal study pairing field data with water level data to understand species richness patterns is a novel, but necessary, approach to island biogeography. Analyzing data in The Massasauga over time may elucidate clearer distribution patterns and predictive models of plant species in the park than the ecological snapshot typically derived from island biogeographical research. Results indicate that island areas change significantly with varied water levels and that species richness changes in concert with changes in area, thus it is imperative for island biogeographers to consider water levels and island areas in relation to the timing of fieldwork. Furthermore, studying the island biogeography of this archipelago over an extended time frame will allow for a better scientific understanding of ecological resilience in a system with unstable water levels. Examination of the dynamic terrestrial-aquatic interface in the Great Lakes is pertinent to many of the conservation policy issues in the region today.

ACKNOWLEDGEMENTS

This material is based upon work supported by the Keck Geology Consortium and the National Science Foundation under Grant No. 2050697. I am grateful to the students' host institutions for providing computing for the students during their Keck experience and to the West Parry Sound Geographic Network for providing aerial imagery of the study area. Thank you to Jenna Otaola, our project's peer mentor, for her leadership and assistance during the summer. Her work was funded by the Wesleyan University Grants in Support of Scholarship program. Thanks also to former student researchers for contributing data for the project.

REFERENCES

MacArthur, R.H. & E.O. Wilson. 1967. The Theory of Island Biogeography. Monographs in Population Biology. No. 1. Princeton: Princeton University Press.

Reznicek, A.A. 1994. The disjunct coastal plain flora in the Great Lakes region. Biological Conservation 68:203-215.

Vigmostad, K.E, editor. 1999. State of the Great Lakes Islands. Paper read at US-Canada Great Lakes Islands Workshop, 1996, at Roscommon, Michigan.

KECK Geology Consortium
Learning Science Through Research
Published by the Keck Geology Consortium
Short Contributions
Keck Geology Consortium
Volume 34
May 2022
doi: 10.18277/AKRSG.2022.34.06

ASSESSING GROUND AND SURFACE WATER QUALITY AT REDOX INTERFACES ACROSS THE SHENANDOAH VALLEY, VIRGINIA

MARGARET A. G. HINKLE, Washington & Lee University
EVA LYON, Washington & Lee University

INTRODUCTION

Emerging Groundwater Quality Issues

In the past decade, an ever increasing number of studies have found that Mn(II) in drinking water is a human health concern with wide ranging negative effects on IQ, infant mortality, and cancer rates, to name a few (Bjørklund et al., 2017; Bouchard et al., 2007, 2011; Hafeman et al., 2007; Khan et al., 2012; Langley et al., 2015; Sanders et al., 2014; Spangler and Spangler, 2009; Spangler and Reid, 2010; Williams et al., 2012). A recent study investigating Mn contamination in groundwater wells across the United States determined ~8% of groundwater wells in Virginia (out of 872 analyzed) have Mn concentrations ≥300 ppb (McMahon et al., 2018b, 2018a), the lifetime chronic exposure health advisory limit for Mn set by the Environmental Protection Agency (U.S. Environmental Protection Agency, 2004). It has been argued that this health advisory limit is set too high (Ljung and Vahter, 2007), with just ≥100 ppb Mn in drinking water leading to some health and developmental effects (Langley et al., 2015; Sanders et al., 2014). Approximately 21% of groundwater wells in Virginia analyzed by McMahon et al. (2018a, b) have Mn concentrations exceeding that threshold. With a majority of the population in the Shenandoah Valley relying on groundwater for their water supply (Virginia Department of Environmental Quality, 2015), Mn may negatively impact the health of tens of thousands of Virginians.

Mn contaminated groundwater wells have previously been identified in several locations throughout VA, including the upper portion of the Shenandoah Valley, VA. Potential sources of Mn and trace metal contamination in VA groundwater include: dissolution of the aquifer, soil-water or sediment-water interactions, Mn mobilization via desorption from mineral surfaces in the soil-water interface. Recent research on Mn contamination in the Roanoke River watershed points to mobilization of Mn associated with carbonate-rich rocks (Kiracofe et al., 2017). Two other recent studies investigating Mn groundwater contamination, one in the Piedmont region of North Carolina (Gillispie et al., 2016) and one surveying the entire United States (McMahon et al., 2018a) both found that soil geochemistry is strongly linked to Mn concentrations in groundwater. In order to predict the likelihood of Mn (or other trace metal) contamination in any drinking water source, identifying the major controls on their concentrations is critical.

Historical & Potential Future Impacts of Mill Pond Dams on Surface Water Quality

Increased aqueous Fe and Mn concentrations (and associated trace metals) in surface water is also linked with the stratification of impounded waters behind dams (Hess et al., 1989; Gordon, 1989; Dortch and Hamlin-Tillman, 1995; Ashby et al., 1999; Munger et al., 2017), negatively impacting surface water quality and surrounding ecosystems. In addition to these geochemical effects, another major consequence of dams includes reservoir infilling with sediments. These legacy sediments are stored behind dams that were constructed in the eastern United States from the earliest days of European settlement until the early 1900s (Walter and Merritts, 2008). Legacy sediments can potentially record evidence of land use changes, such as industrial and agricultural activities.

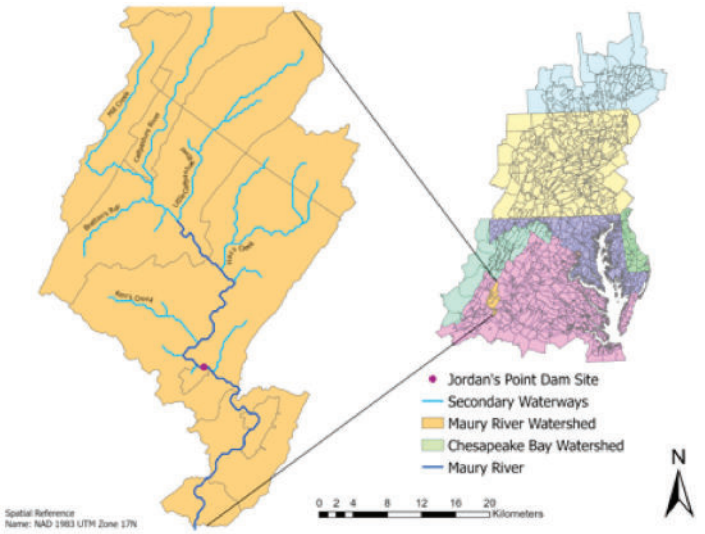

Figure 1. Map of Maury River watershed within the Chesapeake Bay Watershed. Includes the location of Jordan's Point dam in Lexington, VA, a recently removed milldam, and one of several sites sampled for legacy sediments in Rockbridge County. Map by Katie Larkin for her thesis.

The Shenandoah Valley is home to many historical low head dams, primarily used for mills, iron forges, and other hydropower applications. Many of these dams have been breached over the years for a host of reasons.

When these dams are breached, streams can remobilize these legacy sediments, and any potential contaminants that accumulated with them (e.g., Walter and Merritts, 2008; Niemetz et al., 2013), negatively impacting downstream ecosystems via either geochemical contaminants or increased total suspended solids (TSS). We aim to characterize some of these legacy sediments at dams along the Maury River in Rockbridge County, Virginia (Fig. 1) to better assess their potential for erosion into and contamination of the waterway, and downstream water bodies like the Chesapeake Bay (e.g., Hupp et al., 2013; Niemetz et al., 2013). For example, sediment pollution negatively affects the benthic community through several ways, including low dissolved oxygen, sediment contamination, and nutrient loading (Dauer et al., 2000). In addition to the issues of sediment pollution, these sediments can also contain adsorbed trace metals like Cu and Pb (Lutgen et al., 2020), especially when associated with fertilizers and pesticides (Cu) or emissions due to combustion of leaded gasoline (Niemetz et al., 2013). By measuring such trace metals we can assess their potential contribution to the Maury River watershed.

Other geochemical indicators of interest include carbon and nitrogen and their stable isotopes, which we can use to discern land use changes. For example, the ratio of organic carbon to nitrogen in sediment is indicative of organic matter source, with higher values associated with terrestrial vegetation. We can thus use this ratio as an indicator of deforestation in the watershed. By measuring sediment and surface water trace metals, organic carbon content, and stable carbon isotopes, we aim to establish the history of post-colonial fluvial sedimentation in the Maury River watershed. Further, we can assess changes in channel geometry following the removal of dams to determine the potential for sediment pollution from legacy sediments.

Broadly Characterizing Water Geochemistry Across the Shenandoah Valley

With this research, we investigated the role of land use patterns, soil geochemistry, aquifer types, and dams on ground and surface water quality in the Shenandoah Valley region of Virginia. This region was selected because of the high concentrations of Mn in several wells in these areas (McMahon et al. 2018a), variable land use practices throughout the region, and presence of several historical mill pond dams. This work seeks to better understand the controls of Mn and other trace metals in redox active sites such as springs (in which sub/anoxic groundwater meets the oxygenated surface) and impounded waters (in which stratification can occur with depth), as Mn mobility is linked to its redox behavior.

METHODS

With this research we collected and analyzed spring waters to add to the already established well water databases [via the USGS National Water Information System (NWIS) and the Virginia Household Water Quality Program (VAHWQP; www.wellwater.bse.vt.edu)] (Fig. 2), as well as nearby surface waters and soil cores, and investigated the geochemistry and fluvial sedimentology of historical dams. Water samples were analyzed using field probes for in situ pH, dissolved oxygen (DO), temperature, and specific conductivity measurements, and samples were collected for further analysis of cation and anion

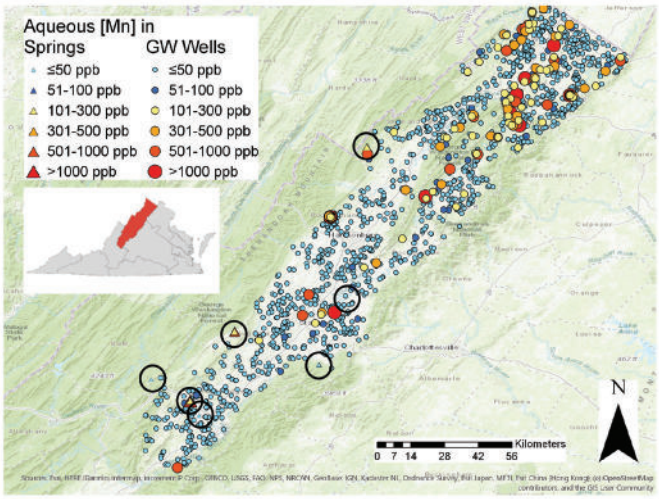

Figure 2. Map of aqueous Mn concentrations in springs (triangles) and groundwater wells (circles) in the Shenandoah Valley, VA, with increasing concentrations increasing the relative size of each data point based on demarcations from ≤50 ppb (light blue) to 51-100 ppb (dark blue) to 101-300 ppb (yellow; above which low level chronic exposure to Mn via drinking water may result in health effects), 301-500 ppb (orange), 501-1000 ppb (light red), to >1000 ppb (dark red). Field sites for springs and seeps are denoted with black circles.

concentrations by ion chromatography (IC) and major elements and trace metal concentrations by inductively coupled plasma-mass spectrometry. Soil samples were analyzed for total element concentrations by X-ray fluorescence and Mn speciation by Mn K-edge X-ray absorption near edge structure (XANES) spectroscopy.

Sediment samples were collected from banks behind breached dams at intervals of 5-10 cm. Samples were then dried and crushed before further analysis. Portable X-Ray Fluorescence (pXRF) measurements were taken to characterize heavy metal concentrations. Elemental abundances of C and N were measured on a Costech ECS 4010 elemental analyzer coupled to a Thermo Electron Delta Plus stable isotope ratio mass spectrometer. A Mastersizer 3000 was used to determine grain size distribution of sediments through time.

To characterize sediment mobilization potential, channel geometry was measured at the site of a recently removed dam site using a TopCon GTS-301 Total Station. Channel armor was measured for grain size using the Wolman pebble count method and a gravelometer.

Figure 3. Photo of the Keck 2022 Advanced team at Natural Bridge, VA. Left to right: Mia Groff, Haley Culbertson, Ani Croy, Maddie Holicky, Kallan Wilde, Margaret Anne Hinkle, Katie Larkin, Noah Willis, Martina Pulido, and Christopher Goldmann (absent: Eva Lyon).

RESEARCH

Our research team included nine students (eight supported by Keck) and two faculty members from five institutions (Fig. 3). We visited 31 sites, of which 24 were springs, seeps, or subsurface environments and seven were dams within the Shenandoah Valley. While all contributed to field work, sample collection, and laboratory analyses, each student took charge of a different component of the project, as follows:

Spring and Groundwater Geochemistry

Ani Croy (Washington and Lee University) examined the geochemistry of water samples collected at 24 springs and seeps visited by the Keck students. Combining the data from field probes with ion chromatography and ICP-MS data, Ani assessed correlations between aqueous Mn concentrations and other ions in solution, pH, DO, depth, most likely aquifer rock type, and more. While the data set taken as a whole indicates that few correlations

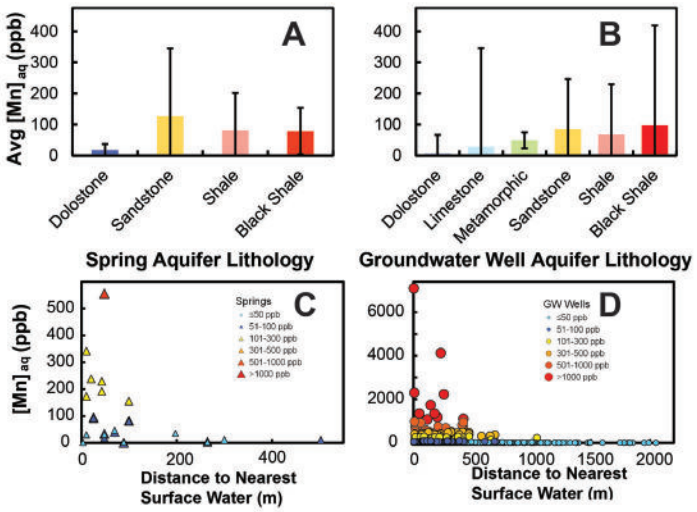

Figure 4. Aqueous Mn in groundwater wells (A,C) and springs (B,D) for average Mn in aquifers with different primary rock types (A,B) and actual aqueous Mn concentrations as a function of distance to nearest surface water bodies (C,D).

exist, when separated out by primary rock aquifer types (sandstone, black shale, and carbonate rocks, the three dominant aquifer types for our field sites), with carbonate aquifers exhibiting relatively low aqueous Mn concentrations, well below thresholds of concern for even low level chronic Mn exposure (Fig. 4A). Conversely, shale, black shale, and sandstone aquifers exhibit much higher average aqueous Mn concentrations (Fig. 4A). Meanwhile, distance to the nearest surface water appears to be correlated with Mn in springs and seeps, with those furthest away from surface water bodies exhibiting the lowest Mn concentrations (Fig. 4B). These results indicate that aquifer lithology serves an important control on spring water geochemistry, and that black shales and sandstones behave very differently than carbonate bearing aquifers.

Chris Goldmann (Trinity University) focused on the aqueous geochemistry and spatial distributions of >1,900 groundwater wells across the Shenandoah Valley, combining data from the VAHWQP and the USGS NWIS database. Mapping the data in ArcGIS, alongside aquifer type, surface lithology, relict Mn ore mines, orchards, surface water maps, and geologic features like faults, dikes, and sills, allowed Chris to determine if correlations exist between such aspects and elevated Mn in groundwater. Chris found that elevated Mn in groundwater in the Shenandoah Valley is most likely geogenic in origin rather than from anthropogenic activities. Chris identified aquifer lithology (Fig. 4B) and distance to surface waters (Fig. 4D) as well as the overall groundwater redox state (determined via principal component analysis) as exerting the strongest controls on Mn concentrations in groundwater wells, consistent with Ani's findings for our field spring and seep sites. Aquifer lithology shows a distinct distribution, indicating that aquifers in karst terrain are more oxic and therefore less likely to have elevated Mn, while those in shales and sandstones are more reducing and therefore at higher risk of elevated Mn.

Noah Willis (Whitman College) researched the interplay between aqueous Mn in our spring and seep water samples and soils by analyzing soils with X-ray fluorescence to determine if there is a correlation between elevated Mn in soils and elevated Mn in the springs and seeps. Noah, like Chris and Ani investigating the geochemistry of waters, identified distinct trends in soil geochemical makeup based on aquifer lithology, with Fe and Mn most correlated in soils from shale and sandstone parent rocks. Soils in regions with sandstone surface lithology were found to have the highest Mn soil content, while those in black shale and carbonate lithologies have similar average Mn soil concentrations (1200 and 1900 ppm Mn, respectively).

Haley Culbertson (Washington and Lee University) investigated soil Mn redox states, general soil properties, and how they relate to aqueous Mn concentrations in our spring and seep field sites. Haley analyzed samples first with SEM-EDS to identify samples of particular interest, and then prepared those select samples for Mn K-edge XANES spectroscopic analyses and analyzed the data by performing linear combination fits on our sample spectra using a suite of Mn oxidation state standards. Haley found soils containing higher Mn(IV) fractions are closest to springs and seeps with low aqueous Mn (and also tend to have higher soil pH), while soils with higher Mn(II) fractions are near springs and seeps with elevated aqueous Mn (and tend to have more acidic soil pH). Haley's work suggests that while lithology does by and large control aqueous Mn concentrations in groundwater and springs, that soils and waters are intimately connected with one another.

Surface Water Impacts by Mill Dams

Martina Pulido (Beloit) measured and analyzed water properties and aqueous geochemistry behind both active and removed dams. She found that waters behind active dams are stratified, fostering low-oxygen conditions in which Mn2+ can accumulate at levels exceeding EPA standards. This finding is concerning, as at least one of these sites is upstream of drinking water intake for Lexington, VA.

Kallan Wilde (St. Norbert College) utilized land use data like historic maps, census data, and aerial photography to identify potential sources of pollution in the Maury River watershed. This involved creating GIS maps corresponding to different periods of time and their associated pollution sources. For example, in a map representing all identified sources prior to 1860, dozens of sources, including mines, forges, mills, and farms, were identified. These maps may be particularly useful in interpreting sedimentological data through time.

Mia Groff (Whitman College) and **Maddie Holicky** (Beloit College) studied the legacy sediment package that accumulated behind dams on the Maury River. Maddie analyzed organic carbon and nitrogen values, and measured heavy metal concentrations to track land use changes through time. She noted three general phases of land use that can be interpreted in the context of activities like deforestation, mining, and metal forging (Fig. 5). Mia measured sediment grain sizes and compared measurements to heavy metal concentrations, noting a negative relationship between Mn and Fe concentrations and grain size. This relationship suggests that these metals are more likely to adsorb onto finer grain sizes like clay.

Katie Larkin (Washington and Lee University) studied the changes in channel morphology following the removal of a low head dam on the Maury River in 2019 (Fig. 1). Katie repeated several channel cross section measurements at areas that were flagged as susceptible to bank erosion following an initial study in 2019. Results show that the channel upstream of the dam has deepened, and nearly 4000 m3 of sediment has been removed in the surveyed reach. These findings support the importance of tracking channel response to dam removal, especially considering the elevated concentrations of heavy metals in some legacy sediment horizons.

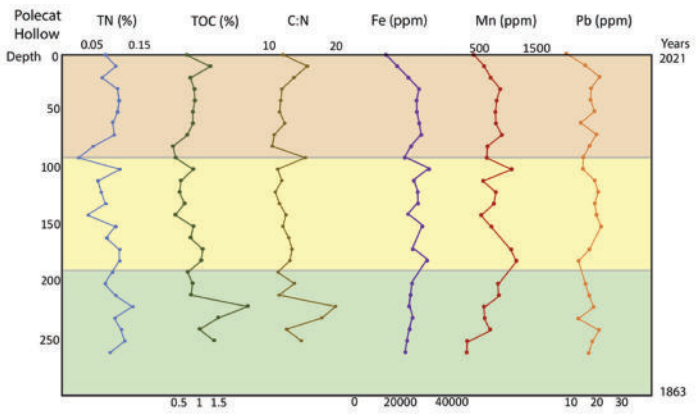

Figure 5. Chemostratigraphic profile for one of the legacy sediment sites (Polecat Hollow). Horizontal color bands represent different phases of land use in the region: Widespread deforestation and mining in the post-colonial era (green), Declining mining and shift to agriculture (yellow) and recent changes, including further reduction in mining activities (orange). Plot by Maddie Holicky for her thesis.

ACKNOWLEDGEMENTS

This material is based upon work supported by the Keck Geology Consortium and the National Science Foundation under Grant No. 2050697. For help with lab analyses we appreciate the support of Emily Falls, Jeffrey Parks, Sarah Teagle, and Angie Gallegos. For assistance with accessing the VAHWQP database (www.wellwater.bse.vt.edu), thank you to Erin Ling, Asa Spiller, and Maddy Schreiber. XANES spectra were collected at beamline 12-BM at the Advanced Photon Source, a U.S. Department of Energy (DOE) Office of Science user facility operated for the DOE Office of Science by Argonne National Laboratory under Contract No. DE-AC02-06CH11357. We particularly thank Benjamin Reinhart for collecting the XANES spectra for this research, particularly considering that COVID-19 required these samples be collected with remote user access. A special thanks to Sarah Wilson for help with logistics and travel. Field work was conducted within the traditional territory of the Yesa People (with descendants including the Monacans) & of the Manahoac People, the indigenous stewards of this land.

REFERENCES

Ashby, S. L., Myers, J. L., Laney, E., Honnell, D., & Owens, C. 1999. The effects of hydropower releases from Lake Texoma on downstream water quality. Journal of Freshwater Ecology, 14, 103–112.

Bjørklund, G., Chartrand, M.S., Aaseth, J., 2017. Manganese exposure and neurotoxic effects in children. Environmental Research 155, 380–384. https://doi.org/10.1016/j.envres.2017.03.003

Bouchard, M., Laforest, F., Vandelac, L., Bellinger, D., Mergler, D., 2007. Hair Manganese and Hyperactive Behaviors: Pilot Study of School-Age Children Exposed through Tap Water. Environmental Health Perspectives 115, 122–127. https://doi.org/10.1289/ehp.9504

Bouchard, M.F., Sauvé, S., Barbeau, B., Legrand, M., Brodeur, M.-È., Bouffard, T., Limoges, E., Bellinger, D.C., Mergler, D., 2011. Intellectual Impairment in School-Age Children Exposed to Manganese from Drinking Water. Environmental Health Perspectives 119, 138–143. https://doi.org/10.1289/ehp.1002321

Dauer, D. M., Ranasinghe, J. A., & Weisberg, S. B. 2000. Relationships between benthic community condition, water quality, sediment quality, nutrient loads, and land use patterns in Chesapeake Bay. Estuaries, 23, 80-96. https://doi.org/10.2307/1353227

Dortch, M. S., & Hamlin-Tillman, D. E. 1995. Disappearance of reduced manganese in reservoir tailwaters. Journal of Environmental Engineering, 121, 287–297.

Gillispie, E.C., Austin, R.E., Rivera, N.A., Bolich, R., Duckworth, O.W., Bradley, P., Amoozegar, A., Hesterberg, D., Polizzotto, M.L., 2016. Soil Weathering as an Engine for Manganese Contamination of Well Water. Environmental Science & Technology 50, 9963–9971. https://doi.org/10.1021/acs.est.6b01686

Gordon, J. A. 1989. Manganese oxidation related to the releases from reservoirs. Journal of the American Water Resources Association, 25, 187–192.

Hafeman, D., Factor-Litvak, P., Cheng, Z., van Geen, A., Ahsan, H., 2007. Association between Manganese Exposure through Drinking Water and Infant Mortality in Bangladesh. Environmental Health Perspectives 115, 1107–1112. https://doi.org/10.1289/ehp.10051

Hess, G. W., Kim, B. R., & Roberts, P. J. W. (1989). A manganese oxidation model for rivers. Journal of the American Water Resources Association, 25, 359–365. doi:10.1111/j.1752-1688.1989.tb03072.x

Hue, N.V., Vega, S., Silva, J.A., 2001. Manganese Toxicity in a Hawaiian Oxisol Affected by Soil pH and Organic Amendments. Soil Sci. Soc. Am. J. 65, 153–160. https://doi.org/10.2136/sssaj2001.651153x

Hupp, Cliff R., Noe, G. B., Schenk, E. R., & Benthem, A. J. 2013. Recent and historic sediment dynamics along Difficult Run, a suburban Virginia Piedmont stream. Geomorphology, 180–181, 156–169. https://doi.org/10.1016/j.geomorph.2012.10.00

Khan, K., Wasserman, G.A., Liu, X., Ahmed, E., Parvez, F., Slavkovich, V., Levy, D., Mey, J., van Geen, A., Graziano, J.H., Factor-Litvak, P., 2012. Manganese exposure from drinking water and children's academic achievement. NeuroToxicology 33, 91–97. https://doi.org/10.1016/j.neuro.2011.12.002

Kiracofe, Z.A., Henika, W.S., Schreiber, M.E., 2017. Assessing the Geological Sources of Manganese in the Roanoke River Watershed, Virginia. Environmental Engineering Science 23, 43–64.

Langley, R., Kao, Y., Mort, S., Bateman, A., Simpson, B., Reich, B., 2015. Adverse neurodevelopmental effects and hearing loss in children associated with manganese in well water, North Carolina, USA. J Environ Occup Sci 4, 62. https://doi.org/10.5455/jeos.20150403060427

Li, M.S., Luo, Y.P., Su, Z.Y., 2007. Heavy metal concentrations in soils and plant accumulation in a restored manganese mineland in Guangxi, South China. Environmental Pollution 147, 168–175. https://doi.org/10.1016/j.envpol.2006.08.006

Ljung, K., Vahter, M., 2007. Time to Re-evaluate the Guideline Value for Manganese in Drinking Water? Environmental Health Perspectives 115, 1533–1538. https://doi.org/10.1289/ehp.10316

Lutgen, A., Jiang, G., Sienkiewicz, N., Mattern, K., Kan, J., & Inamdar, S. 2020. Nutrients and Heavy Metals in Legacy Sediments: Concentrations,

Comparisons with Upland Soils, and Implications for Water Quality. Journal of the American Water Resources Association. 56, 669-691.

McMahon, P.B., Belitz, K., Reddy, J.E., Johnson, T.D., 2018a. Elevated Manganese Concentrations in United States Groundwater, Role of Land Surface–Soil–Aquifer Connections. Environmental Science & Technology 53, 29–38.

McMahon, P.B., Reddy, J.E., Johnson, T.D., 2018b. Data for Elevated Manganese Concentrations in United States Groundwater, Role of Land Surface-Soil-Aquifer Connections. U.S. Geological Survey Data Release. https://doi.org/10.5066/P9Y4GOFQ

Munger, Z. W., Shahady, T. D., Schreiber M.E. 2017. Effects of reservoir stratification and watershed hydrology on manganese and iron in a dam-regulated river. Hydrological Processes, 31, 1622-1635.

Niemitz, J., Haynes, C., & Lasher, G., 2013. Legacy sediments and historic land use: Chemostratigraphic evidence for excess nutrient and heavy metal sources and remobilization. Geology, 41, 47-50. https://doi.org/10.1130/G33547.1

Sanders, A.P., Desrosiers, T.A., Warren, J.L., Herring, A.H., Enright, D., Olshan, A.F., Meyer, R.E., Fry, R.C., 2014. Association between arsenic, cadmium, manganese, and lead levels in private wells and birth defects prevalence in North Carolina: a semi-ecologic study. BMC Public Health 14, 955. https://doi.org/10.1186/1471-2458-14-955

Semu, E., Singh, B.R., 1995. Accumulation of heavy metals in soils and plants after long-term use of fertilizers and fungicides in Tanzania. Fertilizer research 44, 241–248. https://doi.org/10.1007/BF00750931

Spangler, A.H., Spangler, J.G., 2009. Groundwater Manganese and Infant Mortality Rate by County in North Carolina: An Ecological Analysis. EcoHealth 6, 596–600. https://doi.org/10.1007/s10393-010-0291-4

Spangler, J.G., Reid, J.C., 2010. Environmental Manganese and Cancer Mortality Rates by County in North Carolina: An Ecological Study. Biol Trace Elem Res 133, 128–135. https://doi.org/10.1007/s12011-009-8415-9

U.S. Environmental Protection Agency, 2004. Drinking Water Health Advisory for Manganese. Virginia Department of Environmental Quality, 2015. Commonwealth of Virginia State Water Resources Plan.

Walter, R. C., & Merritts, D. J. 2008. Natural streams and the legacy of water-powered mills. Science, 319, 299-304.

Williams, M., Todd, G.D., Roney, N., Crawford, J., Coles, C., McClure, P.R., Garey, J.D., Zaccaria, K., Citra, M., 2012. Toxicological Profile for Manganese.

KECK Geology Consortium
Learning Science Through Research
Published by the Keck Geology Consortium
Short Contributions
Keck Geology Consortium
Volume 34
May 2022
doi: 10.18277/AKRSG.2022.34.07

ANALYZING THE RELATIONSHIPS BETWEEN AQUEOUS MANGANESE AND GEOLOGICAL FACTORS IN GROUNDWATER IN THE SHENANDOAH

MARINA CROY, Washington & Lee University
Project Advisor: Margaret A. G. Hinkle

INTRODUCTION

The human health effects of chronic low exposure to Mn greater than 120 ppb have been well documented in recent years (Bouchard et al., 2007; Bouchard et al., 2011). Increased developmental issues in children and infants are correlated with long-term exposure to Mn in areas where Mn was found to be over the EPA limit of 300 ppb (Langley et al., 2015; U.S. EPA, 2004). Numerous other studies have found that chronic exposure to Mn above even the relatively low limit of 100 ppb can be strongly linked to negative health effects, especially in infants and developing children (Bouchard et al., 2011; Bjørklund et al., 2017; Hafeman et al., 2007, Khan et al., 2012; Sanders et al., 2014; Spangler and Spangler, 2009; Spangler and Reid, 2010). The valence state - the ability of the ions of an element to accept or give electrons - largely determines whether Mn will be in the aqueous or solid phase. A lower valence state (found in more anoxic conditions) will result in Mn moving into (or staying in for the case of groundwater) the aqueous phase. A higher valence state will result in Mn(III)/Mn(IV) precipitating out of solution as Mn (oxyhyr)oxides, lowering the concentration of Mn in the aqueous phase. Thus, more reducing systems like groundwater and springs are of particular concern with respect to Mn exposure via low level chronic ingestion of such drinking water sources. Our field work study area consists of four counties across the Shenandoah Valley: Rockbridge, Augusta, Bath and Shenandoah, whereas the analysis for all groundwater wells spanned the entirety of the Shenandoah Valley in Virginia.

METHODS

A total of forty-two 250 mL water samples from the seven different sites was collected across the study area (Fig. 1). Both filtered (0.2 μm) and unfiltered water samples were collected at each site. When applicable, rocks that were characteristic of the site were also collected so that they may be analyzed for metal precipitates. Filtered samples collected in the field were stored in polypropylene centrifuge test tubes, while unfiltered samples were stored in 250-mL polypropylene bottles sealed with parafilm to preserve their contents, and stored in laboratory refrigerators (at 4°C). Upon returning to the lab, coordinates measured in the field were used to determine the underlying geology of the site, which was correlated

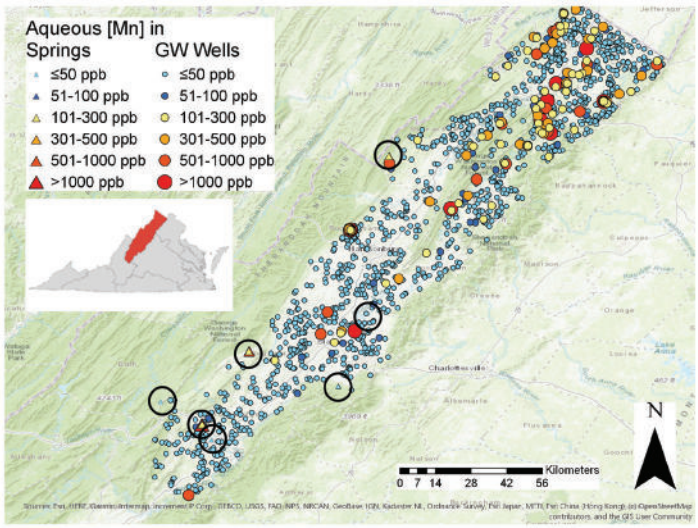

Figure 1. Map of aqueous Mn concentrations in springs (triangles) and groundwater wells (circles) in the Shenandoah Valley, VA, with increasing concentrations increasing the relative size of each data point based on demarcations from ≤50 ppb (light blue) to 51-100 ppb (dark blue) to 101-300 ppb (yellow; above which low level chronic exposure to Mn via drinking water may result in health effects), 301-500 ppb (orange), 501-1000 ppb (light red), to >1000 ppb (dark red). Field sites for springs and seeps are denoted with black circles.

with rock types present at the site. Filtered water samples were diluted by either 1:5 or 1:2 with Milli Q water for analysis by ion chromatography (IC), which analyzed for major ion concentrations (e.g., Ca^{2+}, NO_3^{2-}, SO_4^{2-}, etc.) through IC. The unfiltered, undiluted samples underwent phenolphthalein titration with a bromocresol green-methyl red titration test for [$CaCO_3$] and [HCO^{3-}]. Separate aliquots of filtered spring water samples were acidified to 2% nitric acid (trace metal grade) for analysis via ICP-MS for major and trace elements (e.g., Mn, S, Cr, Fe, Co, Ni, Zn, As, etc.) and diluted with 2% nitric acid in a 1:2 ratio. ICP-MS was performed by the Department of Civil and Environmental Engineering at Virginia Tech. To supplement this research, data from other sources and projects was included in the dataset. Well data, water quality data, and geological map data was obtained from organizations including United States Geological Survey (USGS) National Water Information System (NWIS) and the Virginia Household Water Quality Program (VAHWQP) (McMahon et al., 2018).

RESULTS

ICP-MS analyses found several sites to have aqueous Mn above the 120 ppb limit. Water geochemical analyses also found that some of the samples have high levels of other contaminants (high being defined as concentrations equal to or above safety levels set by the EPA). The drinking standard limits for elements such as lithium (Li), Al, Fe, Mn, and zinc (Zn), were surpassed for several samples, although many of these are considered secondary drinking standards, and thus are not enforceable (Table 1) (U.S. EPA, 2022a,b; Agency for Toxic Substances and Disease Registry (2005), Lindsey et al., 2021).

Interestingly, elevated aqueous Mn concentrations are consistently observed in sandstone and shale aquifers (Fig. 2). Sandstone lithologies exhibit the highest average aqueous Mn in springs and seeps here studied (Fig. 2), along with the largest standard deviation (1σ), with some sites over 500 ppb Mn. Meanwhile, carbonate aquifers have the lowest average aqueous Mn concentrations, with the average and standard deviation below the 100 ppb threshold for chronic exposure health concerns (Fig. 2). The decrease in aqueous Mn in carbonate aquifers may be due the fact

Table 1: Table featuring the EPA secondary drinking standard limits for elements other than Mn analyzed in ICP-MS, as well as any samples with concentrations above the limits.

SampleID	$[Li]_{aq}$ ppb	$[Al]_{aq}$ ppb	$[Fe]_{aq}$ ppb	$[Mn]_{aq}$ ppb	$[Zn]_{aq}$ ppb
EPA drinking water limit (ppb)	10	200	300	300	5000
Rockbridge Pond Spring-01	--	--	467.5	1,321.6	--
Rockbridge Pond Spring-02	--	--	--	172.7	--
Rockbridge Pond Spring-03	--	--	--	341.5	--
Augusta Country Spring Complex-01aa	--	--	1,011.4	555.0	--
Augusta Country Spring Complex-02	--	--	240.3	238.1	--
Shenandoah County Pump Spring-01	--	--	14,339.5	155.3	34,474.7
Shenandoah County Pump Spring-02	--	--	2,479.0	--	--
Shenandoah County Pump Spring-03	--	201.2	1,827.3	--	--
Orkney Spring	12.8	425.8	6,093.8	--	--
Orkney Spring A	13.4	412.8	5,394.5	--	--
Orkney Spring B	13.0	284.3	3,923.9	--	--
Shenandoah County Meadow Spring-01	77.1	--	28,442.0	228.8	16,735.9
Shenandoah County Meadow Spring-02	78.8	296.9	14,567.9	191.7	--

these are weathered carbonates contributing to the karst terrain in the region, thus exhibiting substantial surface water-groundwater connectivity, therefore are likely more oxic, making Mn more stable as Mn oxide minerals (Fig. 3A). Alternatively, carbonate bearing aquifers could have increased bicarbonate concentrations, thereby stabilizing Mn^{2+} in Mn carbonate minerals such as rhodochrosite (Fig. 3B).

Aqueous Mn concentrations exhibit consistently negative correlations with pH and dissolved oxygen (Fig. 4). However, it should be noted that depending on the lithology these correlations can be quite weak (with relatively low R^2 values), albeit the trends are consistent (Fig. 4). Given the nature of Mn thermodynamic stability as it relates to pH and

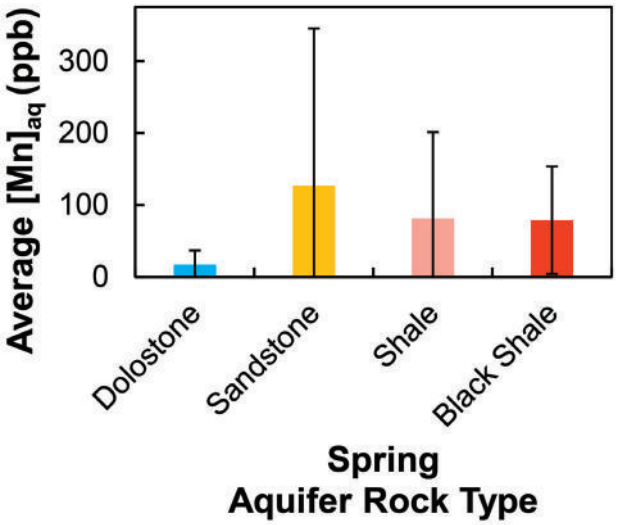

Figure 2. Average [Mn] within each aquifer lithology designated by the primary rock type within the corresponding lithologic unit, with black bars denoting standard deviation of 1σ.

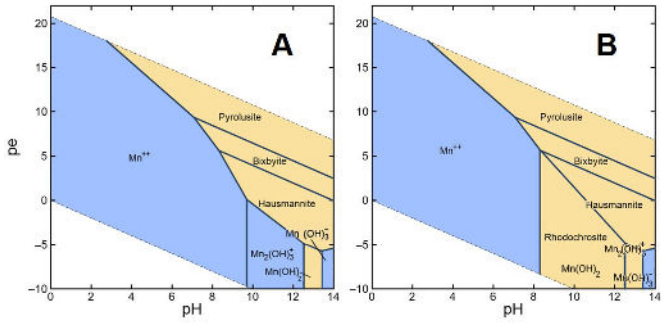

Figure 3. pe/pH diagrams using average [Mn]aq (0.19 ppm) & pH (6.3) of sampled spring sites, with no HCO^{3-} (A) & average $[HCO^{3-}]aq$ from spring sites (56.45 mg/L) (B). Made with Geochemist's Workbench..

reduction potential, with Mn stable as aqueous Mn^{2+} under acidic and reducing conditions (Fig. 3), these negative correlations between Mn and pH and Mn and dissolved oxygen are consistent with its expected behavior. Interestingly, and consistent with the concept that bicarbonate will stabilize Mn in the solid phase in Mn carbonate minerals, all rock types exhibit slightly negative correlations between Mn and alkalinity, although the R^2 values for these are quite low (Fig. 4C).

The lithologic trends continue when examining correlations between aqueous Mn and other trace metals and major elements. Fe, as expected, was found to be strongly positively strongly correlated with Mn in all aquifers, but only when separated out by lithology. The R^2 value for Mn and Fe in sandstone aquifers is 0.93, in black shale aquifers is 0.85, and in carbonate aquifers is 0.42 (Fig. 4F). It should be noted that Fe concentrations in the black shale aquifers are, on average, much higher than Fe concentrations in other aquifers (Fig. 4F). Co also exhibits a similar trend (with R^2 values quite similar to those for Mn and Fe), and thus may demonstrate that aqueous Co concentrations are dependent on Fe, Mn, or some combination thereof (Fig. 4H). In black shale and sandstone aquifers, Mn is positively correlated with S, Co, and Ni (Fig. 4). Mn is negatively correlated with As in black shale aquifers but is positively correlated in sandstone and carbonate aquifers (Fig. 4L).

DISCUSSION

Lithology appears to have a major influence on the geochemistry of springs, due to the effect of sulfur and dissolved organic carbon in redox geochemistry as

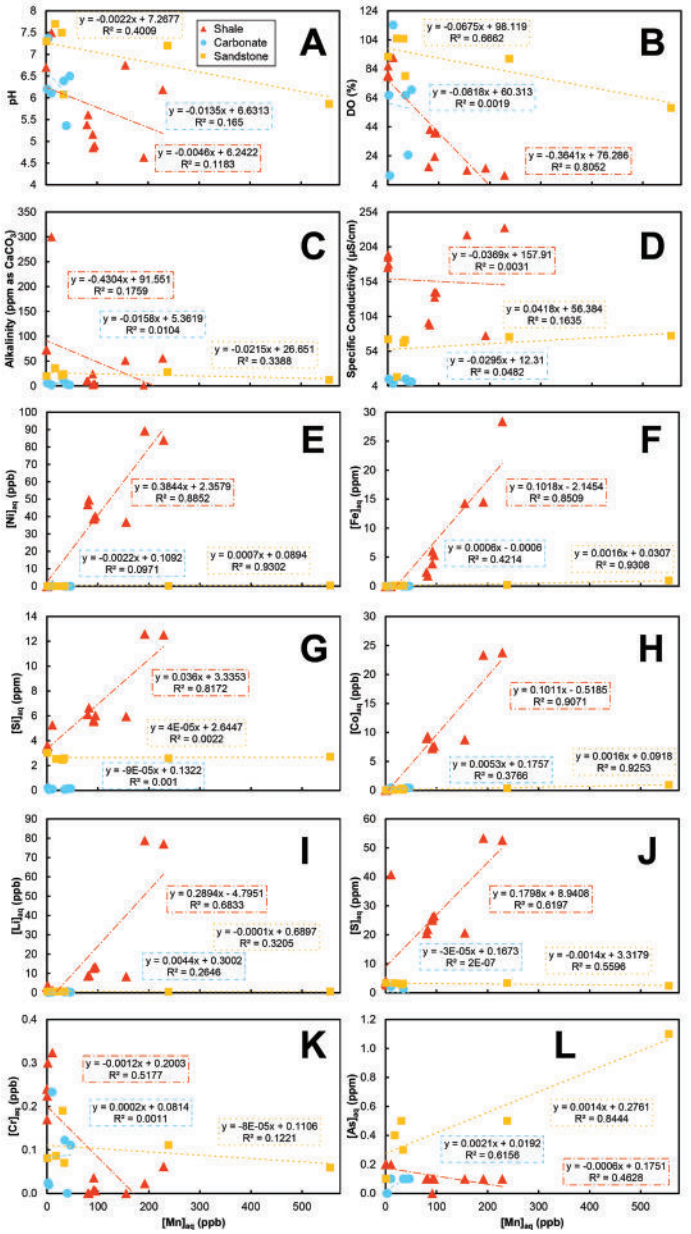

Figure 4. Aqueous [Mn] versus various field parameters: pH (A), dissolved oxygen (B), alkalinity (C), specific conductivity (D), and elements of interest in the aqueous phase: Ni (E), Fe (F), Si (G), Co (H), Li (I), S (J), Cr (K), As (L) separated by aquifer primary rock types with sandstones (orange squares), shales (red triangles), and carbonates (blue circles).

well as the more oxic nature of weathered carbonate aquifers. The presence of sulfides in black shales shifts the reduction potential such that the Mn present in shale aquifers is most stable in a lower valence state (II), which is soluble and results in the Mn staying within the aqueous phase as opposed to entering a higher valence state (III/IV) and precipitating into a solid form, thereby decreasing aqueous Mn(II) concentrations (Fig. 2). In the graph of [S] vs [Mn], the trend of increasing S and increasing Mn in black

shales is an example of this process (Fig. 4). Fe can be used to track the reducing conditions in aquifers, with a suggested threshold of 100 ppb Fe resulting in more anoxic aquifers (Erickson et al., 2019). The black shale aquifers in this study consistently have Fe concentrations above the 100 ppb threshold for anoxic conditions, while carbonate bearing aquifers have much lower Fe concentrations, suggesting that carbonate aquifers are more oxic than black shales in this region. The sulfur-bearing black-shales that create reducing conditions, which cause the Mn to persist in a lower valence state, thus keeping Mn in the aqueous phase, have similar effects on aqueous Fe.

CONCLUSION

Our data indicates that lithology is a major factor affecting groundwater chemistry in the Shenandoah Valley, particularly with regard to the distribution of Mn. The lithology of an aquifer will impact the geochemistry of the water that is stored within it, specifically the redox geochemistry, which will result in a change in the transfer of the electrons and the valence state of elements such as Mn. Thus, it is clear that there is a defined set of cause-and-effects that can be traced in defining where Mn is located (the solid or aqueous phase) where it is likely to move, depending on geochemical and environmental factors. To sum up, aquifer lithology affects the geochemistry within the aquifer, which affects the Mn valence state, which affects the movement of Mn into different phases and forms. Trace metals may bind onto the Mn oxides via sorption processes, resulting in high concentrations of these elements associated with Mn oxides, but may also be released to solution when exposed to reducing conditions with Mn oxide dissolution to aqueous Mn(II). Mn oxides are known as the "scavengers of the sea" due to their highly sorptive properties, as they are able to manipulate the distribution of a range of elements (Tebo et al., 2004). Since Mn(II) is thermodynamically favored in anoxic conditions, and Mn(III)/(IV) are favored in oxic conditions, the state of Mn and presence of Mn oxides can be predicted in groundwater aquifers based on DO. Mn oxides can absorb many different types of ions, and as a result, Mn oxides can control the concentrations of trace metals in natural waters, also allowing the correlation of Mn and elements such as Fe and arsenic (Tebo et al., 2004).

Overall, Mn is an invaluable resource in predicting the mobilization and concentrations of trace elements in groundwater, similar to how Fe can be used to signify reducing or oxidizing conditions. Fe, Si, Ni, Li, S, and Co all have strong positive correlations with Mn, meaning that their concentrations could possibly be predicted in areas where the concentration of Mn is already established. However, due to the close correlation between Fe and Mn, Fe may be as much of a control as Mn on trace metals of interest, and future work may decipher how much each of these two elements plays a role in controlling geochemistry. Future work may also attempt to create a model that can appropriately predict and measure the amount of certain trace metals in an aquifer based on the Mn concentration, or other common water quality measurements such as DO and pH.

ACKNOWLEDGEMENTS

This material is based upon work supported by the Keck Geology Consortium and the National Science Foundation under Grant No. 2050697. I would like to thank Dr. Margaret Hinkle and Dr. Eva Lyon for their guidance on this Keck advanced project. Thanks to Emily Falls, who was integral in teaching me how to use the ion chromatography instrument. Thanks also to the Washington and Lee University Geology Department, as well as fellow seniors Haley Culbertson and Katie Larkin for their assistance in collecting field measurements. This work would not have been possible without funding from the Washington and Lee Geology Department's Edgar W. Spencer Award. Finally, thank you to Virginia Tech Department of Civil and Environmental Engineering for the use of their inductively coupled plasma-mass spectrometry instrument.

REFERENCES

Agency for Toxic Substances and Disease Registry (2005). Public Health Statement: Zinc. CAS#: 7440-66-6.

Bjørklund, G., Chartrand, M. S., and Aaseth, J. (2017). Manganese exposure and neurotoxic effects in children. Environmental Research, 155, 380–384.

https://doi.org/10.1016/j.envres.2017.03.003
Bouchard, M., Laforest, F., Vandelac, L., Bellinger, D., and Mergler, D. (2007). Hair Manganese and Hyperactive Behaviors: Pilot Study of School-Age Children Exposed through Tap Water. Environmental Health Perspectives, 115(1), 122–127. https://doi.org/10.1289/ehp.9504
Bouchard, M. F., Sauvé, S., Barbeau, B., Legrand, M., Brodeur, M.-È., Bouffard, T., Limoges, E., Bellinger, D. C., and Mergler, D. (2011). Intellectual Impairment in School-Age Children Exposed to Manganese from Drinking Water. Environmental Health Perspectives, 119(1), 138–143. https://doi.org/10.1289/ehp.1002321
Carmichael, S., Doctor, D., Wilson, C., Feierstein, J., McAleer, R.,; New insight into the origin of manganese oxide ore deposits in the Appalachian Valley and Ridge of northeastern Tennessee and northern Virginia, USA. GSA Bulletin 2017;; 129 (9-10): 1158–1180. doi: https://doi.org/10.1130/B31682.1
Erickson, M. L., Yager, R. M., Kauffman, L. J., & Wilson, J. T. (2019). Drinking water quality in the glacial aquifer system, northern USA. Science of The Total Environment, 694, 133735. https://doi.org/10.1016/j.scitotenv.2019.133735
Hafeman, D., Factor-Litvak, P., Cheng, Z., van Geen, A., and Ahsan, H. (2007). Association between Manganese Exposure through Drinking Water and Infant Mortality in Bangladesh. Environmental Health Perspectives, 115(7), 1107–1112. https://doi.org/10.1289/ehp.10051
Khan, Kz, Wasserman, G. A., Liu, X., Ahmed, E., Parvez, F., Slavkovich, V., Levy, D., Mey, J., van Geen, A., Graziano, J. H., and Factor-Litvak, P. (2012). Manganese exposure from drinking water and children's academic achievement. NeuroToxicology, 33(1), 91–97. https://doi.org/10.1016/j.neuro.2011.12.002
Langley, R., Kao, Y., Mort, S., Bateman, A., Simpson, B., and Reich, B. (2015). Adverse neurodevelopmental effects and hearing loss in children associated with manganese in well water, North Carolina, USA. Journal of Environmental and Occupational Science, 4(2), 62. https://doi.org/10.5455/jeos.20150403060427
Lindsey, B.D., Belitz, K., Cravotta, C.A. III, Toccalino, P.L., and Dubrovsky, N.M. (2021) Lithium in groundwater used for drinking-water supply in the United States. Science of the Total Environment, v. 767. https://doi.org/10.1016/j.scitotenv.2020.144691
McMahon, P. B., Belitz, K., Reddy, J. E., Johnson, T. D. (2018). Elevated Manganese Concentrations in United States Groundwater, Role of Land Surface–Soil–Aquifer Connections. Environmental Science and Technology, 53(1), 29-38. https://doi.org10.1021/acs.est.8b04055
"Public Health Statement Zinc." Agency for Toxic Substances and Diseases Registry, Department of Health and Human Services, Aug. 2005, https://www.atsdr.cdc.gov/ToxProfiles/tp60-c1-b.pdf. Accessed 14 Apr. 2022.
Sanders, A. P., Desrosiers, T. A., Warren, J. L., Herring, A. H., Enright, D., Olshan, A. F., Meyer, R. E., and Fry, R. C. (2014). Association between arsenic, cadmium, manganese, and lead levels in private wells and birth defects prevalence in North Carolina: A semi-ecologic study. BMC Public Health, 14(1), 955. https://doi.org/10.1186/1471-2458-14-955
Spangler, A. H., and Spangler, J. G. (2009). Groundwater Manganese and Infant Mortality Rate by County in North Carolina: An Ecological Analysis. EcoHealth, 6(4), 596–600. https://doi.org/10.1007/s10393-010-0291-4
Spangler, J. G., and Reid, J. C. (2010). Environmental Manganese and Cancer Mortality Rates by County in North Carolina: An Ecological Study. Biological Trace Element Research, 133(2), 128–135. https://doi.org/10.1007/s12011-009-8415-9
Tebo, B. M., Bargar, J. R., Clement, B. G., Dick, G. J., Murray, K. J., Parker, D., Verity, R., & Webb, S. M. (2004). Biogenic manganese oxides: Properties and mechanisms of formation. Annual Review of Earth and Planetary Sciences, 32, 287–328.
U.S. Environmental Protection Agency. (2004). Drinking water Health advisory for Manganese. https://www.epa.gov/sites/production/files/2014-09/documents/support_cc1_magnese_dwreport_0.pdf.
U.S. Environmental Protection Agency (2022a). "Secondary Drinking Water Standards: Guidance for Nuisance Chemicals." 816-F-10-079.
U.S. Environmental Protection Agency (2022b)

"National Primary Drinking Water Regulations."
EPA 816-F-09-004.

KECK Geology Consortium
Learning Science Through Research
Published by the Keck Geology Consortium
Short Contributions
Keck Geology Consortium
Volume 34
May 2022
doi: 10.18277/AKRSG.2022.34.08

ASSESSING THE IMPACT OF SOIL ON MANGANESE CONTAMINATION IN SPRINGS AND GROUNDWATER IN THE SHENANDOAH VALLEY, VIRGINIA

HALEY CULBERTSON, Washington & Lee University
Project Advisor: Margaret A. G. Hinkle

INTRODUCTION

There are multiple potential geogenic and anthropogenic sources of Mn in surface water and groundwater. Since the discovery of manganese (Mn) in 1774 (Weeks, 1932), it has been utilized for a plethora of purposes in American industry, including infrastructure and agriculture (Johnson, 2006). Mn has also been mined for energy production and fertilizer for decades, the byproducts of which all contribute to Mn entering waterways (Howe and International Programme on Chemical Safety, 2004). In the Blue Ridge Mountains, geogenic sources of Mn are hypothesized to have existed since the Paleozoic era (Pegau, 1958) as a result of clay weathering processes at the contact of the Shady Dolomite and Erwin Formations, forming primarily Mn(III/IV) oxide minerals such as pyrolusite and hollandite (Carmichael et al., 2017; Stose et al., 1919). To the west in the Shenandoah Valley, the origin of Mn ores is thought to be a two-step process involving hydrothermal deposition followed by supergene enrichment. In other words, Mn(III/IV) oxides initially precipitated from a hot solution of mineral enriched water which forced its way through cracks in the Earth's surface, followed by supergene alteration from the downward percolation of mineral- bearing surface water, as evidenced by two distinct mineralogies and geochemical signatures (Carmichael et al., 2017). South of the Shenandoah Valley in the Roanoke River Watershed, Mn ores are believed to have been formed by only supergene processes, with temperatures below 130°C, as indicated by the presence of goethite (Kiracofe et al., 2017). However, rather than a strictly downward percolation model as previously hypothesized (Espenshade, 1954). Kiracofe et al. (2017) suggests Mn was first released from country rock via chemical weathering and carried to reducing conditions by downward percolating groundwater where it was then trapped in mineral structures due to diagenesis and metamorphism. This process is believed to have been followed by the upwelling of anoxic groundwater, releasing $Mn(II)_{aq}$ by chemical weathering, which was then transported to oxic conditions with sufficient microbial support to precipitate Mn(III/IV) oxides (Kiracofe et al., 2017). In all cases, these Mn (oxyhydr)oxide deposits weather and erode through time, transported by aeolian and alluvial processes to eventually end up in the water system.

Because Mn speciation is largely dependent on environmental conditions, with suboxic and anoxic conditions promoting $Mn(II)_{aq}$, drinking water obtained from groundwater sources is of particular concern. Groundwater resources are incredibly relied upon throughout the Shenandoah Valley, as a large percentage of inhabitants rely on springs and groundwater wells as their main source of drinking water (USGS, 2022). Additionally, a redox disequilibrium exists at springs (where the saturated zone meets the topographic surface) as anoxic or suboxic groundwater meets the oxygen-rich surficial environment, encouraging $Mn(II)_{aq}$ to oxidize to Mn(III/IV) oxides. This work investigates the role of soils on Mn concentrations in both springs and groundwater wells throughout the Shenandoah Valley, VA through Mn K-edge X-ray adsorption near-edge structure (XANES) spectroscopy and scanning electron microscopy with energy dispersive X-ray spectroscopy (SEM/EDS).

METHODS AND MATERIALS

Field Sites

The study area of this project consists of four counties across the Shenandoah Valley, including Rockbridge, Augusta, Bath and Shenandoah. The region is characterized by rural mountain landscapes, with historical cities distributed throughout, containing a total population of 145,659. A total of 24 springs (Fig. 1) were selected for sampling based on accessibility, permission, and regions of interest identified from groundwater well data from the Virginia Household Water Quality Project (VAHWQP).

Rockbridge County Sampling Sites

In Rockbridge County, Pond Spring (PS) is currently used to feed a pond that serves as the focal point of an outdoor event center. The spring itself is classified as a seep and located on the west side of the pond, the two slightly separated by a dirt mound covered by grasses, through which water flows. The pond directly east of the mound was a murky white on the day of sampling, possibly due to chemical treatments, but most likely due to decaying organisms (Aswiyanti et al., 2021). Kerr's Creek (KC) is a gaining stream upstream of PS with springs contributing to its flow.

Augusta County Sampling Sites

In Augusta County, Bubbling Springs (BUBS) and Augusta Springs and Wetlands (AWS) are located in the George Washington and Jefferson National Forests. BUBS is a spring-fed pond and is characterized by bubbles believed to be CO_2. The pond bottom is full of yellow, red, black, green, and brown pebbles and the water is extremely clear. In contrast, AWS is a complex of seeps, springs, and creeks. The area has been slightly developed with parking and picnic areas, as well as several post-colonial structures including a spring house, bottling plant foundations, and a hypothesized root cellar.

Disappearing Ponds Complex

Finally, also located within Augusta County and the George Washington and Jefferson National Forests, is the Maple Flats Ponds complex, a series of clay bottom ponds (Fleming and Alstine, 1999). Four of these ponds were included in this study: Frog/Oak Pond (FOP), located nearest to a relict Mn ore mine, Twin Ponds (TPS/N), Deep Pond (DP), and Spring Pond (SP), the latter being the largest and only pond never observed to dry up, and is likely spring-fed. All the ponds contained some water at the time of sampling (August 2021), but exact depth could not be determined because the soft clay bottom prevented wading into the centers. Other than SP, which was surrounded by tall, dense grasses and fruit bushes, the ponds were not dramatically different in appearance from one another. Most have no apparent input or output of water with the exception of precipitation and evaporation. This site was selected as a means to isolate Mn derived from soil weathering versus Mn inputs from groundwater.

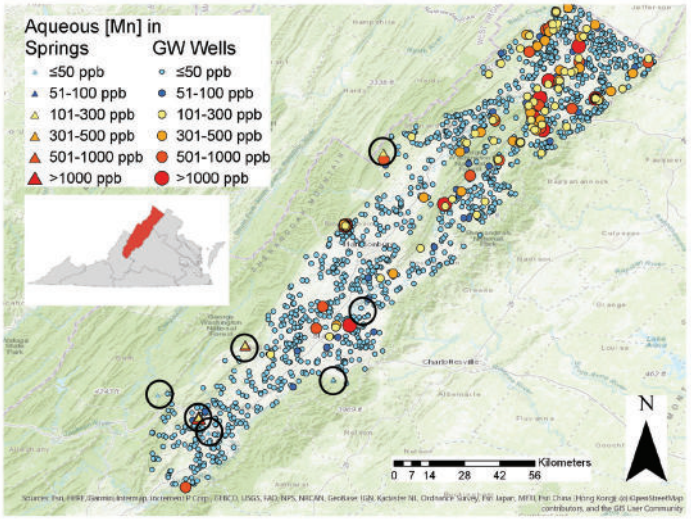

Figure 1. Map of aqueous Mn concentrations in springs (triangles) and groundwater wells (circles) in the Shenandoah Valley, VA, with increasing concentrations increasing the relative size of each data point based on demarcations from ≤50 ppb (light blue) to 51-100 ppb (dark blue) to 101-300 ppb (yellow; above which low level chronic exposure to Mn via drinking water may result in health effects), 301-500 ppb (orange), 501-1000 ppb (light red), to >1000 ppb (dark red). Field sites for springs and seeps are denoted with black circles.

Shenandoah County

The unincorporated town of Shrine Mont (SM) in Shenandoah Co. hosts multiple springs which have undergone over a century of documented use. Because of their history of use, each of the springs, three in total, had some sort of spring house structure built around them out of either wood or stone, with metal pipes used to bring the water to the surface. These

springs included Shrine Mont Orkney Spring (SMOS), Bear Wallow Spring (SMBW), and Tea Spring (SMTS). With the exception of SMBW, extensive Fe oxidation was visible in the form of bright red precipitates coating rocks surrounding the areas.

Soil Analyses

To determine the general composition of the soil samples, small amounts of each sample were mounted to aluminum stubs with double-sided carbon paper for SEM/EDS. These analyses provided elemental distributions and morphologic features across soils and determined the prioritization of samples for XANES spectroscopy. In total, samples analyzed with XANES spectroscopy include AWS03A, KC01A, KC02A, FOP01A, DP01A, and PS02. The "top" and "bottom" of each core was determined by either distinguishable differences in horizon by color or at least 3 cm from the respective end of the core.

Samples and Mn oxidation state standards were analyzed at beamline 12-BM-B, which uses a Si(111) fixed offset double-crystal monochromator with a toroidal focusing and flat harmonic rejection mirrors. XANES spectra of the Mn metal foil were collected at the beginning, end, and multiple mid points to calibrate the monochromators to 6539 eV, the Mn K-edge. Linear combination fits (LCFs) using a suite of XANES spectra standards [manganese (II) chloride [$MnCl_2$], rhodochrosite [$MnCO_3$], manganese (II) sulfate [$MnSO_4$], hausmannite [$Mn(II/III)_2O_4$], bixbyite [Mn,Fe_2O_3], manganite [MnO], feitknechtite [Mn(III)O(OH)], pyrolusite [MnO_2], ramsdellite [MnO_2], KBi, and calcium manganese oxide [$Ca_2Mn_3O_8$], with Mn(IV) standards from Manceau et al. (2012)] determined the average Mn oxidation state (AMOS) of the select soil samples, as well as the fraction of Mn(II/III/IV)s. These LCFs and the total concentration of Mn in the samples determined by XRF from Willis (2022) were used to calculate the actual concentration of Mn(II/III/IV)s per sample.

Total soil moisture content was determined via gravimetric analysis. Soil pH was determined by combining up to 5.0 g of soil with 10 mL of 0.1 M $CaCl_2$. These solutions were mixed with a glass rod and allowed to settle for >30 minutes before the separated solution pH was measured.

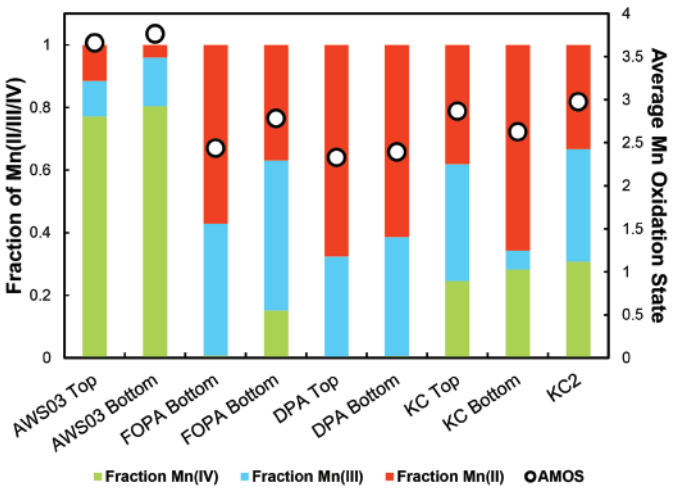

Figure 2. The fractions of Mn(IV) (green), Mn(III) (blue), and Mn(II) (red) and average Mn oxidation state (AMOS; white circles with black outlines) obtained by LCFs for each sample analyzed by Mn K-edge XANES spectroscopy.

RESULTS

Average Mn Oxidation State (AMOS) of Soils of Interest

Substantial Mn(II) (>10%) was found in every sample analyzed by XANES spectroscopy, in varying proportions (Figure 2). Comparing samples within the field sites, the AMOS determined was relatively similar, a trend that was also found within the individual cores. Every soil sample has an AMOS between 2.0 and 4.0, with the exception of PS, whose XANES spectra exhibits a white line at surprisingly high energy beyond all of the Mn(IV) standards and consistent with Mn(VII) (Figure 3). A sample from AWS, AWS03A, exhibits the highest fraction of Mn(IV) with Mn(II/III) comprising just 20-30% (Table 1). In most soil cores, the AMOS is slightly higher in the bottom of the core than the top, similar to Gillispie et al. (2016) which found that the weathering of Mn bearing soils in the Piedmont region of North Carolina contribute to Mn contamination in shallow groundwater wells, with Mn(II/III) minerals near the surface and Mn(III/IV) oxide minerals at depth. There is an exception to this trend in KC01A (Fig. 2), with an AMOS of 2.87 at the top and that of 2.63 at the bottom. KC01A is particularly notable due to the extremely high soil Mn in the bottom of the core and lack of soil Mn in the top (Table 1) and the fact that it is the one sample near a stream rather than a spring/seep.

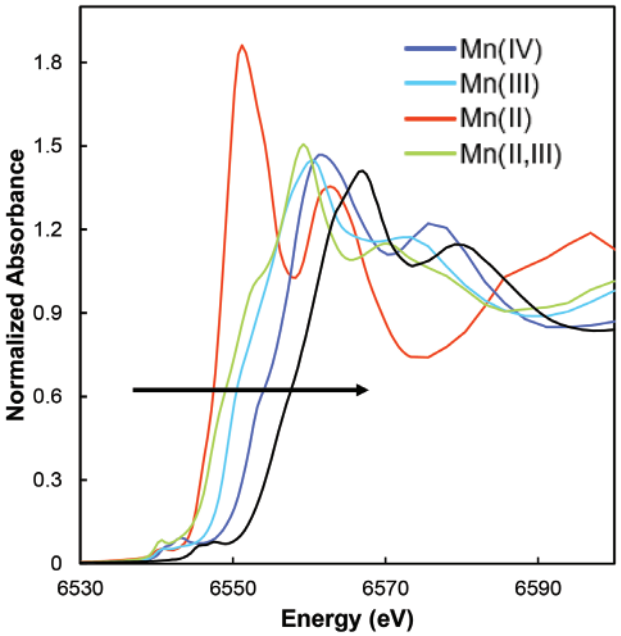

Figure 3. XANES spectra of example Mn oxidation state standards for each oxidation state used for LCFs, with Mn(IV) (dark blue), Mn(III) (light blue), Mn(II/III) (green), and Mn(II) (red) showing the progressive shift toward higher energy with increasing Mn oxidation state, compared with the sample spectra for PS (black). The sample spectra for PS is clearly shifted substantially toward higher energy, beyond that of Mn(IV) standards, indicating its oxidation state is higher than what is normally observed in soil environments.

Paired with the total soil [Mn] determined by XRF, the actual concentration of Mn(II/III/IV) for each sample was calculated (Table 1). Substantial concentrations of soil Mn(IV) were found in cores AWS03A and KC samples. Soil Mn was below the limit of detection for sample FOP01A bottom and the entire DP01A core. Other than these samples, every sample was found to have relatively high concentrations of soil Mn (Table 1) compared to the USGS soils map of the US (Smith et al., 2019).

Relationship Between Mn in Soils and Mn_{aq}

Plotting aqueous Mn in nearby waters vs AMOS and the fractions of Mn(II/III/IV) yields interesting trends. The site-averaged AMOS of soils and $[Mn]_{aq}$ display an inverse relationship ($R^2 = 0.44$), as also occurs for Mn(IV) and $[Mn]_{aq}$ ($R^2 = 0.49$) (Figure 4). When a soil sample has an AMOS closer to 4.0, the spring water collected has a concentration between 0.00 and 5.00 ppm; but when a soil sample has an AMOS closer to 2.0, the corresponding spring water sample $[Mn]_{aq}$ increases substantially. It should be noted that all samples analyzed by XANES spectroscopy happened to have lower aqueous Mn (aside from PS which was removed from this portion of the analysis due to its AMOS of ~+7), thus the maximum aqueous Mn in this data set is just 35 ppm, likely in part because these samples were selected based on observable soil Mn, and higher soil Mn corresponds with lower aqueous Mn.

Soil Mn(II) and $[Mn]_{aq}$ are directly related to one another, with a greater fraction of Mn(II) in soils correlating with higher $[Mn]_{aq}$ in corresponding spring waters ($R^2 = 0.36$). While most commonly existing in oxide minerals and thus usually expected to behave similarly to Mn(IV), Mn(III) also shows a negative correlation relationship with $[Mn]_{aq}$ ($R^2 = 0.60$) (Figure 4).

Table 1. Total soil Mn concentrations, fractions of soil Mn(II/III/IV) and corresponding average Mn oxidation states (AMOS) and actual concentrations of soil-associated Mn(II/III/IV), along with general soil parameters (percent organic matter (OM), percent total organic carbon (TOC), pH, and approximate percentages of sand, silt, and clay based on textural analyses.

Sample	Total [Mn]s (ppm)	fMn(IV)s	f Mn(III)s	fMn(II)s	[Mn(II)]s (ppm)	[Mn(III)]s (ppm)	[Mn(IV)]s (ppm)	[Mn]aq (ppb)	% OM	% TOC	pH	% Clay	% Sand	% Silt	Other Major and Trace Metals Present in Soils
AWS03A-top	1,225	0.77	0.11	0.11	140	139	946	0.90	8%	13%	6.0	35%	10%	55%	Zn,Fe, Cr, Ni, Pb, Ti, Zr
AWS03A- bottom	2,058	0.80	0.16	0.04	84	320	1,655	0.90	9%	16%	6.0	25%	65%	15%	Zn,Fe, Cr, Ni, Pb, Ti, Zr
FOPA- top	176	0.01	0.42	0.57	100	74	1	34.80	7%	13%	5.0	45%	10%	45%	Fe, Pb, Ti, Zn
FOPA- bottom	-	0.15	0.48	0.37	-	-	-	34.80	4%	7%	4.6	45%	5%	50%	Zr, Fe, Cr, Ti,
DP01A- top	-	0.00	0.32	0.68	-	-	-	10.50	8%	13%	4.0	45%	50%	5%	Fe, Ti
DP01A- bottom	-	0.01	0.38	0.61	-	-	-	10.50	1%	3%	3.5	30%	50%	20%	Fe, Ti
KC01A- top	415	0.25	0.37	0.38	158	155	102	9.60	3%	6%	5.6	5%	90%	5%	Fe, Cr, Ni, Ti
KC01A- bottom	17,801	0.28	0.06	0.66	11,698	1,067	5,037	9.60	5%	9%	6.0	0%	100%	0%	Ti, Fe, Cr, Ni, Zr
KC02A	23,754	0.31	0.36	0.33	7,910	8,544	7,300	9.60	4%	7%	6.2	10%	60%	30%	Zr, Fe, Ti, Sn, Cr
PS02A- top	9,301	-	-	-	-	-	-	173-1322	-	-	3.9	-	-	-	-
PS02A- Bottom	12,659	-	-	-	-	-	-	173-1322	-	-	3.1	-	-	-	-

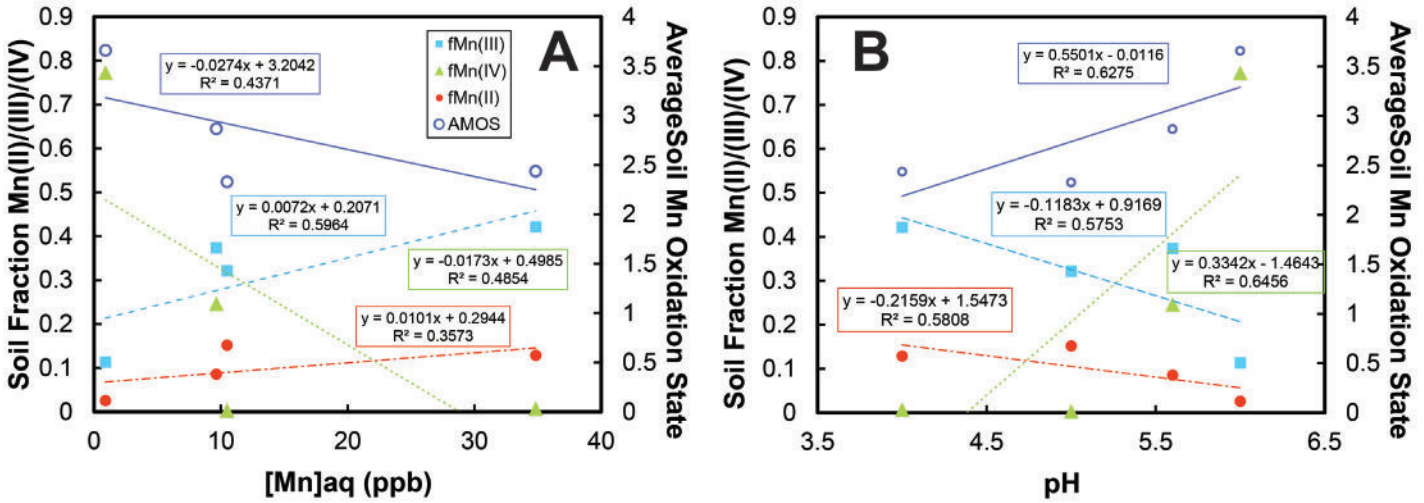

Figure 4. Fraction of Mn(IV) (green triangles), Mn(III) (light blue squares), and Mn(II) (red circles) in soils as well as the AMOS (white circles with blue borders) as a function of aqueous Mn concentrations in nearby springs and seeps (A) and of pH (B).

Soil Characteristics and AMOS Trends

Most of the soils sampled (28/52) contained 50% or greater sand, while the next most common soil component was clay (21/52 samples with greater than 50%), with only 3 samples composed of majority silt (Table 1). Only two cores, both collected from Rockbridge County, have a pH ≥ 7.0, with the other 48 samples being acidic. Soils with confirmed Mns were found to be acidic, with pH levels consistently less than or equal to 6.0 (Table 1). These soils also have very high proportions of silt in comparison to the rest of the samples, with the exception of one sample from Shenandoah County (Table 1). Site averaged AMOS and the fraction of Mn(IV) in samples show a directly correlated relationship with increasing pH, while the fraction of Mn(II) and (III) both show inverse relationships ($R^2 > 0.57$) (Figure 4). These trends are consistent with those shown between the fraction of Mn(II/III/IV) and $[Mn]_{aq}$ in spring waters.

Heavy Metals Associated with Mn_s

Soils which were prioritized for XANES were analyzed with SEM/EDS for a second time, more thoroughly, to determine elemental associations with soil Mn_s. During these analyses, Mns was found as precipitates on other grains without defined boundaries and as distinguishable grains with definitive platy geometry. In every sample, regardless of perceived Mns morphology, Mn was associated with various heavy metal contaminants including chromium (Cr), nickel (Ni), and lead (Pb) (Table 1). Also consistently associated with Mns in soils were Fe and titanium (Ti).

DISCUSSION

Across the Shenandoah Valley, previously analyzed groundwater wells show two contamination "hotspots" (McMahon et al., 2018). Including data from the VAHWQP broadened our groundwater well network to >1,900 wells within the Shenandoah Valley and suggests multiple Mn "hotspots", all of which are in agreement with $[Mn(II)]_{aq}$ found in spring waters by this study, with the exception of PS located in central Rockbridge County (Figure 1). Extremely high [Mntotal]soil found by XRF (Table 1) and AMOS greater than 4 (Figure 3), however, indicates that the regular algae treatments given to the pond may likely contain potassium permanganate (KMn7+O4), with Mn(VII) most stable in the aqueous phase. This input of Mn(VII) would also explain the exceptionally elevated $[Mn]_{aq}$ at PS. These remaining hotspots appear to be strongly associated with black shale and sandstone lithologies, while limestone and dolostone lithologies seem to buffer $Mn(II)_{aq}$ contamination of concerning concentrations (>100 ppb). However, the soils found to contain appreciable concentrations of Mns were from sites located outside of these hotspots and are associated with very low spring $[Mn(II)]_{aq}$.

The correlations between the AMOS, Mn(II), and Mn(IV) with$[Mn]_{aq}$ show expected behaviors, confirming that solid-associated Mn(II) is stable in reducing conditions but less so in oxidizing

conditions. The positive correlation between Mn(III)s and $[Mn]_{aq}$, however, seems to contradict these trends (Figure 4A). This relationship may likely be explained by comproportionation reactions that can occur between Mn(II) and Mn(IV) in certain environments where they coexist (Mandernack et al., 1995), generating Mn(III) as follows:

$$Mn(II) + Mn(IV) \leftrightarrow 2Mn(III) \qquad \text{Eq (1)}$$

Thus, increasing $[Mn(II)]_{aq}$ drives the reaction toward generating more Mn(III) (Zhao et al., 2016). These reactions are typically most common in transition zones, such as wetlands, hyporheic zones, and areas contaminated with other heavy metals (McMahon & Chapelle, 2008), which explains the high [Mn(III)] found in soils at AWS and KC (Table 1), which we would classify as hyporheic zones. These results are consistent with McMahon et al. (2018a) findings that groundwater wells closest to surface water bodies are at higher risk for Mn contamination.

Relationships Between Soil Characteristics and AMOS

The trend displayed between Mn(III) in soils and soil pH can likely also be explained by these comproportionation reactions. Although Mn(IV) is seen to decrease with decreasing pH (Figure 4B), because increasingly acidic conditions make $Mn(II)_{aq}$ stable, the reaction would be expected to become more thermodynamically favorable if Mn(IV) were present in the system; however, previous research has shown that decreasing pH inhibited Mn(IV) comproportionation reactions (in pH conditions of 7.4-8.0) (Mandernack et al., 1995). This trend may conversely be interpreted as $Mn(III)_{aq}$ oxidizing to Mn(IV) with increasing pH conditions, which has been found to play a larger role in the system's redox behavior than previously thought (Johnson, 2006).

CONCLUSION

Because of the negative correlation between soil AMOS and $[Mn]_{aq}$, soils which contain Mn(III/IV) oxides appear to have a buffering effect on Mn_{aq} contamination, as the conditions make the reduction reaction of Mn(IV) more unfavorable in terms of both thermodynamics and kinetics. However, common heavy metal associations with potential contaminants such as chromium, nickel, and lead pose the potential risk of mobilizing to groundwater resources if pH or oxidation conditions change. This work finds that $[Mn(II)]_{aq}$ contamination occurs in a spatially distributed manner throughout the Shenandoah Valley, with [Mn]s in nearby soils providing an indication of possible spring and groundwater contamination. While the region is dominated by limestone and dolostone lithologies, providing buffering protection to springs and groundwater wells, the northern Shenandoah Valley is at higher risk due to the greatest proportion of shale and sandstone aquifers in this area.

ACKNOWLEDGEMENTS

This work was supported by the Keck Geology Consortium and the National Science Foundation under Grant No. 2050697. I would specifically like to thank Dr. Margaret Anne Hinkle, my thesis advisor for making this experience manageable, valuable, and fun. Both Dr. Eva Lyon and Emily Falls also deserve huge thanks for their help with field and lab work. Additionally, without the Keck students, and Ani Croy, Noah Wilson, and Chris Goldmann in particular, this project could not have been brought to its current conclusion in less than a year. XANES spectra were collected at beamline 12-BM at the Advanced Photon Source, a U.S. Department of Energy (DOE) Office of Science user facility operated for the DOE Office of Science by Argonne National Laboratory under Contract No. DE-AC02-06CH11357. A huge thanks to Benjamin Reinhart who collected the XANES spectra for this research, as COVID-19 necessitated that XANES spectra were collected with remote user access. This work was additionally supported by the Johnson Opportunity Grant program at Washington and Lee as well as the Washington and Lee Geology Department's Edgar W. Spencer '53 Geology Field Research Fund.

REFERENCES

Aswiyanti, I., Istiqomah, I., Isnansetyo, A., 2021. Isolation and identification of nitrifying bacteria from tilapia (Oreochromis sp.) pond in Sleman Yogyakarta Indonesia. IOP Conf. Ser. Earth Environ. Sci. 919, 012054. https://doi.

org/10.1088/1755-1315/919/1/012054
Carmichael, S.K., Doctor, D.H., Wilson, C.G., Feierstein, J., McAleer, R.J., 2017. New insight into the origin of manganese oxide ore deposits in the Appalachian Valley and Ridge of northeastern Tennessee and northern Virginia, USA. GSA Bull.
David B. Smith, Frederico Solano, Laura G. Woodruff, William F. Cannon, Karl. J. Ellefsen, 2019. USGS Scientific Investigations Report 2017-5118: Geochemical and Mineralogical Maps, with Interpretation, for Soils of the Conterminous United States [WWW Document]. URL https://pubs.usgs.gov/sir/2017/5118/sir20175118_element.php?el=25 (accessed 3.13.22).
Erickson, M.L., Yager, R.M., Kauffman, L.J., Wilson, J.T., 2019. Drinking water quality in the glacial aquifer system, northern USA. Sci. Total Environ. 694, 133735. https://doi.org/10.1016/j.scitotenv.2019.133735
Fleming, G.P., Alstine, N.E.V., 1999. Plant Communities and Floristic Features of Sinkhole Ponds and Seepage Wetlands in Southeastern Augusta County, Virginia. Banisteria 28.
Gilbert H. Espenshade, 1954. Geology and Mineral Deposits of the James River- Roanoke River Manganese District, Virginia. Geol. Surv. Bull. 1008.
Gillispie, E.C., Austin, R.E., Rivera, N.A., Bolich, R., Duckworth, O.W., Bradley, P., Amoozegar, A., Hesterberg, D., Polizzotto, M.L., 2016. Soil Weathering as an Engine for Manganese Contamination of Well Water. Environ. Sci. Technol. 50, 9963–9971. https://doi.org/10.1021/acs.est.6b01686
Howe, P.D., International Programme on Chemical Safety (Eds.), 2004. Manganese and its compounds: environmental aspects, Concise international chemical assessment document. World Health Organization, Geneva.
Johnson, K.S., 2006. Manganese Redox Chemistry Revisited. Science 313, 1896–1897.
Kiracofe, Z.A., Henika, W.S., Schreiber, M.E., 2017. Assessing the Geological Sources of Manganese in the Roanoke River Watershed, Virginia. Environ. Eng. Sci. 23, 43–64.
Mandernack, K.W., Post, J., Tebo, B.M., 1995. Manganese mineral formation by bacterial spores of the marine Bacillus, strain SG-1: Evidence for the direct oxidation of Mn(II) to Mn(IV). Geochim. Cosmochim. Acta 59, 4393–4408. https://doi.org/10.1016/0016-7037(95)00298-E
McMahon, P. b., Chapelle, F. h., 2008. Redox Processes and Water Quality of Selected Principal Aquifer Systems. Groundwater 46, 259–271. https://doi.org/10.1111/j.1745-6584.2007.00385.x
McMahon, P.B., Belitz, K., Reddy, J.E., Johnson, T.D., 2018a. Elevated Manganese Concentrations in United States Groundwater, Role of Land Surface–Soil–Aquifer Connections. Environ. Sci. Technol. 53, 29–38.
McMahon, P.B., Reddy, J.E., Johnson, T.D., 2018b. Data for Elevated Manganese Concentrations in United States Groundwater, Role of Land Surface-Soil-Aquifer Connections. US Geol. Surv. Data Release. https://doi.org/10.5066/P9Y4GOFQ
Pegau, A., 1958. Virginia Manganese Minerals and Ores A Selected Bibliography with Excerpts. Miner. Resour. Circ. 7.
Stose, G.W., Miser, H.D., Katz, F.J., Hewett, D.F., 1919. Manganese Deposits of West Foot of the Blue Ridge Mountains. Va. Geol. Surv. Bull. 17.
USGS, 2022. USGS Current Conditions for Virginia_Groundwater [WWW Document]. URL https://waterdata.usgs.gov/va/nwis/current/?type=gw (accessed 4.12.22).
Weeks, M.E., 1932. The discovery of the elements. III. Some eighteenth-century metals. J. Chem. Educ. 9, 22. https://doi.org/10.1021/ed009p22
Willis, N., 2022. Analysis of Soil Geochemistry to Better Understand Geogenic Manganese Contamination in the Shenandoah Valley. Keck Geology Consortium Short Contributions, 50.
Zhao, H., Zhu, M., Li, W., Elzinga, E.J., Villalobos, M., Liu, F., Zhang, J., Feng, X., Sparks, D.L., 2016. Redox Reactions between Mn(II) and Hexagonal Birnessite Change Its Layer Symmetry. Environ. Sci. Technol. 50, 1750–1758. https://doi.org/10.1021/acs.est.5b04436

KECK Geology Consortium
Learning Science Through Research
Published by the Keck Geology Consortium
Short Contributions
Keck Geology Consortium
Volume 34
May 2022
doi: 10.18277/AKRSG.2022.34.09

ASSESSING MANGANESE CONCENTRATIONS IN GROUNDWATER ACROSS THE SHENANDOAH VALLEY, VA

CHRISTOPHER GOLDMANN, Trinity University
Project Advisor: Brady Ziegler

INTRODUCTION

Elevated concentrations of aqueous manganese (Mn^{2+}) in drinking water can have a multitude of adverse human health effects and undesirable aesthetic consequences. Chronic exposure to Mn^{2+} concentrations ≥ 100 parts per billion (ppb) can elicit a variety of negative health effects including reduced IQ, increased infant mortality and cancer rates, and increased risk of Parkinson's disease (Bouchard et al., 2011; Langley et al., 2015; Sanders et al., 2014; Spangler and Spangler, 2009; Spangler and Reid, 2010). The Environmental Protection Agency (EPA) has established a lifetime chronic exposure maximum contaminant level (MCL) of 300 ppb (U.S. Environmental Protection Agency, 2004), though negative health effects have been documented with chronic exposure to Mn ≥ 100 ppb (Ljung and Vahter, 2007; Langley et al., 2015; Sanders et al., 2014). Additionally, the EPA has set a 1-day and 10-day health advisory (HA) for acute exposure to Mn^{2+} at 1,000 ppb and a secondary maximum contaminant level (SMCL) for Mn^{2+} at 50 ppb to avoid bitter metallic tastes and staining (U.S. Environmental Protection Agency, 2004).

This study investigates Mn^{2+} concentrations in groundwater in the Shenandoah Valley, Virginia, where at least 36% of the population uses private wells for drinking water (Virginia State Water Resources Plan, 2015; U.S. Census Bureau, 2019). While regular testing and treatment of municipal public water supplies is required by U.S. law, monitoring private supplies is optional. Water quality monitoring services are provided by the Virginia Household Water Quality Program (VAHWQP; www.wellwater.bse.vt.edu) upon request.

The Shenandoah Valley falls within the Valley and Ridge Province, bordered by the Blue Ridge Province to the east and the Appalachian Plateaus Province to the west. The Valley and Ridge Province is geologically complex, with generalized host lithologies including shale, black shale, dolostone, limestone, sandstone, igneous, and metamorphic facies (USGS, 2003).

Mn can be introduced to groundwater through a variety of geogenic and anthropogenic mechanisms. Most commonly, high concentrations of dissolved organic carbon (DOC) in aquifer soils and sediments can stimulate microbial populations and rapidly deplete dissolved oxygen to generate a reducing environment, under which Mn(IV)-oxides, ubiquitous in soils and sediments, are reductively dissolved to aqueous Mn^{2+} (Di-Ruggiero and Gounot, 1990). This reaction is shown in Eq. 1, where CH_2O represents generalized organic matter.

$$2MnO_2 + CH_2O + 3H^+ = HCO^{3-} + 2Mn^{2+} + 2H_2O \quad \text{(Eq. 1)}$$

Thus, environments with shallow anoxic water tables, elevated DOC in host soils, and/or host lithologies containing organic matter (e.g., shale) often contain elevated Mn^{2+} (McMahon et al. 2018). Additionally, soil weathering may increase the quantity of Mn(IV)-oxides available for reductive dissolution. For example, in the Piedmont Plateau of North Carolina, chemical weathering of near-surface soil and saprolite dissolves primary Mn(II,III)-bearing minerals that precipitate as secondary Mn(III,IV)-oxides near the water table. Under reducing conditions, these secondary Mn oxides dissolve and mobilize Mn^{2+} in groundwater (Gillispie et al., 2016).

Possible anthropogenic sources of Mn to groundwater

include, but are not limited to, Mn mines, pesticides, and gasoline. Improperly-reclaimed or abandoned historic Mn ore mines exist throughout the Valley, thus serving as a potential source of Mn^{2+} to groundwater if Mn-bearing minerals are mobilized and exposed to reducing conditions (Hue et al. 2001; Li et al. 2007). The application of fungicides with Mn-containing chemicals Maneb® and Mancozeb® in orchards may lead to Mn^{2+} contamination of groundwater via runoff (Semu and Singh, 1995), and the Mn-bearing molecule methylcyclopentadienyl manganese tricarbonyl (MMT) is used as an additive in gasoline and can accumulate along roadways from engine exhaust which may also introduce Mn^{2+} to groundwater via runoff (Lytle et al., 1995).

The objective of this study is to isolate Mn groundwater contamination mechanisms specific to the Shenandoah Valley. By identifying variables associated with elevated Mn and identifying the primary mechanism by which Mn^{2+} enters groundwater, the Valley's population reliant on private drinking wells can better avoid many of the adverse health effects associated with low level chronic exposure to Mn^{2+} via drinking water.

METHODS

Groundwater Collection and Analyses

This study utilizes well water data from VAHWQP and the United States Geological Survey (USGS) National Water Information System (NWIS). The VAHWQP data set contains samples collected at private residences between 2009 and 2019. Samples were collected from the tap inside privately-owned structures under a single address after five minutes of continuous flushing. Samples were analyzed for NO_3^- and F^- using ion chromatography, while inductively coupled mass spectrometry (ICP-MS) was used to measure all other analytes (Na, Mg, Al, Si, P, SO4, K, Ca, V, Cr, Fe, Mn, Co, Ni, Cu, Zn, As, Mo, Ag, Cd, Sn, Pb, Cl, Ti, Se, Sr, Ba, and U). In concert with the testing of private water supplies, property owners answered questionnaires; topics addressed in the questionnaire included (but were not limited to) whether a water treatment system was present, plumbing construction materials, noticeable aesthetic deficiencies of water, proximity of the property to environmental hazards such as landfills, and whether any member of the household had been sick in the past 30 days.

Data from the USGS NWIS were compiled and reported by McMahon et al. (2018). NWIS data was collected between 1988 and 2017; all samples were collected directly from wells rather than household taps and analyzed with ICP-MS. Data from VAHWQP and NWIS were combined into a single data set, resulting in 1587 unique sampling locations and 1906 individual samples. Thus, 319 samples were collected at duplicate locations at different points in time; samples reporting the highest Mn^{2+} concentrations were prioritized if multiple samples existed for a given location.

Geospatial Analyses

The combined water chemistry data set was imported into ArcGIS Pro 2.8.3 for geospatial analysis. Publically-available geospatial data used in this study include: a shapefile of surface water (streams/rivers) (Virginia Department of Environmental Quality), geologic structures including faults, dikes, and sills (Dicken et al., 2005), generalized lithology (Dicken et al., 2005), historic Mn mine locations (Bureau of Land Management, compiled by www.thediggings.com), orchard proximity (from VAHWQP questionnaire), and roadways (U.S. Census Bureau, Department of Commerce). These data were plotted with the combined VAHWQP/NWIS data set to elucidate potential geospatial controls on elevated Mn concentrations.

Statistical analyses

Multivariate statistical analyses can be useful for large chemical databases to elucidate patterns that inform geochemical mechanisms and processes occurring in a given system. Therefore, the combined VAHWQP/NWIS data set was passed through a principal component analysis (PCA) in an attempt to identify processes impacting groundwater chemistry in the Shenandoah Valley. PCA is a dimension reduction method of multivariate data that aims to identify trends and variation in the data by reducing it to dimensionless latent variables (principal

components) that account for the maximum variance in the multivariate data set. The amount of variance in the data set that is explained decreases with each additional principal component.

PCA output is generally presented as a two-dimensional biplot that compares principal component one (PC1, x-axis) vs principal component two (PC2, y-axis), which explain the most and second-most variance in the data, respectively. Points, known as scores, plot the values of PC1 and PC2 for each sample. Vectors move away from the origin (which represents the geometric mean). The length of a variable's vector indicates the amount of control that variable exerts on the principal component in the vector's direction. Vectors that point in the same direction along a principal component axis are closely related, whereas vectors that point in the opposite direction along a principal component axis are inversely related, but still controlled by that same principal component. For example, if a principal component reflects redox state, one could expect dissolved Fe and Mn vectors to point in the same direction along the principal component axis and point in the opposite direction of dissolved oxygen.

RESULTS

The spatial distribution of Mn^{2+} concentrations in groundwater is depicted in Fig. 1. The majority of elevated Mn^{2+} samples (>100 ppb) are located in the northern part of the Valley and towards the Valley center. Elevated Mn samples occur in curvilinear clusters, and isolated high Mn^{2+} samples surrounded by low Mn^{2+} (<100 ppb) rarely occur. Conversely, groundwater samples near the Valley's southern end and along the eastern and western margins are comparatively low in Mn^{2+}.

Anthropogenic Mn Sources

Fig. 2A displays groundwater Mn^{2+} concentrations with potential anthropogenic Mn inputs such as roads, orchards, and historic Mn mines. Interstate 81 runs the length of the valley from north to south; while there is elevated Mn^{2+} near roadways in the north, this trend is absent in the south. Historic Mn mines are concentrated along ridges near the southeastern margin of the Valley; a cluster of mines also occurs

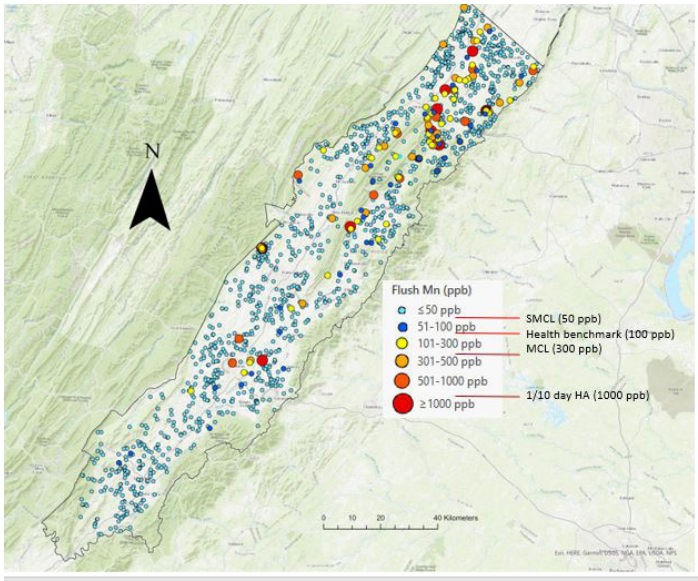

Figure 1. Spatial distribution of groundwater Mn^{2+} concentrations in the Shenandoah Valley.

on the northwestern margin of Massanutten Mountain Range toward the Valley's northern end. While these historic mines reflect the presence of Mn ores, their existence does not seem to influence groundwater Mn^{2+} concentrations in the vicinity. Orchards are sparsely distributed near the Valley's western margin. Given the lack of orchards in proximity to samples with elevated Mn^{2+}, their existence does not seem to influence groundwater Mn^{2+} concentrations in the region.

Geogenic Mn Sources

Fig. 2B displays groundwater Mn^{2+} concentrations along with surface water (streams/rivers) in the Valley.

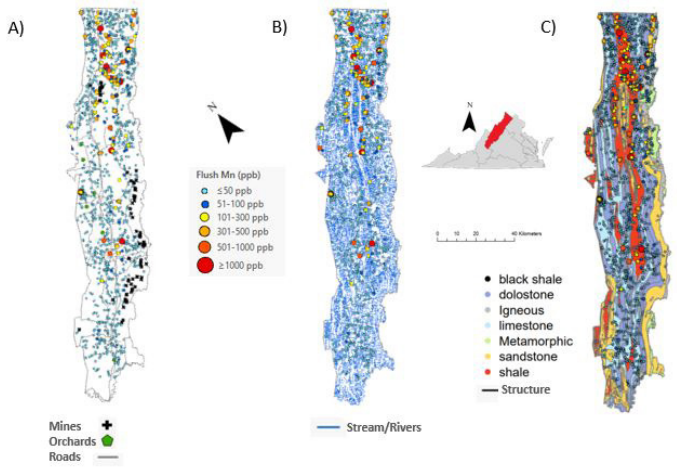

Figure 2. Map of groundwater sample Mn concentrations (ppb) with A) anthropogenic features; B) surface waters; and C) host lithology and geologic structure (faults, dikes, and sills).

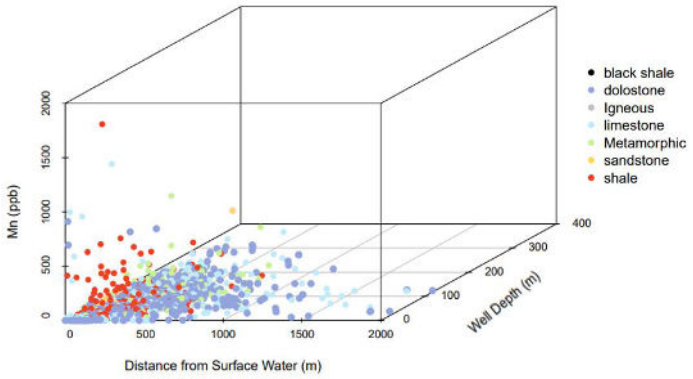

Figure 3. 3D scatterplot of sample Mn concentrations (ppb), distance to surface water (m), and well depth (m): all samples are categorized by host lithology.

Generally, groundwater samples with elevated Mn^{2+} concentrations (>100 ppb) tend to occur in closer proximity to surface water, and Mn^{2+} concentrations decrease with distance. To quantitatively support this observation, the shortest linear distance between sample locations and surface water was calculated and compared in conjunction with well depth and Mn^{2+} concentration (Fig. 3). Due to the dense distribution of surface waters in the valley, the vast majority of samples are within 1000 m of surface water. While the average distance of elevated Mn^{2+} samples from surface water was 206 m, the average distance of all low Mn^{2+} samples (<100 ppb) is notably farther at 304 m. In particular, elevated Mn^{2+} in groundwater often occurs near the headwaters of tributary streams/rivers.

Aquifer lithology carries important implications for groundwater Mn^{2+} concentrations (Fig. 2C). Due to a high average thickness of lithologic units in the region, it is assumed that surface lithology is indicative of aquifer lithology (Trapp, Jr. and Horn, 1997). As is consistent with the findings of McMahon et al. (2018), siliciclastic sedimentary lithologies (shales and sandstones) have the highest average groundwater Mn^{2+}concentrations. A majority of elevated Mn^{2+} samples in the Valley occur in the Martinsburg Formation, which is predominantly shale and underlies the majority of elevated Mn^{2+} samples in the northern part of the Valley as well as a few samples toward the southern extent where it outcrops. However, a few elevated Mn^{2+} samples occur in carbonate lithologies throughout the Valley. This typically occurs near a boundary between carbonate and shale lithologies, thus shales are still in close proximity to these samples.

The percentage of samples in exceedance of aesthetic and health benchmarks (Table 1) help inform lithologic controls on groundwater Mn concentrations in the valley. Only 10 samples exceeded the EPA 1 and 10-day health advisory limit of 1000 ppb, 60 samples exceeded the lifetime chronic exposure MCL of 300 ppb, 111 samples exceeded the 100 ppb potential health benchmark, and 148 samples exceeded the SMCL of 50 ppb. Relative to other lithologies, a higher percentage of samples collected in shale and sandstone lithologies exceeded MCL, SMCL, and HA thresholds. For example, approximately 25% of all samples taken in sandstone and shale exceeded the 50 ppb SMCL, while only 8% of all samples (regardless of lithology) exceeded 50 ppb.

Statistical Analysis

A PCA biplot identifies two principal components that explain the maximum variance among all geochemical analytes in the combined VAHWQP/NWIS data set (Fig. 4). PC1 explains 32.64% of the total variance in the data set, and is heavily influenced by Ca, Mg, and hardness in an elongated, tight cluster of vectors in the direction of positive PC1 space. Other divalent trace metals such as Sr^{2+} and Ba^{2+} exert an influence on PC1 in the positive direction, ultimately plotting with the Ca, Mg, and hardness cluster. This clustering can be explained by the tendency of Sr^{2+} and Ba^{2+} to substitute freely for Ca^{2+} and Mg^{2+} in the carbonate matrix. In contrast, the Na vector points in the opposite direction, into negative PC1 space. No other analytes associate strongly with Na in PC1 space. Interestingly, a substantial number of samples from limestone and dolostone aquifers associate with Na and not Ca or Mg, as would be expected based on matrix mineralogy.

Principal component 2 (PC2) explains 13.08% of the total variance. Nitrate (shown as NO3_N) exerts control on PC2 in the positive dimension and is

Table 1: % of wells in exceedance of:

Lithology	50 ppb	100 ppb	300 ppb	1000 ppb
Black shale (n = 8)	0	0	0	0
Dolostone (n = 757)	2	0.9	1	0
Igneous (n = 4)	0	0	0	0
Limestone (n = 584)	3	2	2	1
Metamorphic (n = 210)	13	10	6	0
Sandstone (n = 16)	25	13	6	0
Shale (n = 326)	26	21	10	2
Overall (n = 1906)	8	6	3	0.5

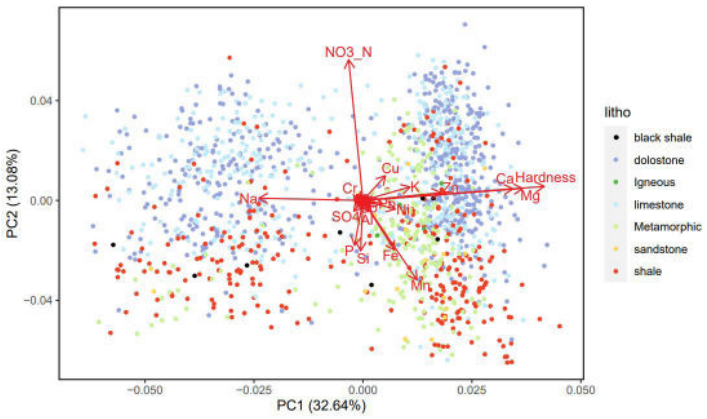

Figure 4. Results of a principal component analysis (PCA) biplot of 25 analytes from the combined VAHWQP and NWIS data set. The following analytes were removed due to incomplete data: Cl, Ti, Se, Sr, Ba, and U.

juxtaposed with Mn and Fe, which are tightly coupled and exert the most control in the negative PC2 dimension. Additionally, Si and P exert control in the negative PC2 dimension, though to a lesser extent than Mn and Fe. Separation by lithology is more prevalent in PC2 than in PC1: while carbonates occur in both positive and negative PC2 space, they are clustered toward the positive and weakly negative PC2 space. In contrast, shales are far more abundant in negative PC2 space.

DISCUSSION

From the PCA, and in conjunction with the VAHWQP questionnaire, it can be inferred that PC1 is reflective of in-home water treatment, including but not limited to water softener systems that remove Ca and Mg in exchange for Na from water softening salts. Thus, untreated samples fall in positive PC1 space and most accurately reflect the groundwater chemistry, whereas treated samples fall in negative PC1 space. A clear separation of samples by host lithology does not occur along the PC1 axis, as might be expected if PC1 is controlled by treatment and is independent of processes occurring in host lithologies. While metamorphic samples tend to fall disproportionately in positive PC1 space, all other lithologies are equally distributed across the PC1 axis. This reinforces the notion that PC1 is water treatment status: whether or not a sample has undergone treatment is completely independent of host lithology.

Given the dichotomy between NO_3^- and aqueous Mn and Fe, PC2 likely evinces redox conditions: positive PC2 space reflects oxidizing conditions while negative PC2 space reflects reducing conditions. This is further supported by host lithology: abundant organic matter within shales typically evokes reducing conditions through decay processes, and the majority of shale samples plot in negative PC2 space. Conversely, the majority of carbonate samples plot in positive PC2 space, thus indicating that weathered carbonates in this karst terrain are more oxic relative to shales.

Most trace metals do not heavily influence either PC1 or PC2, as indicated by relatively short vectors. However, they trend toward positive PC1 space and negative PC2 space, which is indicative of untreated samples under reducing conditions.

CONCLUSIONS

This study has determined that a combination of redox conditions and host lithology is the primary mechanism contributing to elevated Mn^{2+} concentrations in groundwater in select areas within the Shenandoah Valley. Elevated Mn^{2+} samples are located primarily in shale host lithologies, which are associated with reducing conditions that reductively dissolve Mn oxides to mobilize Mn^{2+} to groundwater in the vicinity. Conversely, and as is consistent with the findings of McMahon et al. (2018), weathered carbonates in karst terrains are associated with an oxic environment that stabilizes Mn in the solid phase and reduces the quantity of Mn^{2+} available in groundwater. Overall, those who source drinking water from wells in the Shenandoah Valley should be cautious of consuming untreated water within shale lithologies, whereas water sourced from carbonate lithologies is relatively safe. Future work will involve the isolation of only untreated samples within the VAHWQP data set for further analysis.

ACKNOWLEDGEMENTS

This material is based upon work supported by the Keck Geology Consortium and the National Science Foundation under Grant No. 2050697. I would like to thank the Keck Geology Consortium, the National Science Foundation, the host institution Washington & Lee University, and WLU professors Dr. Margaret

Anne Hinkle and Dr. Eva Lyon for making this research program possible. Thank you to Erin Ling of Virginia Tech for providing access to the VAHWQP data set that informed this thesis. Thank you to Dr. Glenn Kroeger (Trinity University) for offering his ArcGIS expertise and Dr. Kurt Knesel (Trinity University) for providing feedback on initial thesis drafts. Finally, I extend my most sincere gratitude to Dr. Brady Ziegler (Trinity University), who has served as both an advisor and mentor throughout this project.

REFERENCES

Bjørklund, G., Chartrand, M.S., and Aaseth, J., 2017, Manganese exposure and neurotoxic effects in children: Environmental Research, v. 155, p. 380–384, doi:10.1016/j.envres.2017.03.003.

Bouchard, M., Laforest, F., Vandelac, L., Bellinger, D., and Mergler, D., 2007, Hair Manganese and Hyperactive Behaviors: Pilot Study of School-Age Children Exposed through Tap Water: Environmental Health Perspectives, v. 115, p. 122–127, doi:10.1289/ehp.9504.

Bouchard, M.F., Sauvé, S., Barbeau, B., Legrand, M., Brodeur, M.-È., Bouffard, T., Limoges, E., Bellinger, D.C., and Mergler, D., 2011, Intellectual Impairment in School-Age Children Exposed to Manganese from Drinking Water: Environmental Health Perspectives, v. 119, p. 138–143, doi:10.1289/ehp.1002321.

Dicken, Connie L., Nicholson, Suzanne W., Horton, John D., Kinney, Scott A., Gunther, Gregory, Foose, Michael P., and Mueller, Julia A.L., 2005, Integrated Geologic Map Databases for the United States: Delaware, Maryland, New York, Pennsylvania, and Virginia: U.S. Geological Survey Open-File Report 2005-1325, U.S. Geological Survey, Reston, VA.

Di-Ruggiero, J., and A. M. Gounot. "Microbial manganese reduction mediated by bacterial strains isolated from aquifer sediments." Microbial ecology 20.1 (1990): 53-63.

Force, E. R., & Cox, L. J, 1991. Manganese contents of some sedimentary rocks of Paleozoic Age in Virginia. U.S. Geological Survey Bulletin 1916.

Gillispie, E.C., Austin, R.E., Rivera, N.A., Bolich, R., Duckworth, O.W., Bradley, P., Amoozegar, A., Hesterberg, D., and Polizzotto, M.L., 2016, Soil Weathering as an Engine for Manganese Contamination of Well Water: Environmental Science & Technology, v. 50, p. 9963–9971, doi:10.1021/acs.est.6b01686.

Hafeman, D., Factor-Litvak, P., Cheng, Z., van Geen, A., and Ahsan, H., 2007, Association between Manganese Exposure through Drinking Water and Infant Mortality in Bangladesh: Environmental Health Perspectives, v. 115, p. 1107–1112, doi:10.1289/ehp.10051.

Hue, N. V.; Vega, S.; Silva, J. A. Manganese Toxicity in a Hawaiian Oxisol Affected by Soil PH and Organic Amendments. Soil Science Society of America Journal 2001, 65 (1), 153–160. https://doi.org/10.2136/sssaj2001.651153x.

Hue, N.V., Vega, S., Silva, J.A., 2001. Manganese Toxicity in a Hawaiian Oxisol Affected by Soil pH and Organic Amendments. Soil Sci. Soc. Am. J. 65, 153–160. https://doi.org/10.2136/sssaj2001.651153x

Khan, K. et al., 2012, Manganese exposure from drinking water and children's academic achievement: NeuroToxicology, v. 33, p. 91–97, doi:10.1016/j.neuro.2011.12.002.

Langley, R., Kao, Y., Mort, S., Bateman, A., Simpson, B., and Reich, B., 2015, Adverse neurodevelopmental effects and hearing loss in children associated with manganese in well water, North Carolina, USA: Journal of Environmental and Occupational Science, v. 4, p. 62, doi:10.5455/jeos.20150403060427.

Li, M.S., Luo, Y.P., Su, Z.Y., 2007. Heavy metal concentrations in soils and plant accumulation in a restored manganese mineland in Guangxi, South China. Environmental Pollution 147, 168–175. https://doi.org/10.1016/j.envpol.2006.08.006.

Ljung, K., and Vahter, M., 2007, Time to Re-evaluate the Guideline Value for Manganese in Drinking Water? Environmental Health Perspectives, v. 115, p. 1533–1538, doi:10.1289/ehp.10316.

Lytle, C. M.; Smith, B. N.; McKinnon, C. Z. Manganese Accumulation along Utah Roadways: A Possible Indication of Motor Vehicle Exhaust Pollution. Science of The Total Environment 1995, 162 (2), 105–109. https://doi.org/10.1016/0048-9697(95)04438-7.

McMahon, P.B., Belitz, K., Reddy, J.E., and

Johnson, T.D., 2018, Elevated Manganese Concentrations in United States Groundwater, Role of Land Surface–Soil–Aquifer Connections: Environmental Science & Technology, v. 53, p. 29–38.

Sanders, A.P., Desrosiers, T.A., Warren, J.L., Herring, A.H., Enright, D., Olshan, A.F., Meyer, R.E., and Fry, R.C., 2014, Association between arsenic, cadmium, manganese, and lead levels in private wells and birth defects prevalence in North Carolina: a semi-ecologic study: BMC Public Health, v. 14, p. 955, doi:10.1186/1471-2458-14-955.

Semu, E., Singh, B.R., 1995. Accumulation of heavy metals in soils and plants after long-term use of fertilizers and fungicides in Tanzania. Fertilizer research 44, 241–248. https://doi.org/10.1007/BF00750931.

Spangler, A.H., and Spangler, J.G., 2009, Groundwater Manganese and Infant Mortality Rate by County in North Carolina: An Ecological Analysis: EcoHealth, v. 6, p. 596–600, doi:10.1007/s10393-010-0291-4.

Spangler, J.G., and Reid, J.C., 2010, Environmental Manganese and Cancer Mortality Rates by County in North Carolina: An Ecological Study: Biological Trace Element Research, v. 133, p. 128–135, doi:10.1007/s12011-009-8415-9.

Trapp, Jr., H. and Horn, M.A., 1997, U.S. Geological Survey Ground Water Atlas of the United States: Delaware, Maryland, New Jersey, North Carolina, Pennsylvania, Virginia, West Virginia. HA 730-L

U.S. Census Bureau, Department of Commerce: TIGER/Line Shapefile, 2015, state, Virginia, Primary and Secondary Roads State-based Shapefile

U.S. Census Bureau, 2019, Population of Virginia by County.

U.S. Environmental Protection Agency, 2004, Drinking Water Health Advisory for Manganese.

U.S. Geological Society, 2003. Virginia geologic map data.

Virginia Department of Environmental Quality, Office of Ecology, Water Monitoring & Assessment Program

Virginia State Water Resources Plan, 2015.

Yager, R.M., Voss, C.I., and Southworth, S., 2009, Comparison of alternative representations of hydraulic-conductivity anisotropy in folded fractured-sedimentary rock: modeling groundwater flow in the Shenandoah Valley (USA): Hydrogeology Journal, v. 17, p. 1111–1131, doi:10.1007/s10040-008-0431-x.

KECK Geology Consortium
Learning Science Through Research
Published by the Keck Geology Consortium
Short Contributions
Keck Geology Consortium
Volume 34
May 2022
doi: 10.18277/AKRSG.2022.34.10

ASSESSING THE GRAIN SIZE OF LEGACY SEDIMENTS AND POTENTIAL FOR HEAVY METAL CONTAMINATION IN ROCKBRIDGE COUNTY, VA

MIA GROFF, Whitman College
Project Advisor: Kirsten Nicolaysen

INTRODUCTION

In Rockbridge County, VA studying legacy sediment grain size and elemental abundances elucidates decades of major flood events, land use changes, and the presence and mobility of heavy metals. Chesapeake Bay drains a huge catchment that includes the Maury River watershed in western Virginia (Fig. 1). The Maury River provides water for many communities (Fig. 2), making it vital to monitor and study the water and sediments for potential contaminants. Inorganic metals of concern include both manganese and lead (Niemitz et al., 2012; Kiracofe et al., 2017). Manganese can be toxic and harmful to humans - especially infants and children - at chronic low levels (Bjørklund et al., 2017). The occurrence of these elements in sediments can be traced back to the underlying lithology and the mining history of the region.

Over the decades, impounded reaches and their connected floodplains accumulated sediments and may have captured heavy metals. Now, because of dam removal, the concern is remobilization. Though it is uncertain whether these heavy metal elements will be linked in the sediment with larger precipitated particles or in clays as bonded cations. Smaller clay particles have higher surface area and may be able to adsorb and absorb toxic elements depending on water redox and pH characteristics. On the other hand, larger particles may include heavy metal oxides and hydroxides which have been deposited in the legacy sediments (Pavlowsky et al., 2017).

The focus of this research is on the grain size and heavy metal composition of a 2.6 m stratigraphic column taken from sediment layers that accumulated behind a dam at Polecat Hollow (Fig. 2). Correlations between grain size and metal elements within the stratigraphic column can signify aspects about the environment of deposition.

Figure 1. A map of the State of Virginia showing the locations of the towns of Lexington and Buena Vista relative to the Maury River, James River, and to Chesapeake Bay.

BACKGROUND

The Maury River drains from the Valley and Ridge Province of Western Virginia and meets the James River at a confluence south of the towns of Lexington and Buena Vista (Fig. 1). The Maury River watershed is mainly located in Ordovician age limestone, sandstone and dolostone deposits of the Beekmantown, Lincolnshire Edinberg and Martinsburg Formations near Goshen Pass (Wilkes et al., 2007). The lithology includes deposits high in manganese, and mineralization along faults in the area has created ores valuable enough to mine. There is evidence for extensive mining in Rockbridge County, including 23 mines or quarries and 17 foundries (Wilde, 2022). Three of these mines were located near our sample site, close to the town of Lexington (Wilde,

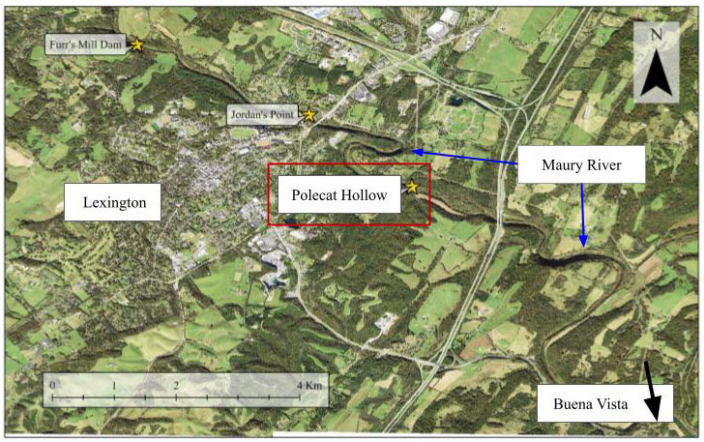

Figure 2. An aerial photograph of the town of Lexington with three of our sample sites shown along the Maury River and depicted by the yellow stars; Polecat Hollow is outlined by a red box. Aerial photo obtained from USGS Earth Explorer (EROS) database.

2022).

Over 64 different dam structures have been built in Rockbridge County, many of them now have been breached or removed (Wilde, 2022). Reid's Lock and Dam at Polecat Hollow existed from prior to 1863 until 1930 when it was removed. There are two recorded historic floods for the time during which Reid's Lock and Dam were operational, one in 1893 and one in 1896 (USGS, 2022). This is pertinent because higher volumes of water are able to transport more sediment and larger grain sizes.

Grain size analysis determines the distribution of the diameter of particles within a sample. Creating grain size distributions (GSD) for each sample shows the nature of the grain size spread, from which I interpret the differences between layers. In addition, this study explores manganese, lead, and iron abundances by examining the interactions of these heavy metals with clay rich layers and then large sand abundant layers.

METHODS

Field Sampling

We collected both sediment samples at eight different sites concentrated mostly within the Maury River watershed. The focus of this research on grain size changes through time includes only sediment samples collected from Reid's Lock and Dam, colloquially referred to as Polecat Hollow (sample site KDPH, Fig. 2). KDPH is located just downstream of the town of Lexington.

At Polecat Hollow, we sampled from the northern side of the channel about 100 m upstream of the dam remnants. The process began with scraping away any accumulated colluvium to create a vertical 2.6 m stratigraphic column. A tape measure was placed with 0 cm at the top horizon, or ground surface level and measured down to water level. We took ~10 g samples every 10 cm by using a lab grade steel spatula (Fig. 3). During collection, descriptions of the layering included the apparent grain size, color, and texture.

Sample Preparation

Removal of organic matter from each of the 16 samples chosen for grain size analysis ensured the complete separation of particles. The process involved repeatedly allowing 4-8 g samples to bathe in 30% hydrogen peroxide until the organics were absent from the sample (ISO, 2009). I deduced this by watching the samples during addition of H2O2, and stopping the process once they ceased to generate gas by oxidation. Finally, I included Sodium Hexametaphosphate to ensure particle separation. Samples did not require sieving during preparation; all of the samples contained only particles < 2 mm when they were collected.

Grain Size Analysis

At Whitman College the Mastersizer 3000 by Malvern Instruments collects grain size data through a multistep process ending with laser diffraction. The method begins with adding processed sediment to a swirling water bath to an obscuration of laser light between 10 and 15%. The water bath then sonicates the sample for a minute to ensure complete suspension and separation of particles. Next, the water and sample feed continually through a tube into the laser chamber. The sample analysis procedure was set to take 5 measurements of each batch and at least 3 distinct batches were run for each sample from KDPH. For example, the sample collected at a depth of 20 cm at Polecat Hollow would be analyzed with three separate aliquot runs, as PH-20a, PH-20b and PH-20c. The laser collects data by shooting light through the water and suspended grains and collects information about the angles of diffracted light.

Figure 3. A photo of one of the stratigraphic columns studied by our team. We sampled starting at the top using the tape measure, flags for marking, and lab spatulas to collect the sample. The same method was used at KDPH.

Collected GSD data used in interpretation included the D10, D50 and D90 (distribution percent which is the size of the particle below which exists the given percent distribution), the percent sand, silt, clay, and the percent volume density of particles for 100 bins from 0.01 microns to 3500 µm in diameter. The distinctions for clay, silt, and sand were < 4 µm, 4-62.5 µm and > 62.5 µm respectively. These GSD graphs expressed each of the three measured batches and the calculated average of three runs (Fig. 4).

RESULTS

Grain size distribution of the KDPH stratigraphic sequence varies from sand dominant to silt dominant in somewhat rhythmic layers. Overall, silt is usually most abundant at depths greater than 20 cm. Figure 4 displays a typical GSD from a layer with high clay content - 50 cm (PH-50) - and one with high sand content at 140 cm (PH-140). The sample PH-50 shows slight bimodal distribution with a small peak centering around 0.5 µm and a broad peak at 50 µm. In contrast, PH-140 shows a single peak near 100 µm with a slight skew towards smaller grain size. To compare the percent sand, silt, and clay, PH-50 shows 20% clay, 72% silt, and 7% sand whereas PH-140 has 6% clay,

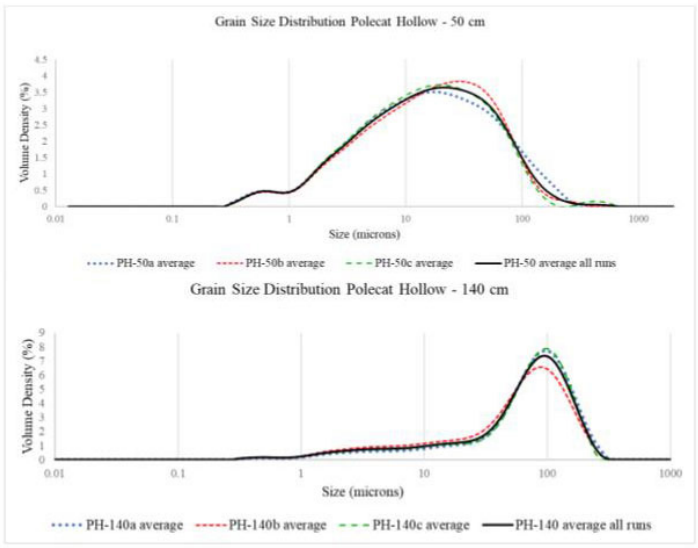

Figure 4. Two grain size distribution graphs, one from a depth of 50 cm and another from 140 cm. The red, green, and blue lines are the three measured runs. The black line is the calculated average of the three runs and shows the average GSD for these samples.

26% silt, and 68% sand.

Mean grain sizes for the entire stratigraphic profile sampled ranged from 11.7 µm to 197.6 µm (Fig. 5).The largest mean grain size of 198.6 µm was recorded at depth 0 cm. The average of all sample means (the average D50) is 56.8 µm. The average percent clay in the 16 samples was 12% with the average silt and sand being 49% and 39% respectively; although there were large ranges of variability in both silt and sand percent volumes. Silt dominates samples in three layers and sand is most abundant in four layers of the column at KDPH.

I performed X- Ray Diffraction analysis to determine the mineral identities present and found quartz as the only distinguishable mineral.

DISCUSSION

At the top of the column the larger grain size and lower relative abundances of Fe, Mn, and Pb suggest a distinct change in depositional environment, which is probably due to the removal of the dam in 1930.

The data show some positive correlation between median grain size (D50) and the abundance of Mn, Pb, and Fe (Fig. 5). At the top of the column, at 0 cm, we see the largest particle size. On the other hand, concentrations for Mn, Pb, and Fe are at low at the top

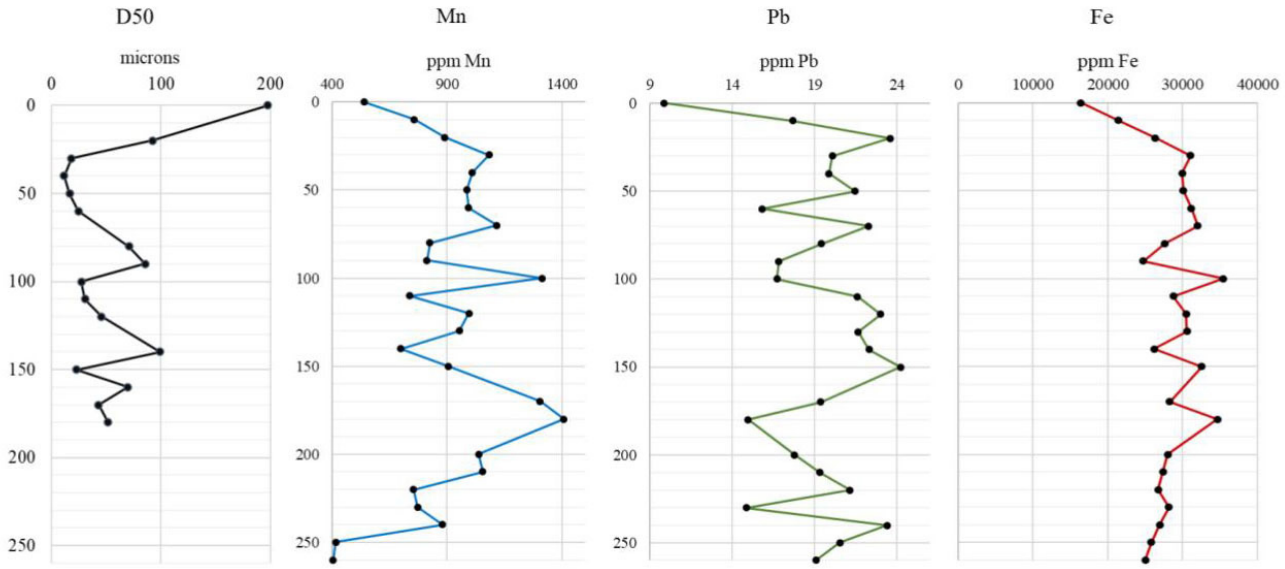

Figure 5. The average D50 value for each KDPH sample depicted stratigraphically and placed next to similarly oriented graphs depicting the abundance of Mn, Pb, and Fe throughout the column. The elemental abundance data gathered and provided by Madeline Holicky at Beloit College.

of the column (and the least abundant of all samples for both Fe and Pb. Following this trend, other spikes in D50 occur at depths of 90 and 140 cm. At these horizons, all metals have lower concentrations. This is consistent with the hypothesis that layers with larger particles will have overall lower surface area and therefore not allow as much heavy metal adsorption as smaller, more clay rich layers in the stratigraphic column. The sample depths with smaller mean grain sizes include 40, 100 and 150 cm. Between these three samples the variation of general elemental abundances fluctuates a bit more, though the trend shows overall greater concentrations of Mn, Pb, and Fe. This is especially apparent at a sample depth of 100 with Mn and Fe. The amount of Pb at this depth is low, which might suggest a complex relationship between abundance of Pb with the abundances of Mn and Fe - Mn and Fe tend to trend similarly throughout the column, with both showing alignment of peaks and troughs.

CONCLUSION

Grain size analysis of a stratigraphic column of millpond sediments along the Maury River in Rockbridge County elucidates the relationships between grain size and heavy metal abundances. The legacy sediments studied at Polecat Hollow have overall grain size means in the range of clay, silt and sand. The association of smaller particles with higher Mn and Fe abundance suggests the metals are correlated with clay abundance. The larger particles therefore are generally not compositionally inclusive of the highest amounts of Mn, Fe, and Pb. The larger sediments at the top of the column are likely associated with the removal of Reid's Lock and Dam signifying a distinct change in depositional environment. The top 30-40 cm of the stratigraphic column has much larger grain sizes, with lower levels of heavy metals. This can be pertinent for contamination studies and for monitoring the region. This also can inform the future of dam removal in relation to legacy sediment remobilization. Legacy sediments have overall grain size means in the range of silt and the active floodplain has much larger grain sizes, with lower levels of heavy metals. The history of land use in this column was more difficult to deduce because we lack age constraints and accumulation rates of sediments during the time the dam was active.

ACKNOWLEDGEMENTS

This material is based upon work supported by the Keck Geology Consortium and the National Science Foundation under Grant No. 2050697. I would like to thank my research mentors and advisors Kirsten Nicolaysen and Eva Lyon. I am grateful for the help and support of Nick Bader, Pat Spencer, Elliot Broze, and Emily Falls. Thanks to fellow Keck researchers, especially Maddie Holicky, Kallan

Wilde, and Noah Willis. Thank you to the Whitman Geology Department as well for support and providing resources such as lab material and for the use of the Mastersizer 3000.

REFERENCES

Bjørklund, G., Chartrand, M.S., Aaseth, J., 2017, Manganese exposure and neurotoxic effects in children. Environ Res. v. 155 p. 380-384.

Holicky, M., 2022, Assessing land use changes using the legacy sediments of Shenandoah valley, Virginia, [BA thesis: Beloit College]

International Organization for Standardization, 2009, Soil quality - Determination of particle size distribution in mineral soil material - Method by sieving and sedimentation

Kiracofe Z., Henika W., Schrieber M., 2017, Assessing the geological sources of manganese in the roanoke river watershed, Virginia, Environmental & Engineering Geoscience, v. 23, p. 43-64

Niemitz, J., Haynes C., Lasher G., 2012, Legacy sediments and historic land use: Chemostratigraphic evidence for excess nutrient and heavy metal sources and remobilization, Geology, v. 41, p.47-50

Pavlowsky, R. T., Lecce, S.A., Owen, M. R., Martin, D. J., 2017, Legacy sediment, lead, and zinc storage in channel and floodplain deposits of the Big River, Old Lead Belt Mining District, Missouri, USA, Geomorphology, v. 299, p. 54-75

Wilde, K., 2022, Analysis of land use in Rockbridge County, VA from precolonial times to current day and consequences for riparian ecosystems [BA thesis: St. Norbert College] (in press)

Wilkes, J. P., Spencer, E.W., Evans, N. H., Campbell, E.V. M., 2007, Geologic Map of Rockbridge Co, Virginia, Department of Mines, Minerals, and Energy. 1:50,000

KECK Geology Consortium
Learning Science Through Research
Published by the Keck Geology Consortium
Short Contributions
Keck Geology Consortium
Volume 34
May 2022
doi: 10.18277/AKRSG.2022.34.11

ASSESSING LAND USE CHANGES USING THE LEGACY SEDIMENTS IN THE SHENANDOAH VALLEY OF VIRGINIA

MADELINE HOLICKY, Beloit College
Project Advisor: James Rougvie

INTRODUCTION

Between the 17th and 19th centuries, thousands of dams were put in place in the state of Virginia to provide waterpower for agricultural and industrial purposes which caused an increased rate of sedimentation in the floodplains behind these dams (Walter and Merritts, 2008; Pizzuto and O'Neal, 2009; Balascio et al., 2019). These sediments are more formally known as legacy sediments because of the location and time frame in which they were deposited (Walter and Merritts, 2008; James, 2013; Balascio et al., 2019). These sediments are of interest because when dams are removed the legacy sediments are remobilized, and can release harmful pollutants that have built up in these sediments into the waterways (Walter and Merritts, 2008; Pizzuto and O'Neal, 2009; Kirwan et al., 2011, Palinkas et al., 2019; Balascio et al., 2019). This study hypothesizes that the changes in elemental and isotopic composition in these sediments reflect the changes in land use in the Maury River watershed in Virginia. The Maury is a tributary of the James River, which is part of the Chesapeake Bay Watershed (Fig. 1).

This project is part of a Keck Geology Consortium project focused on the historical and potential future impacts of millpond dams on surface water quality. This research will support the overall project by providing data regarding changes in land use since colonial times, the presence of geochemical pollutants in the sediments, and how those can affect the water quality in the Chesapeake Bay watershed.

Proxies

The proxies used in this study are as follows: total organic carbon (TOC), total nitrogen (TN), carbon

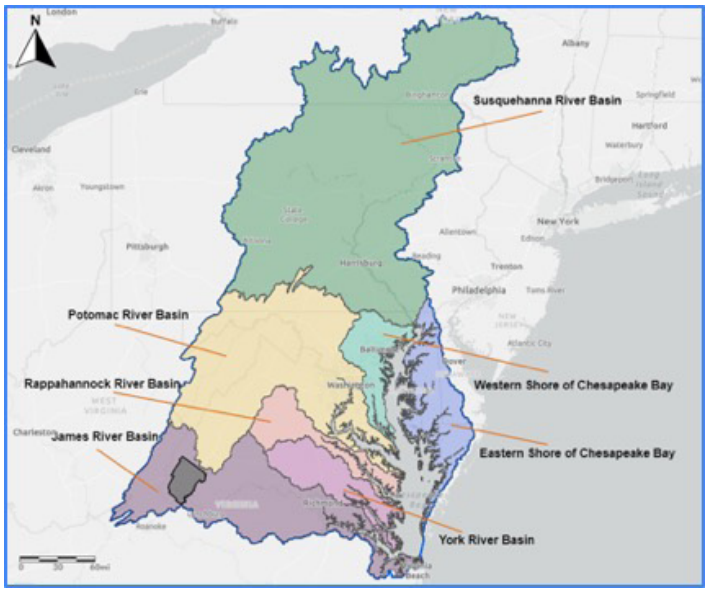

Figure 1. Chesapeake Bay Watershed. Rockbridge County is the gray polygon within the James River Basin. Map by Kallan Wilde.

to nitrogen ratio (C:N), nitrogen isotopes ($\delta^{15}N$), carbon isotopes ($\delta^{13}C$), and trace metals (Mn, Fe, Pb). The carbon to nitrogen ratio distinguishes between the amount of aquatic organic matter and terrestrial organic matter. TOC represents the fraction of organic matter that accumulated, while C:N values identify increases and decreases in the deposition of land organic matter from changes in land use (Meyers, 1997; Dean, 1999; Meyers, 2001). $\delta^{15}N$ and $\delta^{13}C$ values can indicate trends relating to anthropogenic activities such as fossil fuel burning and atmospheric fallout (Holtgrieve et al., 2011; Dean et al., 2014). Changes in phytoplankton in lake matter can also cause an increase in nitrates, used to complement the C:N values to show an increase in land usage such as an increase in agriculture following deforestation (Hecky and Kilham, 1988; Meyers, 1997; Meyers, 2001; Balascio et al., 2019). The trace metals are proxies for different land uses such as mining, metal forging, and construction (Niemitz, et al., 2013;

Balascio et al., 2019).

METHODS

Sampling

Samples from the banks behind removed dams were collected at numerous locations, including Polecat Hollow and Jordan's Point (Fig. 2). In the vertical river banks, a sediment sample was taken every 5 to 10 centimeters from the top of the bank to the bottom (Fig. 3). We interpreted the bottom of the bank to be the present water level of the river, based on the presence of in situ tree stumps dated to the late 1700s, consistent with the onset of milling activity in the region (Iosso and Harbor, 2020).

Elemental Analysis

Sediments were dried overnight for 48 hours in an oven at 35°C and were ground using a mortar and pestle to homogenize the samples for total carbon and nitrogen analyses. A subset of samples was rinsed with HCl to remove inorganic carbon before pulverization and elemental analysis. Carbon and nitrogen elemental concentrations and stable isotope ratios for dried and powdered sediment samples were determined using a Costech ECS 4010 elemental analyzer coupled to a Thermo Electron Delta Plus stable isotope ratio mass spectrometer at Washington and Lee University. Carbon and nitrogen isotope data were calibrated using the USGS-40 standard. Elemental C and N were corrected based on an acetanilide standard. Duplicate measurements of unknowns were used to establish precision: standard deviations were better than 0.007 for %N, 0.08 for %C, 0.1 for $\delta^{15}N$, and 0.5 for $\delta^{13}C$.

PXRF

Samples were analyzed using a Thermo Fisher Scientific Niton XL3t GOLDD++ Handheld XRF using the Test All Geo analysis mode at Beloit College. The standards used were NIST 2709a (180-649) San Joaquin Soil, Thermo Fisher 180-647 SiO2 blank, USGS SGR-1b Green River Shale, USGS SBV-1 Brush Creek Shale, AMIS 0547 Dolomite, Olifantsfontein, South Africa, AMIS 0461 Limestone, South Africa, and USGS W-2 Diabase. Mn, Fe, and Pb were calibrated based on these standards using the method of Rowe et al. (2012).

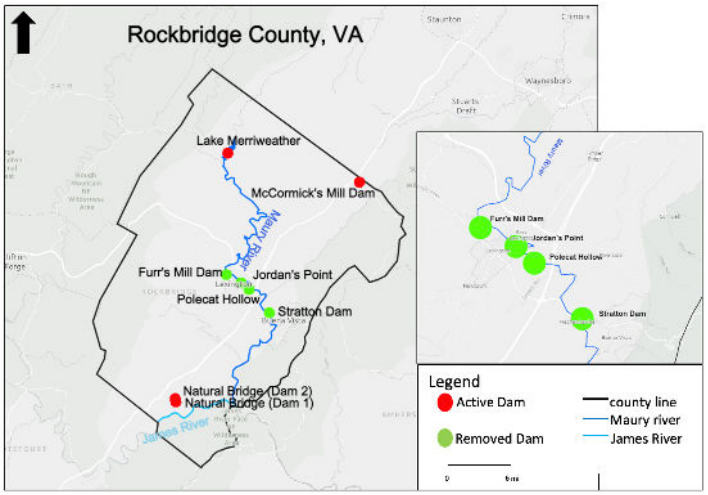

Figure 2. Legacy sediment and water sampling sites in Rockbridge County, VA. Red pins are sample collection sites at extant dams and green pins are sample collection sites where the dam has been removed. The inset map is a close-up map of the sites on the Maury River. The only sites reviewed in this study are Jordan's point and Polecat Hollow. Map by Kallan Wilde.

RESULTS

We assigned three broad temporal zones to the stratigraphy to contextualize changes through time at each site. These zones were based on trends in the proxies, some of which were consistent between sites.

Jordan's Point

The lowermost zone of interest is from 350 to 140 cm. In this zone, there are increases in C:N and $\delta^{13}C$ and they parallel one another throughout the column (Fig. 4). $\delta^{15}N$ steadily increases throughout this part of the column, and Fe and Mn increase until they decrease above 200 cm. Notably, the trace metals (Fe, Mn, Pb) are sampled at a coarser resolution in this zone, which limits our ability to compare their trends to the other proxies.

The middle zone of Jordan's Point chemostratigraphic column is from 140 to 60 cm. A major spike occurs in the C:N at 140 cm, and TC and TN steadily increase. $\delta^{15}N$ is invariable for the middle zone. There is a large spike in both Mn and Pb at the beginning of this zone after which they decrease. Fe decreases slightly over the course of this zone (Fig. 4).

The uppermost zone is between 60 and 0 cm and is

Figure 3. A photo of a student collecting samples from a bank at the Jordan's Point locality.

distinguished by the overall decrease in C:N, $\delta^{15}N$, $\delta^{13}C$, and the trace metals. There is a slight increase in both the C:N and $\delta^{13}C$ followed by a decrease in both until 0 cm. At 60 cm a sharp decrease in the $\delta^{15}N$ is present, the same trend occurs with the Mn, Fe, and Pb. The TN and TC increase from 60 to 0 cm (Fig. 4).

Polecat Hollow

The lowermost zone of interest is from depths of 260 to 190 cm. In this zone the TOC and C:N trends both increase at 230 cm after which they decrease. TN also spikes at 220 cm, but in less magnitude than C:N and TOC. The Mn and Fe trends increase steadily until a depth of 190 cm, which marks the end of the zone. Throughout the zone Pb ranges from 8 to 21 ppm (Fig. 5).

The middle zone of interest is from 190 to 90 cm. TN, TOC, C:N, Fe, and Mn do not vary often throughout this part of the column, except for their increases at 100 cm. The Pb concentrations are relatively invariant (Fig. 5).

The uppermost zone begins at a depth of 90 cm where a few of the trends change. There is a large increase in C:N and a slight increase in TOC at a depth of 20 cm, after which both trend to lower values. TN increases at the beginning of this zone and then stays fairly consistent. Fe and Mn decrease at 30 cm until depth of 0 cm while Pb starts to decrease at 20 cm until 0 cm (Fig. 5).

DISCUSSION

Both Jordan's Point and Polecat Hollow localities show trends that relate to the hypothesis. These trends are divided into zones of interest, which represent three broad intervals of time: 1. post-colonial forest clearing activities and early agriculture and mining in the Shenandoah Valley region, 2. the stabilization and continuation of agriculture in the area and the decrease in mining, and 3. an overall increase in the effects of anthropogenic activities like farming and burning of fossil fuels as discussed below. Both sites show these three broad zones, albeit at different levels in the bank stratigraphy (Fig. 4, 5).

The zones are referred to by depth from the bottom of the column to the top. The dates for the top and bottom of the column were assigned based on when the dam was put into place (bottom) and the present (top) assuming the sedimentation rate was constant. A constant sedimentation rate is unlikely, but there is not currently an established age model that would more accurately represent changes in sedimentation rate through time. The river is still capable of overtopping its banks and depositing sediments after dam removal (Kirwan et al., 2011; Palinkas et al., 2019, Iosso and Harbor, 2020), hence the date of 2021 at the top of the bank.

The assigned zones for Polecat Hollow and Jordan's Point somewhat align. While the zones and some of the trends in both represent the same three changes in land use, there are differences in the lengths of the zones along with differences in the trends overall (Fig. 4, 5). Because sedimentation rate changes while the dams are in place due to the removal of trees in the surrounding landscape, along with intense weathering events, and then changes significantly after the dams are removed due to changes in mean water level, (Iosso and Harbor, 2020), it is very difficult to cross-compare the localities' chemostratigraphy by layer.

The geochemical analysis of sediments at Jordan's Point reveal land use changes based on elemental changes seen in the chemostratigraphy. The lowermost

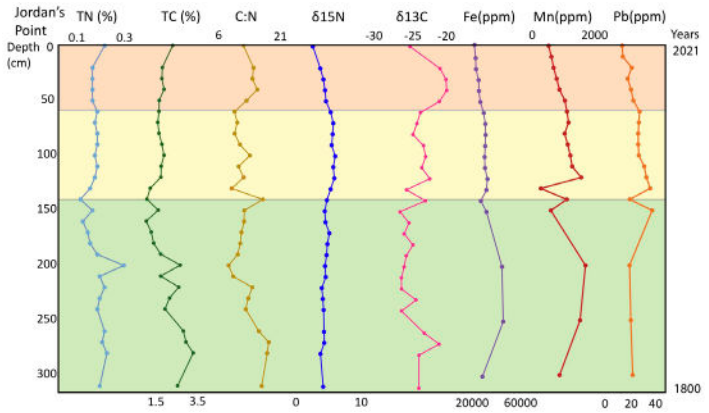

Figure 4. Chemostratigraphic profile for Jordan's Point. Zones of interest are as follows: lowermost (green), middle (yellow) and uppermost (orange).

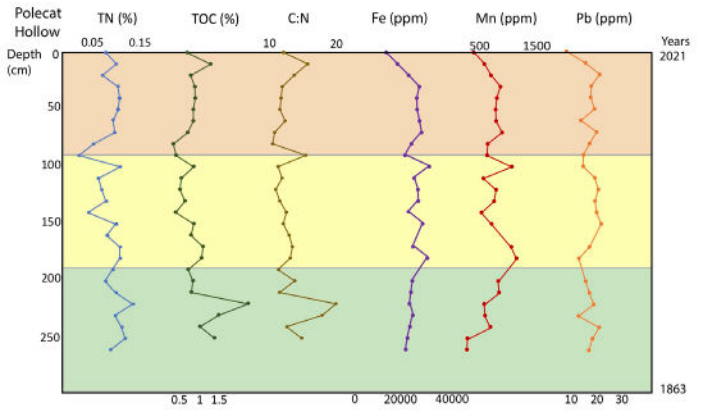

Figure 5. Chemostratigraphic Profile for Polecat Hollow. Zones of interest are as follows: lowermost (green), middle (yellow) and uppermost (orange).

zone is characterized by an increase in C:N and TC in the lower depths of the column, which suggests an increase in deforestation. Likewise, the concentrations of Fe and Mn increase over this zone. These trends are likely related due to the burning of trees to power metal forges during the late 1800s into the early 1900s. (Miller, 1996; Wilkinson and McElroy, 2007; Pavlowsky et al. 2017; Niemietz et al. 2013; Balascio et al. 2019). These same trends in C:N, TOC, Fe, and Mn occur in the lowermost zone of Polecat Hollow (Fig. 5). Thus, it appears that deforestation can be correlated with the increase in heavy metals related to mining and forging of these elements in the region as (Miller, 1996; Wilkinson and McElroy, 2007; Pavlowsky et al., 2017; Niemietz et al., 2013; Balascio et al., 2019).

The increasing trends for trace metals Fe and Mn correlate with changes seen in C:N and may be attributed to increases in mining and smelting in the area (Balascio et al., 2019; Pavlowsky et al., 2017, Scott 2015). Scott (2015) describes the fourteen furnaces that operated between 1820 and 1920 and the large number of iron ore deposits present in the area. The furnaces needed a great amount of iron ore to operate; on average it took 10 tons of ore to make one ton of pig iron (Scott, 2015). The increases in Fe and Mn in the lowermost zone at Jordan's Point may be related to this increase in mining and forging activity (Fig. 4).

The middle zone of Jordan's Point likely represents the decline in mining in the area and the stabilization of agricultural practices. There are increases in TOC, C:N, Fe and Mn in Polecat Hollow's middle zone which can also be attributed to these land changes. Balascio et al. (2019), describes how Lake Matoaka showed significant fluctuations in TOC and C:N due to the terrestrial-derived organic matter due to early agricultural practices in the area. In this zone, there is also a slight increase in Pb followed by Mn, and which may all be related to the increase in agricultural activity in the early 1900s (Niemitz et al., 2013, Balascio et al., 2019). Niemitz et al. (2013) relates the presence of heavy metals in agricultural soils and sediments surrounding farms to fertilizer usage. The increases in both Fe, Mn and Pb could be a reflection of the increase in fertilizer usage, such increases are also seen in the middle zone of Polecat Hollow in the Fe and Mn (Niemitz et al., 2013; Balascio et al., 2019) (Figure 4, 5)

The uppermost zone for both sites is characterized by a decrease in C:N and all of the trace metals. At Jordan's Point, where isotopic values were measured, there are declines in $\delta^{15}N$, and $\delta^{13}C$. The decrease in $\delta^{15}N$ is consistent with the atmospheric fallout of isotopically depleted nitrogen seen by Holtgrieve et al. (2011), which is due to the increased, widespread industrial N production in the past half-century. This change in $\delta^{15}N$ is also related to $\delta^{13}C$. A shift to lower $\delta^{13}C$ after ~1950 CE may be attributed to the increased consumption of fossil fuels and increased use of fertilizers (Dean et al., 2014).

Throughout most of this zone at both sites Fe and Mn decrease gradually until the end of the column, which could be attributed to the shift away from the Fe and Mn mining and smelting operations (Figure 4, 5). According to Scott (2015), the mining of iron ore and

the iron industry in general, decreased significantly after the 1920s (Miller, 1996). This could explain the general decrease of C:N and TOC throughout this zone in Polecat Hollow's chemostratigraphy because if less mining was happening, then less deforestation to power forges would occur (Meyers, 1997; Dean, 1999; Meyers, 2001; Balascio et al., 2019).

CONCLUSION

Based on the trends in the chemostratigraphic data, the hypothesis of this research can be supported. Although the age control of that data is lacking, there are general trends whose order is consistent with the overall history. Because of the trends relating to the mining of iron ore, and agriculture, it is reasonable to conclude that the sediments deposited behind 19th century milldams preserve a record of human activities in the Maury River watershed.

There were some limitations to the study, including the lack of absolute time constraints for the data, which made interpreting the timing of changes in land use difficult. Another consideration is the effect of fluvial processes on these sediments. This study was conducted on Maury River bank sediments, whereas many of the studies that apply similar methodologies are based on lake sediment archives. Thus, there could be influences on these geochemical data that are not accounted for in our interpretations.

With more research on the legacy sediments, there will be a greater understanding of the intensity that human activities long term and short term have on fluvial sediments and how those sediments impact the environment overall.

ACKNOWLEDGEMENTS

This material is based upon work supported by the Keck Geology Consortium and the National Science Foundation under Grant No. 1659322. The Keck team, Dr. Margret Anne Hinkle, Dr. Eva Lyon and my peers, Martina Pulido, Mia Groff, Katherine Larkin, Noah Willis, Kallan Wilde, Marina Croy, Christopher Goldmann, and Haley Culbertson all assisted in collecting the data and managing this project. In addition, I would like to thank Dr. James Zambito and James Rougvie, along with the entire Geology Department at Beloit College. Along with this, I would like to thank my family and friends for support throughout this entire process.

REFERENCES

Balascio, N.L., Kaste, J.M., Meyer, M.G., Renshaw, M., Smith, K., and Chambers, R.M., 2019, A high-resolution mill pond record from eastern Virginia (USA) reveals the impact of past landscape changes and regional pollution history: Anthropocene, v. 25, DOI :10.1016/j.ancene.2019.100190

Dean, J. R., Leng, M. J., Mackay, A.W., 2014, Is there an isotopic signature of the Anthropocene?: The Anthropocene Review. v. 1, p. 276-287. DOI:10.1177/2053019614541631

Dean, W. E., 1999, The carbon cycle and the biogeochemical dynamics in lake sediments: The Journal of Paleolimnology, v. 21, p. 375-393.

Deniro, M. and Epstein, S., 1981, Influence of diet on the distribution of nitrogen isotopes in animals; Geochimica et Comochimica Acta, Abstract, v. 45, p. 341-351, DOI:10.1016/0016-7037(81)90244-1

Dodoye-Alali, B., 1998, Terrace correlation from soil study along the Maury River, Virginia in Eleventh Keck Research Symposium in Geology Proceedings. Carleton College.

Hecky. R.E., and Kilham, P., 1988, Nutrient limitation of phytoplankton in freshwater and marine environments: a review of recent evidence on the effects of enrichment: Limnol. Oceanography, v.33, p. 796-822.

Holtgrieve, G.W., Schindler, D.E., Hobbes, W. O., Levitt, P.R., Ward, E.J., Bunting, L., Chen, G., Finney, B.P., Gregory-Eaves, I., Holmgren S., et al., 2011, A coherent signature of anthropogenic nitrogen deposition to remote watersheds of the northern hemisphere: Science, v. 334, 6062, p. 1545-1548. DOI:10.1126/science.12122267

James, L.A., 2013, Legacy sediment: Definitions and processes of episodically produced anthropogenic sediment: Anthropocene, v. 2, 16-26. DOI: 10.1016/j.ancene.2013.04.001

Kirwan, M.L., Murray, A.,B., Donnelly, J.P., Corbett, D.,R., 2011, Rapid Wetland expansion during

European settlement and its implication for marsh survival under modern sediment delivery rates: Geology, v. 39, 507-510. DOI: 10.1130/G31789.1

Miller. J. R., 1997, The role of fluvial geomorphic processes in the dispersal of heavy metals from mine sites: Journal of Geochemical Exploration, v. 58, 101-118.

Meyers, P.A., 1997, Organic geochemical proxies of paleoceanographic, paleolimnologic, and paleoclimatic processes: Organic Geochem, v. 27, 213-250. S0146-630(97)00049-1

Meyers, P.A. and Teranes, J.L. 2001, Sediment Organic Matter in Last W.M and Smol, J.P. (eds.), Tracking Environmental Change Using Lake Sediments: Physical and Geochemical Methods, Kluwer Academic Publishers, Dordrecht, v. 2, p 239-269.

Iosso, C., and Harbor, D. 2020, Impacts of Low-Head Dam Construction and Removal with Little Channel Sediment Storage: Case Study from the Maury River, Virginia, Undergraduate Thesis, Washington and Lee University, 27 p.

Niemitz, J., Haynes, C., and Lasher, G. 2013, Legacy sediments and historic land use: Chemostratigraphic evidence for excess nutrient and heavy metal sources and remobilization, Geology v. 41, p. 47-50., DOI: 10.1130/G33547

Palinkas, C.M., Testa, J.M., Cornwell, J.C., Li, M., Sanford, L. P., 2019, Influences of a River Dam on Delivery and Fate of Sediments and Particulate Nutrients to the Adjacent Estuary: Case Study of Conowingo Dam and Chesapeake Bay: Estuaries and Coasts, v. 42, p. 2072-2095 DOI:10.1007/s12237-019-00634-x

Pizzuto, J., and O'Neal, M., 2009, Increased mid-twentieth century riverbank erosion rates related to the demise of mill dams, South River, Virginia: Geology, v. 37, p. 19-22 DOI:10.1130/G25207A.1

Pavlowsky, R.T., Lecce, S.A., Owen, M.R., Martin, D.J., 2017, Legacy sediment, lead, and zinc storage in channel and floodplain deposits of the Big River, Old Lead Belt Mining District, Missouri, USA: Geomorphology, v. 299, p. 54-75, DOI: /10.1016/j.geomorph.2017.08.042

Rowe, H., Hughes N., and Robinson, K., 2012, The quantification and application of handheld energy-dispersive x-ray fluorescence (ED-XRF) in mudrock chemostratigraphy and geochemistry: Chemical Geology, v. 324-325, p. 122-131, DOI:10.1016/j.chemgeo.2011.12.023

Trout, W.E., 1992, The Maury River Atlas, Virginia Canals and Navigation Society. v. 2 Wilkinson, B.H. and McElroy, B.J., 2007, The impacts on continental erosion and sedimentation: Geological Society of America Bulletin, v. 119, p. 140-156. DOI: 10.1130/B25899

Walter, R. C., and Merritts, D. J. 2008, Natural streams and the legacy of water-powered mills: Science, v. 319, 299-304.

KECK Geology Consortium
Learning Science Through Research
Published by the Keck Geology Consortium
Short Contributions
Keck Geology Consortium
Volume 34
May 2022
doi: 10.18277/AKRSG.2022.34.12

MEASURING CHANGES IN CHANNEL MORPHOLOGY AND VOLUME OF MOBILIZED SEDIMENT FOLLOWING THE REMOVAL OF A LOWHEAD DAM IN ROCKBRIDGE COUNTY, VA

KATIE LARKIN, Washington & Lee University
Project Advisor: Eva Lyon

INTRODUCTION

Dam removals have increased in frequency in the 21st century (USGS Dam Removal Information Portal, 2020), and the environmental and geomorphological impacts of dams have been a popular topic of scientific study. Dams contribute to the fragmentation of rivers, in which a free-flowing channel is restricted to a number of slow-velocity or slackwater reaches (Graf, 1999). Slowed water velocity allows fine grains to settle, causing a localized buildup of fine sediment and depleting downstream areas of this material. By interrupting the natural movement of eroded solids and waters in rivers and changing the flux between reservoirs, fluvial systems begin to interact differently with the land through which they run (Marren, 2014). Dams are able to propagate signals up and downstream upon their emplacement; they cause an increase in local base level and cause a significant obstruction in the channel (e.g., Leopold & Bull, 1979; Merritts et. al, 2013; Dow et. al., 2020). Similarly, the removal of dams has the potential to interrupt the equilibrium state of a river, causing bank instability and incision into the riverbed, among other geomorphological reactions (Simon, 1994). Short-term studies on dam removals have been well-studied over the last few decades, but long-term channel impacts are far less understood (e.g., Merritts et. al., 2013).

The Maury River, a 42.8-mile-long tributary of the James River, is characterized by a coarse bed load and armor, consisting mostly of rounded Cambrian Keefer, Rose Hill, and Tuscarora sandstone cobbles and angular Ordovician Edinburg limestones. The Jordan's Point Dam (Fig. 1), a low head structure dating back to 1805, is one of numerous mill dams and lock-and-dam structures constructed on the Maury River in response to increased industrial activity. After a 70-year obsolescence, the structurally unsound dam was removed in May 2019; WLU student Chantal Iosso (2020) established baseline conditions following the removal of the dam and predicted future conditions. Notably, she found that the dam did not store significant quantities of fines during its emplacement. My investigation aims to characterize channel change over the last two years, using Iosso's data for comparison, in order to define the extent of post-removal channel restructure and adjustment. I will also provide quantitative data estimating change in channel area and the approximate volume of sediment mobilized since the dam removal.

Figure 1. The Jordan's Point Dam, seen looking upstream, in March 2019. The structures downstream of the dam are concrete pylons, which were part of an old railroad bridge (Young, 2019); they have since been moved and now reside on river left downstream of the dam.

METHODS

Field methods

Cross sections were measured in Summer 2021. Locations were selected based on cross sections measured in Iosso and Harbor (2020) (Fig. 2). The sections immediately above and below the dam experienced the most channel change and restructuring since 2019, and were thus subject to repeat measurement. Cross sections were measured using a TopCon GTS-301 Total Station to capture changes in elevation or channel morphology, both of which can indicate changes in river behavior. Channel width is thought to have undergone negligible change from 2019 to 2021 due to the relatively short time frame of the study; channel adjustments of this magnitude generally occur on a longer timeframe (e.g., Simon, 1994; Wolman and Leopold, 1957; Merritts et al., 2013).

Channel bed grain size analyses followed the Wolman pebble count procedure using a gravelometer. Three samples were measured at every meter along the transect. We calculated the mean grain size, or d_{50}, with this formula:

(smallest grain size (mm) x # obs.) + … (largest grain size (mm) x # obs.)/ (total obs.)

We calculated d_{90} by multiplying total observations by 0.9, then noting the value of the corresponding observation. During these calculations, any specimen with a grain size larger than 180 was assigned a size of 180+ millimeters and a phi value of 256, pertaining to the next largest size on a gravelometer. Given the exceptionally coarse nature of the alluvium, such an adjustment was performed numerous times. The focus of the grain size sampling was to understand longer-term changes in bed armor size and river competency.

Analytical methods

The resulting cross section plots constructed in Microsoft Excel were used to calculate channel measurements in three dimensions, including wetted perimeter, change in channel area, and volume of alluvium removed. Wetted perimeter was calculated using Pythagorean's Theorem. Waterline positions

Figure 2. Aerial view of 2019 and 2021 cross section locations. Inset map shows location of dam in the Maury River watershed.

noted during fieldwork were used to denote the boundaries of these measurements. Channel area was calculated based on changes in bed elevation made visible by the cross section projections. Trapezoidal under-curve area was calculated for each year; 2019 and 2021 under curve areas were subtracted from each other to determine total change in channel area.

The total volume of material removed between each cross section was calculated using a piecewise integration, which took distance and change in channel area at each cross section into account. The resulting value estimates the entire volume of sediment removed by extrapolating the results from each cross section onto the entire 376-meter-long study area.

Critical shear stresses for the d_{50} and d_{90} were calculated in order to gauge changes to the mobile fraction of alluvium; the following critical shear stress equation, developed by Shields (1936) and modified by Fischenich (2001) was used:

$$\tau_{cr} = 0.06 \times g(\rho_s - \rho_w)d \times \mathrm{Tan}\varphi$$

Where τ_{cr} is the critical shear stress, g is the acceleration due to gravity, ρ_w is the density of water, ρ_s is the density of the substrate, d is the particle size of interest, and φ is angle of repose of the substrate. Substrate density was assigned a value of 2659 kg/m^3 according to the bulk density of Tuscarora sandstone, a major unit making up the bed load in the Maury River (Manger, 1963).

RESULTS

Degradation, or localized removal of channel sediment, is the dominant channel response in all cross sections. Where alluvium has been removed, the "pockets" of removed alluvium tend to be lenticular in shape. Pockets in the upper reaches tend to be shorter and deeper, occurring more as concentrated zones rather than vast degradational areas found in the lower reaches (Fig. 3). In comparing the 2019 and 2021 cross sections, the thalweg seems to have migrated from the center of the river to river left and changed in profile from a sharp 'v-shape' to a gentler-sloped and wider zone of high-velocity flow, particularly in the upper reaches. Despite the consistent trend of degradation, channel shape is variable between the upstream and downstream areas.

In the upper reaches (Cross Sections 6, 7, and 8), degradation signals were strong and channel restructure was relatively consistent in shape and distribution. Repositioning of the thalweg to the center of the channel and significant erosion of material has resulted in a trapezoidal channel shape, particularly at Cross Sections 6 and 7 (Fig. 3); the thalweg is located on river left at Cross Section 8.

In the reaches just above the dam (4 and 5), the trend of degradation continues to a varying extent. Cross Section 5 remained practically unchanged between 2019 and 2021 and experienced only minor degradation. Cross Section 4 was subject to a high degree of degradation, and the elevation of the channel bottom has been reduced by a noticeable amount.

Degradation continues at and below the dam, though to a lesser magnitude than observed upstream. Channel roughness increased between 2019 and 2021 at Cross Section 3 (site of the dam), and numerous small v-shaped breaks in the dam structure have developed. The channel at Cross Section 1 below the dam is wider, flatter, and generally symmetrical in shape. Degradation in this area is minor, but distributed throughout the entire channel instead of in pockets.

Channel area (Fig. 4) increased between 2019 and 2021 at every cross section. Minimal change in area was observed at the dam (Cross Section 3) and the maximum observed change in area occurred just upstream at Cross Section 4. Percent change in channel area was disproportionately large at Cross Section 6. Taking the changes in channel area into account, an estimated 3,934.7 m^3 of alluvium has been mobilized between 2019 and 2021 over the course of the 376-meter study site.

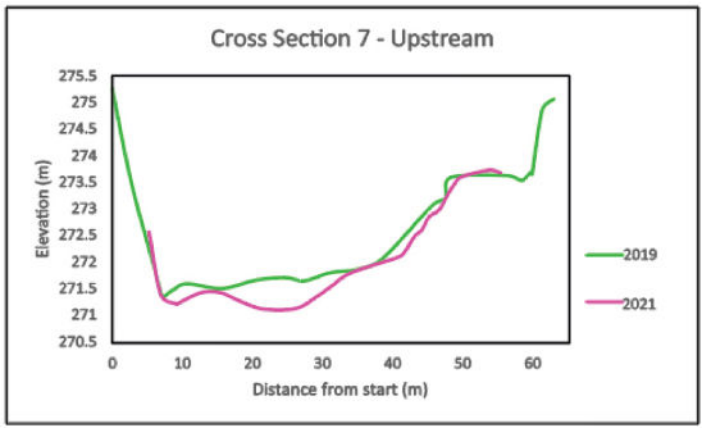

Figure 3. Example cross section from the upper reach, about 300 meters upstream of the removed dam.

Both average grain size and grain size distribution increased between 2019 and 2021. 2019 d_{50} values for Cross Sections 4, 7, and 8 were the same, but a higher d_{90} value was recorded for Cross Section 4. 2021 measurements recorded the highest d_{50} value for Cross Section 1, and the highest d_{90} values for Cross Section 4. The d_{90} at Cross Section 4 is double that of Cross Sections 7 and 8, exceeding the 1.67x difference observed in 2019. Between 2019 and 2021, the percent increases in d_{50} from downstream to upstream (4 to 8) are 187%, 111%, and 101%. The percent increases in d_{90} are 105%, 70.6%, and 70.6%. Greatest changes in average and 90th-percentile grain sizes are present at cross section 4, just upstream of the former dam site. Shear stresses have declined between 2019 and 2021 at each cross section. Critical shear stress increases at each cross section reflect the aforementioned changes in grain sizes between 2019 and 2021.

DISCUSSION

Channel cross sections recorded a change in channel area from 4-25 m^2, with proximity to the dam and channel substrate acting as the largest controls. Lowest levels of degradation were recorded at Cross Section 5, the only location where limestone bedrock makes up a significant part of the channel. Mobilization

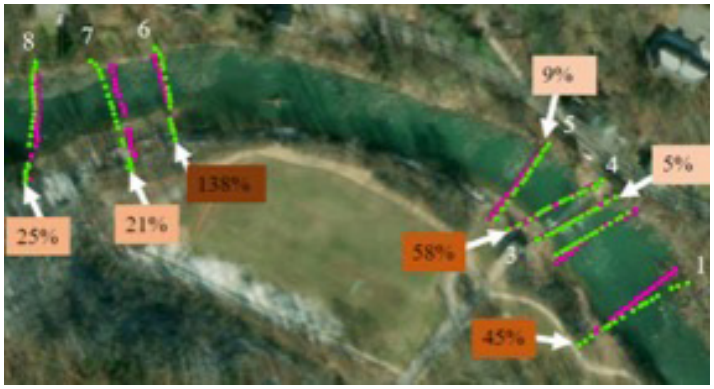

Figure 4. Calculated change in channel area between 2019 and 2021.

of this limestone bedrock is heavily dependent on numerous conditions; entrainment, or 'quarrying' of bedded carbonates is controlled by the location and orientation of fractures as well as hydraulic conditions (Miller, 1991). The evolution of bedrock channel systems in response to disturbances is also understood to operate on a longer timeframe than alluvial systems. Thus, the retention of channel structure at this location makes sense given the channel substrate.

The highest degree of degradation occurred just upstream of the dam at Cross Section 4, where the erosive effect of dam breaching would be strongest. Distribution of degradation downstream of the dam was measurable (7 m^2) but shallow and relatively evenly distributed within the channel, as opposed to the pocketed removal visible in the upper reaches. Iosso (2020) recorded higher channel bed elevations in a sediment ramp immediately upstream of the dam, but this was the only significant buildup of sediment in the channel recorded in 2019. Iosso hypothesized that grain sizes as large as cobbles (64-256 mm) were able to be transported over the dam during high flow. Pearson and Pizzuto (2015) made similar observations, noting that transport of sediment over a low-storage impoundment was aided by a sediment ramp. Degradation at Cross Section 4 has likely recorded the mobilization and leveling of this ramp, as opposed to the incision of a legacy sediment package.

Changes in channel bed armor makeup reflect the changes in flow conditions made evident by the cross sections. Percent change in grain size decreases in magnitude moving upstream, given the inverse relationship between geomorphic signal intensity and distance from the disturbance (Simon & Hupp, 1987). Additionally, bed armor grain sizes in the upper reaches tend to be smaller than those at and downstream of the dam site; a wider range of values was also observed in the lower reaches. The growing range of grain sizes and diversity of channel structure is reflective of a restoration of unobstructed flow, in which flow conditions and sediment behavior differ greatly depending on location (Kibler et al., 2011). This is in contrast to the prior dammed status of the river, wherein the river was restricted to a dammed 'pool' and was subject to slackwater conditions.

HEC-RAS modeling by Iosso (2020) found that a significant increase in sediment transport capacity was likely for the 500 meters of river upstream of the dam; given the extent of degradation and coarsening of the riverbed, this prediction appears to have been correct. At the time of sampling, Iosso found that d_{90} cobbles were mobilized by events as small as 2-year floods; however, her recorded d_{90} values of 74-150 mm are comparatively smaller than the 128-256 mm range observed in 2021. Floods are known to serve as major geomorphic events that have the potential to mobilize a large range of cobbles. Between 2019 and 2021, peak discharge was recorded as a 1.5 year flood (USGS NWIS, 2022). Elevated transportation capacity has likely played a major role in the shaping of the channel. The relatively minor peak discharge between 2019 and 2021 was able to transport material, meaning that high-discharge events will continue to erode the mobile fraction of the subarmor. Currently, interplay between sediment load and transport capacity continue to define the extent of equilibration; as the bed armor coarsens, mobile sediment supply is increasingly limited. As expected from the increase in grain size, critical shear stress of d_{90} sediment in 2021 (112.4 - 224.9 N/m^2) is notably higher than 2019 (65.9 - 109.8 N/m^2), and no observations support a significant change in flow conditions following Iosso's work.

CONCLUSIONS

Between 2019 and 2021, conditions in the Maury River have been conducive to mass mobilization of sediment and channel restructure. The degradation of almost 4000 m^3 of sediment from the 376 meter reach is consistent with observations from other dam removals (e.g., Merritts et. al, 2013; Kibler

et. al, 2011; etc), though this degradation has likely occurred to a lesser extent due to the coarseness of the alluvium. Bed armor grain size analyses support an immediate winnowing of fine sediment stored in the channel was induced by the dam removal and subsequent base level fall. Mobilization of remaining larger cobbles is ongoing, but peak sediment flux has likely already occurred (e.g., Merritts et al., 2014).

ACKNOWLEDGEMENTS

This material is based upon work supported by the Keck Geology Consortium and the National Science Foundation under Grant No. 2050697. This research was also supported by the Edgar W. Spencer (‘53) Geology Field Research Fund. I also thank Keck Advisors, Drs. Eva Lyon and Margaret Anne Hinkle, fellow students Ani Croy, Haley Culbertson, Christopher Goldmann, Mia Groff, Maddie Holicky, Martina Pulido, Kallan Wilde, and Noah Willis. Finally, thanks to Chantal Iosso and Dr. David Harbor, whose work helped form the foundation of this study.

REFERENCES

Dow, S., Snyder, N.P., Ouimet, W.B., Martini, A.M., Yellen, B., Woodruff, J.D., Newton, R.M., Merritts, D.J., and Walter, R.C., 2020, Estimating the timescale of fluvial response to anthropogenic disturbance using two generations of dams on the South River, Massachusetts, USA: Earth Surface Processes and Landforms, v. 45, p. 2380–2393, doi:10.1002/esp.4886.

Graf, W.L., 1999, Dam nation: A geographic census of American dams and their large-scale hydrologic impacts: Water Resources Research, v. 35, p. 1305–1311, doi:10.1029/1999WR900016.

Fischenich, C., 2001, Stability Thresholds for Stream Restoration Materials: Engineer Research And Development Center Vicksburg Ms Environmental Lab, https://apps.dtic.mil/sti/citations/ADA392430 (accessed April 2022).

Kibler, K., Tullos, D., and Kondolf, M., 2011, Evolving Expectations of Dam Removal Outcomes: Downstream Geomorphic Effects Following Removal of a Small, Gravel-Filled Dam1: Evolving Expectations of Dam Removal Outcomes: Downstream Geomorphic Effects Following Removal of a Small, Gravel-Filled Dam: JAWRA Journal of the American Water Resources Association, v. 47, p. 408–423, doi:10.1111/j.1752-1688.2011.00523.x.

Leopold, L.B., and Bull, W.B., 1979, Base Level, Aggradation, and Grade: American Philosophical Society, 35 p.

Leopold, L.B., and Wolman, M.G., 1957, River channel patterns: Braided, meandering, and straight: U.S. Government Printing Office Professional Paper USGS Numbered Series 282-B, 50 p., http://pubs.er.usgs.gov/publication/pp282B (accessed April 2022).

Manger, G. E., Porosity and bulk density of sedimentary rocks, 1963, doi:10.3133/b1144E.

Marren, P.M., Grove, J.R., Webb, J.A., and Stewardson, M.J., 2014, The Potential for Dams to Impact Lowland Meandering River Floodplain Geomorphology: The Scientific World Journal, v. 2014, p. 1–24, doi:10.1155/2014/309673.

Merritts, D. et al., 2013, The rise and fall of Mid-Atlantic streams: Millpond sedimentation, milldam breaching, channel incision, and stream bank erosion, in The Challenges of Dam Removal and River Restoration, Geological Society of America, doi:10.1130/2013.4121(14).

Miller, J.R., 1991, The Influence of Bedrock Geology on Knickpoint Development and Channel-Bed Degradation along Downcutting Streams in South-Central Indiana: The Journal of Geology, v. 99, p. 591–605, doi:10.1086/629519.

Pearson, A.J., and Pizzuto, J., 2015, Bedload transport over run-of-river dams, Delaware, U.S.A.: Geomorphology, v. 248, p. 382–395, doi:10.1016/j.geomorph.2015.07.025.

Shields, A. (1936) Application of similarity principles and turbulence research to bed-load movement. California Institute of Technology , Pasadena, CA. (Unpublished)

Simon, A., and Hupp, C.R., 1987, Channel Evolution In Modified Alluvial Streams: Transportation Research Record, p. 9, http://pubs.er.usgs.gov/publication/70014832 (accessed April 2022).

Simon, A., 1994, Gradation processes and channel evolution in modified West Tennessee streams; process, response, and form: Professional Paper, doi:10.3133/pp1470.

Wildman, L.A.S., and MacBroom, J.G., 2005, The

evolution of gravel bed channels after dam removal: Case study of the Anaconda and Union City Dam removals: Geomorphology, v. 71, p. 245–262, doi:10.1016/j.geomorph.2004.08.018.

KECK Geology Consortium
Learning Science Through Research
Published by the Keck Geology Consortium
Short Contributions
Keck Geology Consortium
Volume 34
May 2022
doi: 10.18277/AKRSG.2022.34.13

THE GEOCHEMISTRY OF RELICT MILL POND WATERS AND STRATIFIED RESERVOIRS IN THE SHENANDOAH VALLEY, VA

MARTINA PULIDO, Beloit College
Project Advisor: James Rougvie

INTRODUCTION

An assessment of stratified reservoirs and their impact on aqueous geochemistry is imperative to mitigate the effects of Mn and N contamination. Seasonally stratified reservoirs allow metals, such as manganese (Mn) and iron (Fe), to accumulate in the water column due to reducing conditions, and be released to downstream rivers through dam discharge (Munger et al., 2017). Dam removal can remobilize and release soluble contaminants from impounded sediments to water systems, and transport them downstream along with the now remobilized sediments (Niemetz et al., 2013; Curran and Coveleski, 2021). Mn and N are of particular interest, due to their known impacts on human and environmental health. This study aims to better understand contaminants in water systems for the purpose of improving water quality.

Manganese is a naturally occurring metal that has been identified as a potential contaminant in Roanoke County groundwaters (Kiracofe et al., 2017) and dam impacted water (Munger et al., 2017). In oxic waters, insoluble Mn is trapped in benthic sediments as Mn (oxyhydr)oxide minerals or bound to stream sediments via sorption processes, as evidenced by changes in aqueous Mn concentrations downstream of dams (Gordon et al., 1984; Hess et al., 1989; Dortch & Hamlin-Tillman, 1995; Ashby et al., 1999). In anoxic conditions (such as those at depth within a lake or reservoir), Mn can be reduced to Mn^{2+} which is most stable in the aqueous phase, thereby allowing the metal to become heavily concentrated (Davison, 1993). If waters are released via a bottom sluice gate or dam tailrace, Mn^{2+} can be transported downstream, and may be present in the flowpath for months after leaving reducing conditions (Munger et al., 2017). When the tailrace transports anoxic impounded sediments and water, the contaminants accumulate further downstream, thereby impacting community and environmental health.

Elevated concentrations of Mn^{2+} and other contaminants in water have a negative impact on the quality of human life. When ingested over extended periods of time even in relatively low concentrations, Mn^{2+} presents symptoms of headaches, depression, and learning impairments in children (Spangler and Spangler, 2010). Consequently, the EPA has established an unenforceable Health Advisory (of 300 ppb Mn) in drinking water to decrease Mn^{2+} health effects (EPA, 2004).

The greatest threat to the Chesapeake Bay Watershed is eutrophication– the excessive nutrient enrichment as a result of phosphorus and nitrogen in water causes hypoxia, and a decrease in aquatic life (EPA, 2021). P and N are of particular interest as, when released from legacy sediments post-dam removal, they are difficult to control (Riggsbee et al., 2011). Phosphate is an anion that is naturally derived from phosphorus in phosphate minerals,which are mined for agricultural and industrial use (Florida Industrial and Phosphate Research Institute 2017). Phosphorus and nitrogen can enter watersheds as runoff from industrial, agricultural, and household cleaning products (European Environmental Agency, 2005). Increased P in water systems leads to eutrophication, creating anoxic water conditions ideal for Mn^{2+} solubility. Monitoring and identifying sources of excessive N and P enrichment is imperative to restoring watershed health. When a dam tailrace transports remobilized sediments, impounded waters, and soluble metals, the downstream water and ecosystems may be polluted with Mn^{2+}, N, and P.

The area of focus is the Maury River in Rockbridge County, Virginia (VA), located in the James Basin of the Chesapeake Bay Watershed. The Maury River contains many structures; our focus is a combination of six obsolete as well as operating dams. Most obsolete dams are along the river, with Lake Merriweather at its headwaters (Fig. 1). McCormick's Mill Dam is located outside of the Maury River watershed. Sites were selected to evaluate changes in water geochemistry as a function of stratification and location. In this assessment, we analyze aqueous geochemical characteristics to evaluate potential pollutants, with a focus on soluble aqueous manganese ([Mn^{2+}]), phosphorus and total nitrogen (TN).

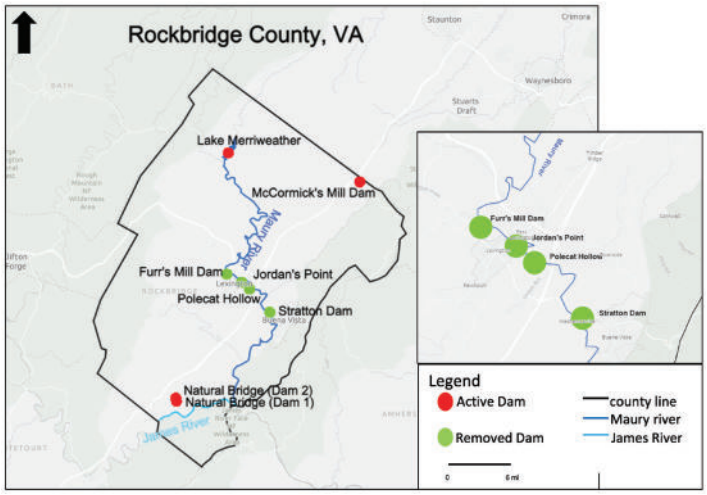

Figure 1. Sample sites in Rockbridge County, VA. Red points show operating dams. Green points show demolished dams. Figure by Kallan Wilde.

METHODS

Data collected included GPS coordinates, water at varying depths, and field data. To collect in situ water chemistry field data (pH, dissolved oxygen, temperature, and specific conductivity), a YSI 556 Multi-Probe System (MPS) was lowered to the desired depth. All bottled samples were immediately sealed and promptly refrigerated upon return to the lab. One aliquot of each sample was filtered; another aliquot was filtered and acidified. A phenolphthalein titration with a bromocresol green-methyl red titration test was used to collect alkalinity measurements. Filtered but unacidified samples were analyzed for major cation (e.g., Ca^{2+} , Mg^{2+}, Na^{+}, K^{+}, NH_4^{+}) and anion (e.g., Cl^{-}, SO_4^{2-}, NO^{3-}, NO^{2-}) concentrations by ion chromatography (IC) analysis. TN was calculated as the sum of ammonia (NH_4^{+}), nitrate (NO^{3-}), and nitrite (NO^{2-}). To perform the inductively coupled mass spectroscopy (ICP-MS) analysis (P, Cl, K Al, Fe, Mn), the filtered and acidified samples were diluted with a 1:1 ratio with 2% nitric acid solution (trace metal grade).

Sites of interest included reservoirs behind extant dams, and former dam localities where pockets of stagnant water remained (Fig. 1). Extant dams were found at Lake Merriweather (LM), McCormick's Mill Dam (MMD), and Natural Bridge Dam (NBD). Obsolete dams include Polecat Hollow (PH), Stratton's Dam (SD), Furr's Mill Dam (FMD), and Jordan's Point (JP).

RESULTS

As expected, DO and temperature change as a factor of depth. At McCormick's Mill, where sampling was repeated every 3-4 months, DO increases from summer to winter as expected due to the temperature dependence of gas solubility (Fig. 2A). Temperature decreases with depth, as expected. The aqueous Mn concentration generally increases from shallow waters to deep waters (Fig. 2B). Total nitrogen varies with depth, initially decreasing, before increasing towards the bottom of the reservoir (Fig. 2C).

Lake Merriweather has the largest range of Mn^{2+} concentrations, and the greatest TN concentration of all sample sites (Fig. 3A). Over 25% of data collected at LM lies above the EPA human health advisory benchmark of 300 ppb (HA). The upper quartile is $\log(Mn^{2+})=1.93$. The lower quartile is $\log(Mn^{2+})=0.55$. McCormick's Mill Dam contains the second highest concentration of Mn^{2+}. All other obsolete dams contained Mn^{2+} concentrations that did not exceed EPA standards, but show a medium-large distribution (Fig. 3). In comparison, NBD has negligible Mn^{2+} concentrations, and the smallest distribution of data. Mn^{2+} concentrations that exceed EPA standards are at LM and MMD.

The highest concentration and distribution of TN is at Lake Merriweather. TN exceeds HA EPA guidelines at all sites (Fig. 3B) (EPA, 2009). Phosphorus does not exceed SMCL EPA limits at any site on the Maury

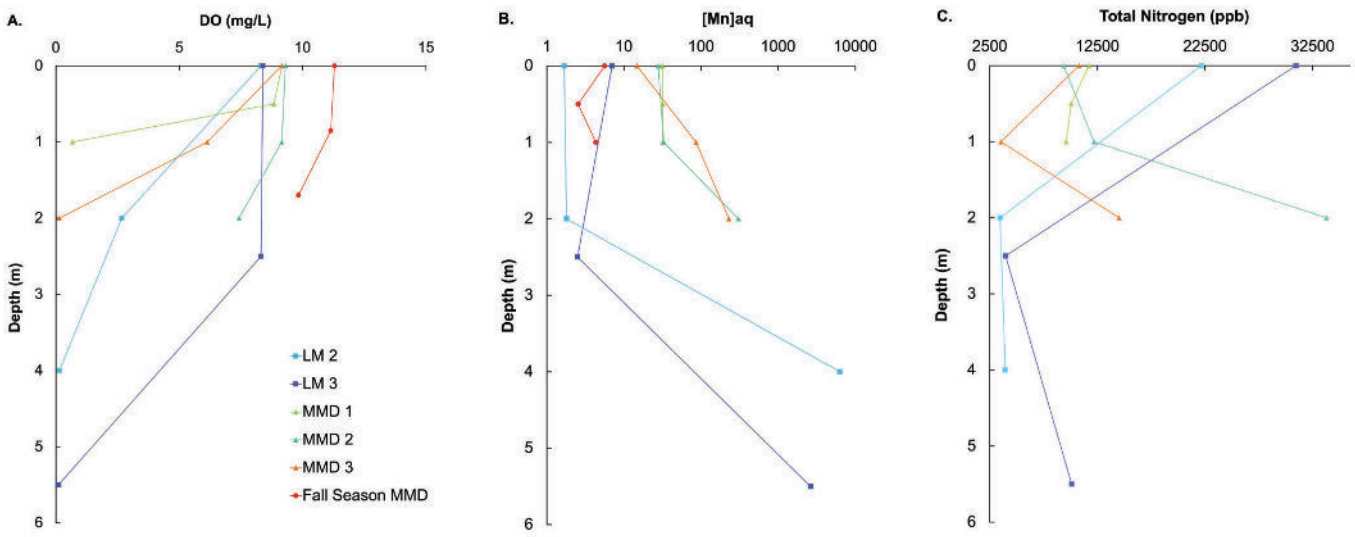

Figure 2. A) Relationship between dissolved oxygen (mg/L) and depth. DO decreases with depth for samples from Lake Merriweather (LM) and McCormick's Mill Dam (MMD). Chemoclines for (B) Mn(II) and (C) total nitrogen. Mn(II) increases with depth for both samples from LM and all samples from MMD collected in summer. Only the water sampled in fall from MMD had no clear relationship between Mn(II) and depth.

River (Figure 3D). Iron exceeds SMCL only at Lake Merriweather (Fig. 3C). The highest concentrations for aqueous Mn^{2+}, TN, and Fe are found at Lake Merriweather. The largest concentration of P can be found in the non-stratified reservoirs.

All non-stratified sites and Lake Merriweather have similar hydrochemical facies (Fig. 4). These samples present a calcium cation type, and a bicarbonate anion type, which corresponds to a calcium bicarbonate type. The samples demonstrate that weak acids exceed strong acids. Finally, we can determine that alkaline earths exceed alkalis in these samples.

With some minor differences in anion and cation concentrations, MMD exhibits similar hydrochemical facies to other sites (Fig. 4). The sample demonstrates that weak acids exceed strong acids and that alkaline earths exceed alkalis. Furthermore, MMD has higher total dissolved solid (TDS) than all other sites.

IMPLICATIONS OF THIS WORK

Are waters behind dams stratified?

Three dams were tested for stratification: LM, MMD, and NBD. LM and MMD are stratified, with temperature and DO decreasing with increasing depth. NBD is not stratified; its reservoir is not large enough to allow for significant changes in temperature and DO with depth. Similarly, all other sites (obsolete dams) are not stratified.

Stratified reservoirs are characterized by changes in temperature and DO with depth. Furthermore, this study investigated the stratified characteristics of specific conductivity; conductivity increases with depth. Greater conductance reflects an increase in total dissolved solids. Lastly, LM can be categorized as 'more stratified' than MMD – its lower temperature and DO correspond with a low specific conductivity and higher concentrations of Mn^{2+}.

Are contaminants, including Mn, present behind dams?

All sites contain aqueous Mn^{2+} (Fig. 2A) with variable concentrations. Mn^{2+} exceeds the Environmental Protection Agency (EPA) human health benchmark at LM and MMD (Fig. 3A), the only two stratified reservoirs. At these two sites, Mn^{2+} increases with depth, where low oxygen conditions exist. Lake Merriweather performs regular flushes; water mixing as a result of water mobilization oxidizes the reservoir. Under such conditions, soluble Mn may be mobilized, but eventually decreases in concentration downstream via oxidative precipitation or sorption processes (Gordon et al., 1984; Hess et al., 1989; Dortch & Hamlin-Tillman, 1995; Ashby et al., 1999; Munger et al., 2017). This scenario can serve as a model for 'dam removal' and the resulting impacts on water chemistry. If a dam is removed, then the reservoir no

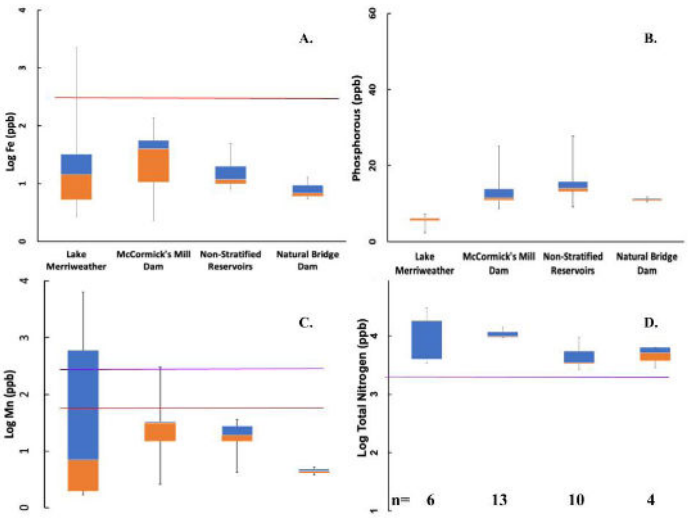

Figure 3. Box plot showing log(Mn^{2+}) distribution between LM, MMD, and the non-stratified reservoirs of the Maury River. Non-stratified reservoirs contain Polecat Hollow, Stratton's Dam, Jordan's Point, and Furr's Mill Dam. Lower boundary has Natural Bridge Dam. Blue boxes are the upper quartile of data; orange boxes are the lower quartile. Red line marks EPA Secondary Maximum Contaminant Level (SMCL) log(50 ppb), purple line marks EPA Health Advisory (HA) log(300 ppb).

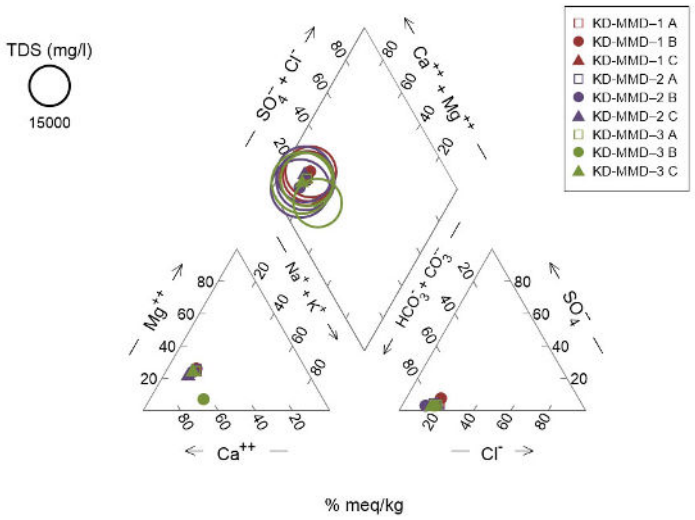

Figure 4. Piper diagram showing hydrochemical facies for waters from behind McCormick's Mill Dam (MMD). Different colored markers represent three sampled sites within the reservoir.

longer stratifies, and soluble materials are remobilized in an oxidized environment, eventually changing to insoluble forms. Less aqueous Mn^{2+} results in less Mn contamination.

Three other aqueous elements of interest (Fe, N, and P) were studied, though only one was not found at high concentrations. Iron is not the focus of this study, but it was found to increase in concentration as a factor of depth at LM and MMD similar to Mn. Concentrations of phosphorus do not exceed EPA standards at any sites. There are elevated concentrations of TN throughout all sites tested on the Maury River (Fig. 3D). Future impacts suggest that high TN concentrations in water will acidify and aggravate eutrophication downstream.

How do stratified reservoirs compare to non-stratified reservoirs?

All sites can be categorized as a calcium and magnesium bicarbonate type (Fig. 4), according to their hydrochemical facies (Piper, 1944). However, three sites deviate from this trend: LM, MMD, and NBD. These three sites vary in their chemical composition, but there is one link between them: active dams. Two of the three sampling sites at LM have calcium magnesium sulfate type waters; MMD has a high TDS, and greater ionic concentrations; NBD has a calcium magnesium sulfate type at depth. At these stratified reservoirs, specific conductivity and alkalinity increase with depth. LM is found in a shale bedrock, while MMD is within a limestone bedrock. The surrounding karst terrain increases alkalinity, the buffering capacity of the solution, and conductivity. High alkalinity and high conductivity are consistent with high TDS observed at MMD.

CONCLUSION

Contaminant solubility of the Maury River is dependent on stratified conditions, impacting the aqueous chemistry downstream, and influences in-situ chemical characteristics as well. The stratification of reservoir dams like LM and MMD, at the head of the Maury River, promotes ideal conditions for the solubility of aqueous Mn^{2+} and Fe^{2+}. Impounded water at depth creates oxygen-reducing conditions ideal for aqueous Mn^{2+} solubility and high conductivity. Lake Merriweather and McCormick's Mill Dam contain the highest aqueous Mn^{2+} concentrations. These sites are stratified reservoirs, but other chemical characteristics vary. Lake Merriweather is overall less conductive, less oxygenated, and colder than McCormick's Mill Dam.

Some elements are not influenced by the stratification, such as silicon and phosphorus. Sources of silicon, phosphorus, and total nitrogen can be derived from

surrounding bedrock or land use. LM source material is derived from the surrounding shale bedrock, and all other sites lie within a limestone bedrock. The bedrock runoff can be accumulated at both stratified and non-stratified sites. TN is potentially present as a result of surrounding agricultural land use and wastewater runoff. Future investigations could involve an analysis of the aqueous chemistry of high TN waters in comparison to Maury River reservoirs. Similarly, silicon inputs and elevated concentrations are dependent on location and proximity to the river, as opposed to stratified conditions. Phosphorus does not show significant impacts in the Maury River, perhaps due to lower input of P.

The findings of this study are indicative of the Maury River's susceptibility to some water contaminants from active impoundments. Elevated Mn^{2+} concentrations found at the stratified reservoirs pose a potential health risk in the case of dam failure or reopening the bottom drain sluice gate, closed since 2012 per Virginia Department of Environmental Quality orders (Stuart, 2012). While there are low P concentrations throughout the sites here analyzed in the Maury River, high TN behind these impoundments may increase the risk of eutrophication downstream. Contaminant conditions are influenced by reservoir size and stratified conditions, and are reflected by changes in TDS.

ACKNOWLEDGMENTS

This material is based upon work supported by the Keck Geology Consortium and the National Science Foundation under Grant No. 2050697. Additional funding for this project was generously provided by the Washington and Lee Office of the Provost and Geology Department. In addition to Washington and Lee University Geology advisors Margaret Anne Hinkle and Eva Lyon, we wish to thank Sarah Wilson and Emily Falls (W&L Geology). Data collection could not have been possible without the assistance of Jeffrey Parks, Sarah Teagle, and Keck students Chris Goldman and Ani Croy. Additionally, this study would like to thank Beloit College Advisor Jim Rougvie for endlessly reviewing, editing, and supporting this process. Finally, the author is thankful to Julia Hwang and Jo Medusa, for reminders of perseverance and accomplishment.

REFERENCES

Ashby, S. L., Myers, J. L., Laney, E., Honnell, D., & Owens, C. (1999). The effects of hydropower releases from Lake Texoma on downstream water quality. Journal of Freshwater Ecology, 14, 103–112.

Davison, W. (1993). Iron and manganese in lakes. Earth Science Reviews, 34, 119–163.

Dortch, M. S., & Hamlin-Tillman, D. E. (1995). Disappearance of reduced manganese in reservoir tailwaters. Journal of Environmental Engineering, 121, 287–297.

Environmental Protection Agency U.S., 2013, Addressing nutrient pollution in the Chesapeake bay: https://www.epa.gov/nutrient-policy-data/addressing-nutrient-pollution-chesapeake-bay (accessed December 2021).

Environmental Protection Agency U.S., 2009, Total Nitrogen, National Service Center for Environmental Publications: https://nepis.epa.gov/Exe/ZyPURL.cgi?Dockey=P10070OQ.txt (accessed April 2022).

European Environment Agency, 2005. Source apportionment of nitrogen and phosphorus inputs into the aquatic environment. European Environment Agency Report 7, Office for Official Publications of the European Communities: Luxembourg. ISBN 92-9167-777-9. 48 pp.

Gordon, J. A., Bonner, W. P., & Milligan, J. D. (1984). Iron, manganese, and sulfide transformations downstream from Normandy Dam. Lake and Reservoir Management, 1, 58–62.

Henika,W.S., Kiracofe, Z.A.,Schreiber M.E., 2017, Assessing the Geological Sources of Manganese in the Roanoke River Watershed, Virginia: Environmental & Engineering GeoScience, v. 23, p. 43–64.

Hess, G. W., Kim, B. R., & Roberts, P. J. W. (1989). A manganese oxidation model for rivers. Journal of the American Water Resources Association, 25, 359–365.

Munger, Z.W., Shahady, T.D., and Schreiber, M.E., 2016, Effects of reservoir stratification and watershed hydrology on manganese and iron in a dam-regulated river: Hydrological Processes, v.

31, p. 1622–1635.
Niemitz, J., Haynes, C., and Lasher, G. 2013, Legacy sediments and historic land use: Chemostratigraphic evidence for excess nutrient and heavy metal sources and remobilization: Geology, v. 41, p. 47–50.
Piper, Arthur (1944). “A graphic procedure in the geochemical interpretation of water-analyses”. Transactions, American Geophysical Union. 25 (6): 914–928. Bibcode:1944TrAGU..25..914P. doi:10.1029/TR025i006p00914.
Riggsbee, J.A., Wetzel, R., and Doyle, M.W., 2012, Physical and plant community controls on nitrogen and phosphorus leaching from impounded riverine wetlands following dam removal: Nutrient leaching following dam removal: River Research and Applications, v. 28, p. 1439–1450.
Spangler, J. G.; Reid, J. C. Environmental manganese and cancer mortality rates by county in North Carolina: An ecological study. Biol. Trace Elem. Res. 2010, 133 (2), 128−135.
Stuart, Sandra (2012). “Impounding Structure Regulations.” Virginia Administrative Code, Title. 4, Agency. 50, Ch. 20.

KECK Geology Consortium
Learning Science Through Research
Published by the Keck Geology Consortium
Short Contributions
Keck Geology Consortium
Volume 34
May 2022
doi: 10.18277/AKRSG.2022.34.14

ANALYSIS OF LAND USE IN ROCKBRIDGE COUNTY, VA, FROM PRECOLONIAL TIMES TO CURRENT DAY AND CONSEQUENCES FOR RIPARIAN ECOSYSTEMS

KALLAN R. WILDE, Saint Norbert College
Project Advisor: Nelson Ham

INTRODUCTION

In 1816 Virginia implemented one of the earliest programs of infrastructure improvements, called The Fund for Internal Improvement, designed to enhance commerce after the American Revolution. The program was implemented in response to a sense of urgency within the state to share in the wealth of the new country. Virginia implemented improvements to its extensive river system, which facilitated these commercial needs (McKee, 2003). By 1860 there were approximately ten navigation-dam structures and at least thirty mill-dam structures operating along waterways in Rockbridge County, VA (Rockbridge Co., Va. [186]).

Emplacement of dams caused a decrease in stream velocity, which allowed suspended sediments to settle behind the dam structures. These sediments, hereafter called legacy sediments, can hold a record of changes in land use such as agriculture, timbering, and development that have replaced indigneous stewardship (Walter and Merritts, 2008). The goal of this study is to learn how dam emplacement or removal and land use in Rockbridge County, Va affected the waterways, in particular the Maury River, over time.

The study area is located in the James and Maury River watersheds. Geologically, Rockbridge County is located in the Valley and Ridge province of Virginia. Bedrock in the region is primarily composed of limestone, calcareous shale, and dolomite; however, there are some exposures of sandstone and conglomerate in the region as well (Wilkes, 2007). Four dam sites were sampled from Rockbridge County, VA along the Maury River. This study uses maps and other historical data to construct GIS visualizations of past and present land use, and create estimates of floodplain and water levels during the various intervals of history in the watershed. Age dating of sediment sampled in river banks was attempted to create a more accurate timeline of watershed history.

METHODS

During summer 2021, sediment and water samples were collected from eight dam sites in Rockbridge County, VA (Figure 1). After sample collection, laboratory analyses were completed to create a historical record of environmental changes from pre-colonial times to present day and to identify potential water contaminants. These samples are being examined by me and four other colleagues from various universities and colleges as part of the Keck Geology Consortium 2021 Advanced Project. Samples were taken from the banks of removed dams for geochemical analysis and to establish sedimentation rates. Samples were collected every 5-10 cm from near-vertical outcrops. Organic material was isolated from the bank sediments collected using the Center for Mass Spectrometry's standard operating procedures with the intent to radiocarbon (C14) date the sediments collected, but could not be radiocarbon dated due to concerns of potential contamination from lab procedures. Future work for this study will involve re-sampling to construct an age model using Pb-210.

My study was focused on identifying potential pollution sources for the Maury River watershed from historical data sets. ArcGIS software was used to

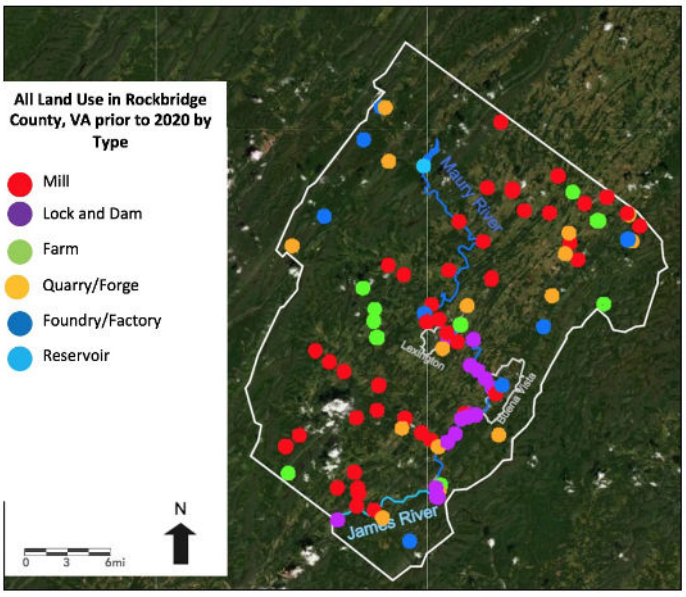

Figure 1. Land use in Rockbridge County, VA prior to 2020 organized by type.

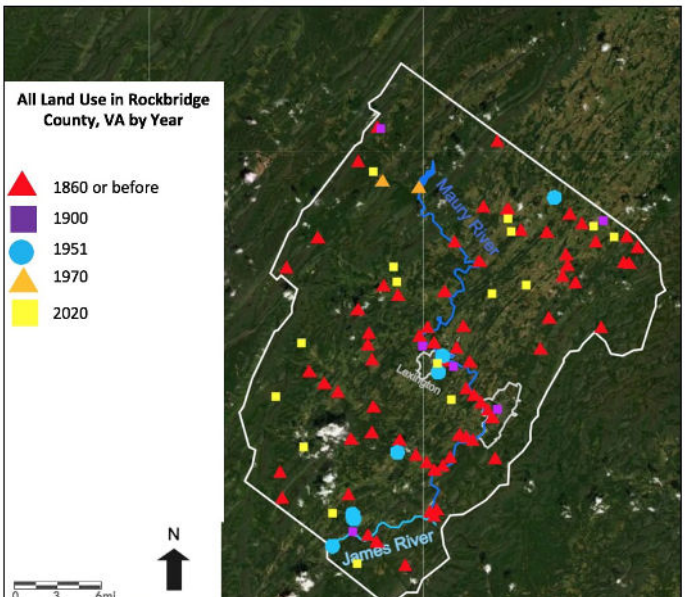

Figure 2. All land use in Rockbridge County, VA categorized by year.

create maps at various points in history to construct a visual timeline of events and evolution of land use in the region over time. Data for these maps was collected using historical maps, aerial photos, LiDAR data, census data and other historic documents. Maps and photos were converted into .tiff files and georeferenced onto the base layer. Data from these files was then highlighted using polygon, line, and point feature classes.

2D models were made to compare water levels in 1964, 1977, and 2018 to compare topography from the beginning, middle, and end of the study timeframe. These years were selected based on available topographic maps and to show changes in the landscape through time. The modeling was done by creating DEMs from the available topographic maps and LiDAR data, and then highlighting the various elevations in the county with different colorations. 3D models of areas downstream of Jordan's Point and Lake Merriweather were made by taking the 2D map and converting it to a local scene, exaggerating the elevation by 2.00 to give depth to the map, and zooming into the sites of interest.

Discharge data for areas downstream of these two dam sites was accessed from the USGS Water Data Online Mapper (USGS, 02024000 and USGS 02021500). The data was then imported to Excel to create graphs depicting change in discharge downstream of two dam sites: one showing before and after dam emplacement (Lake Merriweather) and one showing before and after dam removal (Jordan's Point).

RESULTS AND FUTURE WORK

The Fund for Internal Improvement allowed Virginia to implement improvements to its extensive river system to facilitate its commercial needs (McKee, 2003). Figures 1 and 2 illustrate how land use in the region has changed since the implementation of the internal improvement through 1970. Figure 3 depicts current day land use as of 2020.

During the study timeframe, a total of at least sixty-four dams, including approximately forty-five mill dams, fifteen lock dams, and four reservoir dams, have operated in the county. Approximately seventeen furnaces/foundries and twenty-three iron mines/quarries have operated in the county. Approximately twenty farms that operated/are operating in the county have been accounted for, but this number is certainly an undercount. Locations of farms found in census records were difficult to find due to lack of old property records, and have not been marked on the maps (Rockbridge Co., Va. [186], U.S. Department of the Interior, and Rockbridge County, Va.)

There was insufficient data from pre-colonial and early colonial times to put together a map for these periods, but based on the timelapse maps we know most of the European land use practices were put in place before

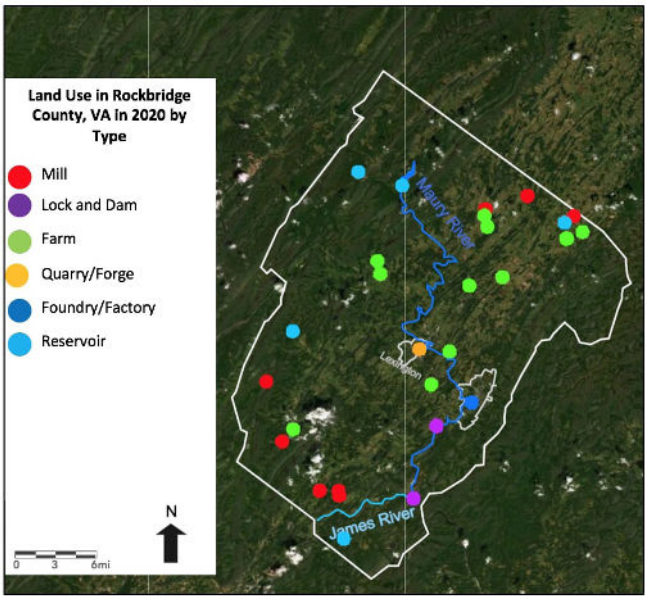

Figure 3. Land use in Rockbridge County, VA in 2020 categorized by type.

the 1860s. We know of some dams that were built and operated during pre-colonial or early colonial times. One of the sampled dams, McCormick's Mill Dam, was created before 1760 but the exact date of construction is unknown. There are other dams that have recorded construction dates predating our study timeframe. These include Pogues (Red) Mill (1765-present), Beatty's Mill (1750-?), and Hay's Creek Mill (1760-1957). There are likely others that fall in this category, but specifics for many of these old dams are unknown. The first modern reservoir dam was the dam at Lake Merriweather, which was created for recreation in 1966 (McKee, 2003 and U.S. Department of the Interior).

There were also six furnaces that operated in the region prior to our study timeframe: Bath Iron Works (1820-1860), Jordan Furnace (1800-1860), McCormick Furnace (1834-1854), Moore's Furnace (1849-1853), Mount Hope (1849-1853), and Vesuvius Furnace (1828-1854). Operation dates for Grant's Furnace, McCowen Iron Works, and Lebanon Forge are unknown and unlisted on the maps created (Scott, 2015).

The timeline of land-use changes shows that the majority of improvements to the county occurred between the Revolutionary War and the Civil War. Progression of land use slowed down after the Civil War. Information regarding land use in the region after the 1900's was difficult to acquire, and the maps during this time period reflect this. The drop in land use during the 1900's from the 1860's could be in part due to destruction of certain industry operations during the war. Lock and dam structures had almost disappeared by 1950. In the 1970's we started to see land use move away from our major waterways. We also see the first reservoir dam installed during this time. Current day land use is dominated by farms and most land use takes place farther away from our major waterways than what was previous practice. Lock and dam structures are no longer in use. Mining is less common now than it had been in the 1800's to 1900's. Reservoir dams are more popular now, be it for recreation, power, or water supply. Very few mills are still in operation compared to the beginning of the study at which they were at their peak.

The 2D and 3D models (Fig. 4) show that, historically, the Maury had higher water levels in the regions with dams than current day with these dams removed. The Lake Merriweather dam had lower water levels than current day with a dam in place.

The annual discharge data downstream of Lake Merriweather at Rockbridge Baths was examined from 1929 to the present day. The graph (Fig. 5) shows that after dam installation, the range of peak discharge values increases from before the dam was installed. This is an indication that the dam has created a disruption to natural flow conditions. It is worth noting that this dam is "flushed" periodically when sediment infilling behind the dam becomes an issue, which could be partly responsible for some of the discharge peaks seen on the graph after dam installation.

CONCLUSIONS

The maps created for this study show a decrease in land use over time and a shift from operations centered around major waterways such as the James and Maury Rivers to areas that are in contact with minor tributaries to these major waterways. The maps also show a shift in industry from more milling and mining operations in the 1800's to more farming in the present day.

The 2D and 3D models show that the Maury and James river water levels are lower now than they were with the heavy dam intervention during the mid 1800s

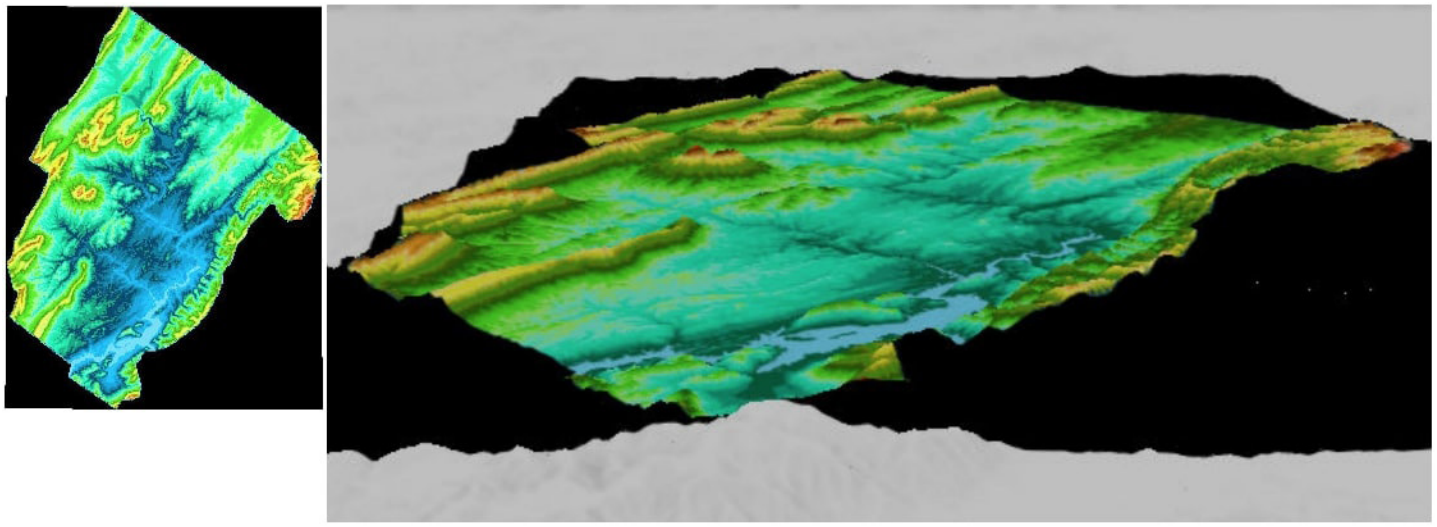

Figure 4. A) 2018 2D rendering of Rockbridge County based on elevation. B) 3D rendering of Rockbridge County based on the 2D model.

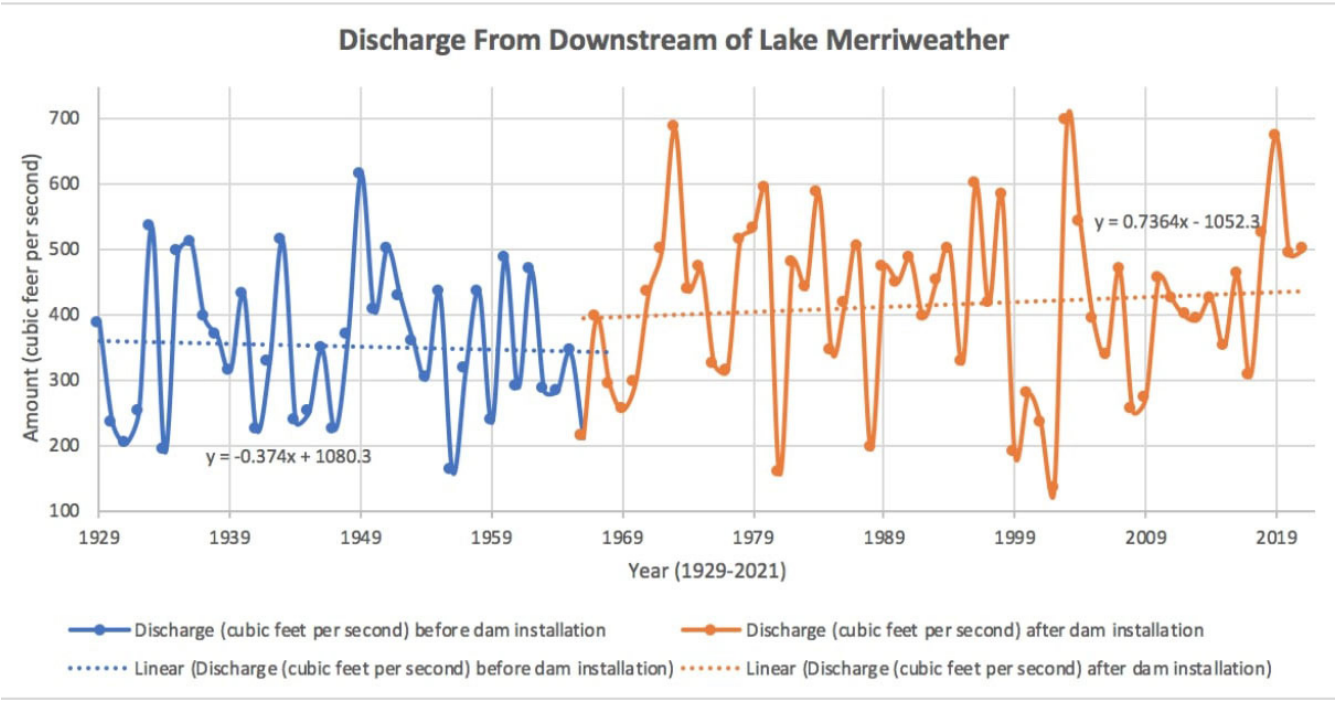

Figure 5. Yearly discharge data downstream of Lake Merriweather Dam graphed with a trendline. Information collected from USGS National Water Information System Mapper. Site: 02021500..

through the 1900s and also lower than in the 1950s.

We are able to determine that high water levels correspond with high discharge, and low water levels correspond with low discharge. The emplacement of dams caused a decrease in stream velocity allowing legacy sediments to settle out behind the dam structures. As the dams are removed, we run the risk of these sediments remobilizing and spreading contaminants throughout the waterways.

ACKNOWLEDGEMENTS

This material is based upon work supported by the Keck Geology Consortium and the National Science Foundation under Grant No. 1659322. A special thank you to Washington and Lee University Geology administrative assistantSarah Wilson, and lab technician Emily Falls for helping with logistics, travel, and lab situations. And a final thank you to all the Shenandoah Valley Keck participants who aided

in initial field and lab work: Mia Groff, Madeline Holicky, Katie Larkin, Martina Pulido, Marina Croy, Christopher Goldman, Noah Willis, and Haley Culbertson. Another special thank you to SNC's Tim Flood for his assistance with microscopes and photomicrographs, and Jeff DuMez from Brown County USGS for his assistance and guidance with ArcGIS troubleshooting.

Field work was conducted within the traditional territory of the Yesa People (with descendants including the Monacans) & of the Manahoac People, the indigenous stewards of this land.

REFERENCES

Army Map Service, Corps of Engineers, Department of the Army, Roanoke, VA. USGS, 1949. Map.

Army Map Service, Corps of Engineers, Department of the Army,Roanoke, VA. USGS, 1963. Map.

Balasico, N.L., Kaste, J.M., Meyer, M.G., Renshaw, M., Smith, K., Chambers, R.M., 2019, A high-resolution mill-pond record from eastern Virginia (USA) reveals impact of past landscape changes and regional pollution history, Anthropocene, v. 25, p. 2213-3054.

Blackburn, J.E., Walker, H.D., Fischer, W.A., Amherst, VA. USGS, 1939. Map.

Fowler, A.T., Ogle, A.J., Buckey, C.W., Wells, C.S., Stump, C.W., Buena Vista, VA. USGS, 1939. Map.

Gannett, H., Thompson, G., Fischer, L.C., Bien, M., Lexington, VA. USGS, 1894. Map.

Gannett, H., Thompson, G., Bien, M., Fletcher, L.C., Rockbridge, VA. USGS, 1894. Map.

Krishnaswamy, S., Lal, D., Martin, J.M., Meybeck, M., 1971, Geochronology of lake sediments, Earth and Planetary Science Letters, v. 11, i 1-5, p. 407-414.

McKee, M. M., 2003, The Internal Improvement Movement in Virginia: Early Canals, River Navigations, Roads,Turnpikes, Bridges, and Railroads, Records and Resources at the Library of Virginia. www.lva.lib.va.us

Natural Bridge, VA. USGS, 1894. Map.

Niemitz, J., Haynes, C., Lasher, G., 2013, Legacy sediments and historic land use: Chemostratigraphic evidence for excess nutrient and heavy metal sources and remobilization, Geology, v. 41, no. 1, p. 47-50

Pike, A., Bean, H.A., Sisson, G.E., Buckey, C.W., Law, J.A., Lexington, VA. USGS, 1932. Map.

Pike, A., Thompson, W.C., Blackburn, J.E., Clement, S.E., Parker, S.L., Watkins, J.L., Ford, R.V., Doane, F.E., Vesuvius, VA. USGS, 1936. Map.

Rockbridge Co., Va. [186] [Map] Retrieved from the Library of Congress, https://www.loc.gov/item/2002627465/.

Rockbridge County, Va. Google Earth, https://earth.google.com/web/ .

Scott, N. H., 2015, A river of iron: A history of mining, smelting and transporting iron in the Virginia counties of Alleghany, Augusta, Botetourt and Rockbridge, CreateSpace Independent Publishing Platform.

U.S. Department of the Interior. (n.d.). National Register of Historic Places (U.S. National Park Service). National Parks Service. https://www.nps.gov/subjects/nationalregister/index.htm

U.S. Geological Survey, Department of the Interior, Roanoke, VA. USGS, 1971. Map.

USGS, 02024000 Maury River Near Buena Vista, VA, National Water Information System: Mapper.

USGS, 02021500 Maury River at Rockbridge Baths, VA, National Water Information System: Mapper.

Wilkes, G. P., Spencer, E. D., Evans, N.H., and Campbell, E. V. M., 2007, Geology of Rockbridge County, Virginia, Virginia Division of Mineral Resources, Publication 170.

KECK Geology Consortium
Learning Science Through Research
Published by the Keck Geology Consortium
Short Contributions
Keck Geology Consortium
Volume 34
May 2022
doi: 10.18277/AKRSG.2022.34.15

ANALYSIS OF SOIL GEOCHEMISTRY TO BETTER UNDERSTAND GEOGENIC MANGANESE CONTAMINATION IN THE SHENANDOAH VALLEY

NOAH WILLIS, Whitman College
Project Advisor: Nick Bader

INTRODUCTION

Manganese contamination in drinking water poses serious long-term health risks even at low concentrations if exposure is chronic. Children and infants are especially at risk, with the potential for neurodevelopmental defects, including problems with memory, attention, and motor skills (Williams et al., 2012). In the United States there is no legally binding standard for manganese in drinking water, only a secondary unenforceable aesthetic standard of 50 parts per billion (Spangler et al., 2010). However, recent studies have shown that exposure to as little as 100 ppb can pose a serious health risk (Williams et al., 2012). Manganese contamination can be anthropogenic and geogenic in nature. A recent study indicates that certain hydrogeologic provinces are more prone to having groundwater contaminated with manganese (Erickson et al., 2019). This current paper focuses on the Shenandoah Valley region of Virginia.

Because manganese contamination can be geogenic in nature, an understanding of an area's geology and hydrology is useful. Virginia's geology generally represents the products of advancing and retreating ocean shorelines, and the deformation resulting from the tectonic collisions that built the Appalachians in the Paleozoic Era (Torsvik, 2017). Our area of study lies in the Valley and Ridge province. The valleys are usually underlain by the Edinburg Formation, a limestone of Ordovician age. The ridges are usually composed of sandstones (Heller et al., 2018). The limestone has been preferentially weathered to create the valleys, leaving the sandstone in place as the ridges that generally run north-south.

One of these valleys, The Shenandoah Valley, lies mostly in north-central Virginia, with its northern terminus in Maryland. It is bounded by the Appalachian Plateau province to the west, and the Blue Ridge Mountains to the east. The Shenandoah River eventually runs into the Chesapeake Bay, flowing south to north for much of its course. Our study examines springs from six different sites throughout the Shenandoah Valley spanning from Shenandoah County to Natural Bridge, VA. This encompasses Rockbridge County in the south, through Augusta, Rockingham, and Shenandoah Counties. Whereas the southern end of our area of study may lie in the culturally defined Shenandoah Valley, hydrologically it does not. Our area of study can be broken into two different watersheds: the Shenandoah Watershed to the north and the James River Watershed to the south, which exits the Shenandoah Valley running from west to east through a gap in the Blue Ridge. Streams in this region are generally gaining streams, recharged with groundwater, responding quickly to precipitation events (Swain et al., 1991). Due to the tectonic history of the area the strata that compose the Valley and Ridge dip steeply in many places. Therefore, most wells will only penetrate the unit found on the surface, making surface lithology a good proxy for what unit a well will draw water from (Trapp et al., 1997).

Manganese is naturally found at around 600 ppm in upper continental rocks worldwide and 260 ppm in soils on average in the Eastern United States (see Cannon et al., 2017 for review). Manganese is a redox active element with +2, +3, +4, +5, +6, and +7 oxidation states (Railsback, 2003). The oxidation state of manganese controls whether or not manganese is

bio-available or not when consumed. Of the oxidation states most commonly found in natural systems (+2,+3, and +4), soluble manganese is most stable as Mn^{2+}, being found in anoxic conditions, while more oxic conditions, like a well mixed stream, oxidize manganese to Mn^{3+} or Mn^{4+}, precipitating out and forming minerals such as pyrolusite, todorokite, or buserite (Cannon et al., 2017).

In the Shenandoah Valley, Mn oxide ores are commonly found in fault breccias contained within the Antietam Sandstone (Carmichael et al., 2017). It is thought that this Mn originates from Mn dissolved in water percolating downward, into more reducing conditions, allowing it to remain as soluble Mn^{2+}. As water then upwelled and discharged through springs along faults, or directly into streams, the manganese was oxidized, forming the oxide ores that exist today (Carmichael et al., 2017). This model explains the occurrence of manganese oxides in fault breccia and ancient alluvium within the Shenandoah Valley. The goal of this project is to analyze the complex relationships that govern the redox state of manganese in groundwater in the Shenandoah Valley today. Through analyses of soil samples we hope to gain a better understanding of the redox chemistry that controls the oxidation state of manganese in groundwater.

METHODS

Field Methods and Sample Treatment

Water samples were collected from a series of springs and seeps across the Shenandoah Valley (Fig. 1) as close as possible to the point where water emerged from the subsurface. 250 mL polypropylene bottles were primed three times with spring water before sampling. An aliquot of each sample was filtered in the field with 0.22 µm filters, discarding the first 1 mL of filtrate and saving the filter paper for microscopic analysis of the filtered solids. Two aliquots of filtered water were collected, one simply taken back to the lab and refrigerated at 4°C for ion chromatography analyses (to determine major anion and cation concentrations). The other aliquot was acidified to 1% nitric acid (trace metal grade) upon returning to the lab and then refrigerated for major element and trace

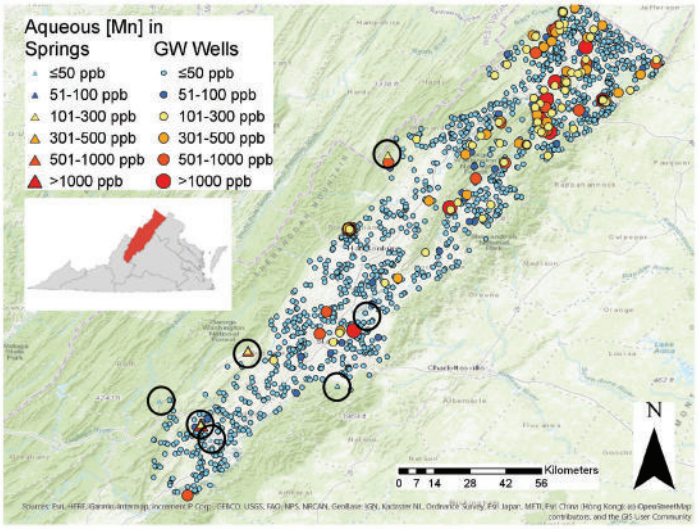

Figure 1. Map of aqueous Mn concentrations in springs (triangles) and groundwater wells (circles) in the Shenandoah Valley, VA, with increasing concentrations increasing the relative size of each data point based on demarcations from ≤50 ppb (light blue) to 51-100 ppb (dark blue) to 101-300 ppb (yellow; above which low level chronic exposure to Mn via drinking water may result in health effects), 301-500 ppb (orange), 501-1000 ppb (light red), to >1000 ppb (dark red). Field sites for springs and seeps are denoted with black circles.

metal analyses via inductively coupled plasma-mass spectrometry. In the field, a YSI probe was used to measure dissolved oxygen (DO), specific conductivity, temperature, and pH.

Soil cores were collected as close as possible to the spring or pond itself. Additional cores were also taken up- and down-gradient of each spring and seep. Cores were sealed in polyethylene bags and then refrigerated upon return to the lab.

The Munsell soil classification is a system used to sort samples of damp soil into different discrete color categories. We used this system to separate soil cores into different color-based horizons. A subsample was collected from each Munsell defined horizon, and dried at 105o Celsius overnight. Samples were then ground in an agate mortar and pestle for 8 minutes to create a fine powder. An aliquot of sample was used to make slides for X-Ray Diffraction (XRD) and the rest was set aside for total elemental analyses by X-ray fluorescence (XRF) and later soil sequential extractions to assess the mobility of elements of interest.

XRF Analyses

Samples were dried and ground following the protocols outlined above were then packaged in pXRF cups. A Thermo Scientific Niton XL3t pXRF was set to analyze samples with the "test all geo" program for 120 seconds. The instrument was calibrated for Mn with USGS standards SGR-1b, AGV-2, and BCR-2. At the start of each run, an initial calibration was performed with the three standards, five samples were analyzed, and then a second calibration was performed with the same three standards. No systematic drift associated with a drop in battery voltage was noticed upon analysis. A calibration curve was created with the standards and used to determine the concentrations of Mn and Fe in each soil subsample.

RESULTS

When plotted, data from pXRF analysis of soil samples visually shows a positive correlation between total Fe concentration in soil and total Mn concentration in soil, however owing to the wide range of Fe concentrations, only has an R^2 of 0.074 (Fig. 2). A breakdown of total Fe concentration in soil and total Mn concentration in soil by aquifer lithology reveals no real trends in any of the aquifer lithologies. (Fig. 3).

Data from pXRF analysis of soil samples and ICP-MS analysis of water samples reveals that there is a positive correlation between total Mn concentration in soil samples and aqueous Mn concentration in water samples taken from carbonate aquifers, with an R^2 of 0.54 (Fig. 4). The same data set shows a slight negative correlation between total Mn concentration in soil samples and aqueous Mn concentration in water samples taken from sandstone aquifers, with an R^2 value of 0.34 (Fig. 4). There is no meaningful trend one way or the other in black shale aquifers (Fig. 4).

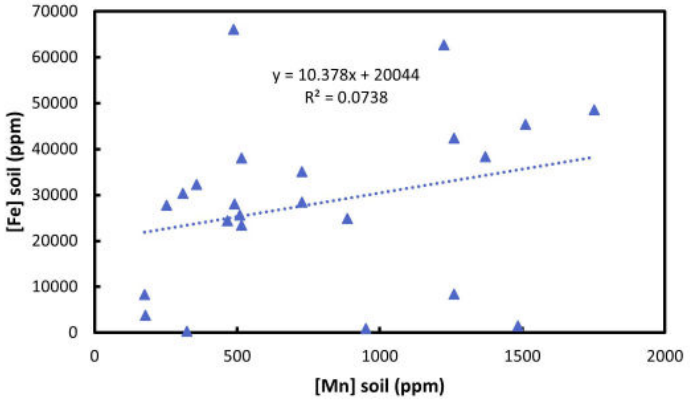

Figure 2. Plot of total Fe concentration versus total Mn concentration in soil samples.

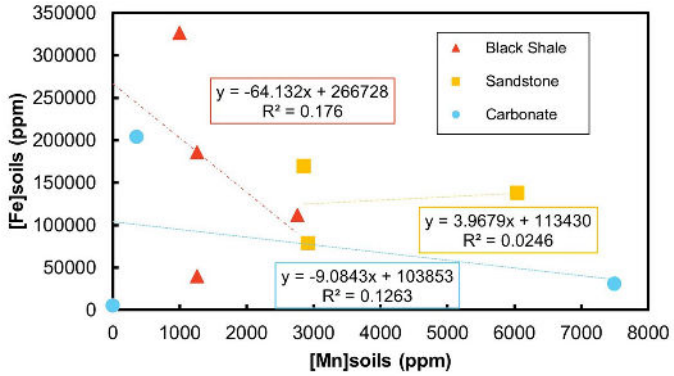

Figure 3. Plot of total Fe concentration in soil versus total Mn concentration in soil broken down by aquifer lithology. Balck shale sites shown in red triangles, sandstone sites shown in yellow squares, and carbonate sites shown in blue circles.

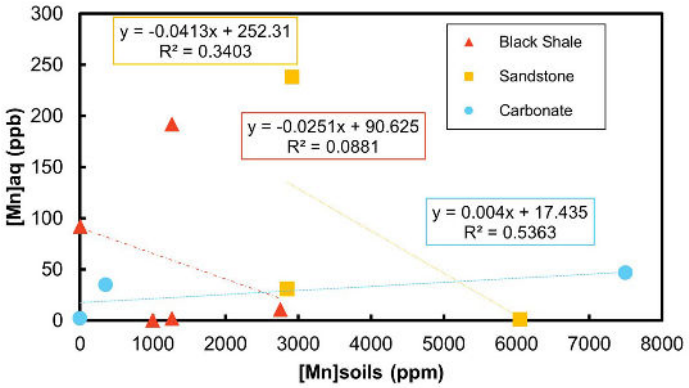

Figure 4. Plot of total Mn concentration in soil samples versus aqueous Mn concentration in water samples broken down by aquifer lithology. Black shale sites shown in red triagnes, sandstone sites shown in yellow squares, and carbonate sites shown in blue circles.

DISCUSSION

Black shale aquifers do not exhibit a meaningful correlation between aqueous Mn and total soil Mn. There is a potential negative correlation between aqueous Mn and total soil Mn in sandstone aquifers, with an R^2 of 0.34 (Fig. 2). This negative correlation between aqueous Mn and total soil Mn as observed in sandstone aquifers makes sense; as a system becomes more oxidizing, more Mn oxidizes and precipitates from spring water and becomes trapped in the soil.

However, carbonate aquifers display a positive correlation between aqueous Mn and total soil Mn. It should be noted that all carbonate soil samples in

this data set were obtained from the Maple Flats Pond complex, a group of ponds with thick clay layers overlying Antietam quartzite alluvial cobbles on top of carbonates (Buhlmann et al., 1999). Dissolution of the carbonates resulted in the formation of these sinkhole ponds, while the thick clay layer allows these ponds to periodically fill and retain water for extended periods of time (Fleming & Alstine, 1999). Thus, these ponds are unique systems in that there is no contribution of Mn to these waters from groundwater systems (with the exception of Spring Pond), thus all Mn in these ponds must be derived exclusively from soil weathering. Therefore, if aqueous Mn can only be derived from soil weathering in these cases, it follows that increasing soil concentrations will result in increased aqueous Mn in the corresponding springs and seeps.

One alternative explanation that does bear mentioning is that carbonate aquifers often have higher bicarbonate concentrations than other aquifer rock types and therefore stabilize manganese carbonate minerals such as rhodochrosite, $MnCO_3$. Rhodochrosite is more soluble (with a pKsp value of 10.39) than Mn (oxyhydr)oxide minerals such as birnessite (pKsp of 15.62), pyrolusite (pKsp of 17.84), and manganite (pKsp of 18.26) (Harris, 2016). However, the alkalinity of these waters from the Maple Flats Pond complex are no greater than the springs and seeps in sandstone and shale aquifers here studied (Croy, 2022), thus this explanation is less likely than the soil weathering hypothesis.

Although there are no clear correlations between total Fe concentration in soil and total Mn concentration in soil when broken down by lithology (Fig. 3), plotting all data together reveals a positive correlation (Fig. 2). The broad range of Fe concentrations makes the observed small R^2 very likely, even though it is clear there is a general positive relationship between total soil Fe concentration and total soil Mn concentration (Fig. 2). Generally speaking, a positive correlation between total Fe concentration in a soil core and total Mn concentration is logical. Mn and Fe behave similarly from a redox perspective (Harris, 2016). Both aqueous Fe and Mn are most stable as divalent cations. When oxidized to 3+ they will precipitate out as an Mn/Fe (oxyhydr)oxide mineral.

Overall bulk Mn concentrations found in this study differ somewhat from what past studies have found. A survey of wells from across the United States found bulk Mn concentrations of anywhere between 300 to 800 ppm (Cannon et al., 2017). Data from pXRF analysis in this current study returned bulk Mn concentrations much higher than found in Cannon et al. (2017). The data in Cannon et al. (2017) was collected around wells all across the United States, including data from areas that may not be particularly susceptible to having elevated levels of Mn in groundwater. Considering that the average bulk Mn concentration in soil worldwide is 650 ppm, some samples from Cannon et al. (2017) clearly have bulk Mn concentrations below average. It is also worth considering that Cannon et al. (2017) used data collected from around wells, not springs. Soil around springs is much more likely to interact with groundwater than soil around a well (Tolman, 1937). Surface or rainwater that might be more likely to interact with soil around a well, may be very different from groundwater from a chemical perspective.

CONCLUSION

Understanding what factors are correlated with high manganese concentrations in groundwater is a public health imperative. Analyzing the chemistry of the soil around springs is a good way to help build that understanding. This study found that there is a general positive correlation between total Fe concentration in soil and total Mn concentration in soil. This study also found that different aquifer lithologies display different relationships between total Mn concentration in soil and total aqueous Mn concentration, with carbonate aquifers displaying a positive relationship and black shale and sandstone aquifers displaying negative relationships. These relationships give valuable information about the source of Mn contamination in systems. A positive correlation between total Mn concentration in soil and total aqueous Mn suggests that the soil itself may be the major source of aqueous Mn contamination. A negative correlation suggests that the redox conditions of a system control where Mn appears in the system. A more oxidizing system may cause Mn to end up as oxides in soil, whereas a more reducing system may cause Mn to mobilize and end up in the water.

ACKNOWLEDGEMENTS

This material is based upon work supported by the Keck Geology Consortium and the National Science Foundation under Grant No. 2050697. I would like to thank Margaret Anne Hinkle and Eva Lyon for being the Keck directors for the project, Emily Falls and Sarah Wilson for all their help at Washington and Lee, Nick Bader for help with writing, Kirsten Nicolaysen for supervision in lab, Nate Boland for guidance when I had questions, the Whitman Chemistry Department and Frank Dunnivant for equipment and reagents, all fellow Keck students for help with field work and sample prep, and all landowners for granting access.

REFERENCES

Buhlmann, K., Mitchell, J., Smith, L., 1999, Descriptive Ecology of the Shenandoah Valley Sinkhole Pond System in Virginia: Banisteria, Number 13.

Cannon, W. F.; Kimball, B. E.; Corathers, L. A. Manganese; Schulz, K. J., DeYoung, Jr., John H., Seal II, R. R., Bradley, D. C., Series Eds.; Professional Paper; Report 1802L; Reston, VA, 2017; p 40. https://doi.org/10.3133/pp1802L.

Carmichael, S.K., Doctor, D.H., Wilson, C.G., Feierstein, J., McAleer, R.J., 2017. New insight into the origin of manganese oxide ore deposits in the Appalachian Valley and Ridge of northeastern Tennessee and northern Virginia, USA. GSA Bulletin 129, 1158–1180.

Croy, M., 2022, Analyzing the Relationships Between Aqueous Manganese and Geological Factors in Groundwater in the Shenandoah Valley: Keck Short Contributions, v. 34.

Fleming, Gary P. and Nancy E. Van Alstine,. 1999, Plant Communities and Floristic Features of Sinkhole Ponds and Seepage Wetlands in Southeastern Augusta County, Virginia. Banisteria 13, 67 - 94.

Gounot, A., 1994, FEMS Microbio. Rev., 14(4), 339–349.

Harris, D.C., 2016, Quantitative Chemical Analysis, W. H. Freeman and Company, 792 p.

Health Canada., 2019, Water and Air Quality Bureau (Catalogue No H144-39/2017E-PDF)

Heller, M.J., Carter, M.W., Wilkes, G.P., and Coiner, L.V., 2018, Geology of the Cornwall quadrangle, Virginia, Virginia Division of Geology and Mineral Resources, Publication 184, 1:24,000.

Kiracofe, Z.A., Henika, W.S., Schreiber, M.E., 2017. Assessing the Geological Sources of Manganese in the Roanoke River Watershed, Virginia. Environmental Engineering Science 23, 43–64.

Lindsey, B.D., Zimmerman, T.M., Chapman, M.J., Cravotta III, C.A., Szabo, Z., 2014, US Geological Survey Circular 1354, 107 p.

Malcolm Williams, DVM, Ph.D., G. Daniel Todd, Ph.D., Nickolette Roney, M.P.H., Jewell Crawford, M.D., Charleton Coles, Ph.D., 2012, US Department of Health and Human Services, Agency for Toxic Substances and Disease Registry: Toxicological Profile for Manganese.

McMahon, P.B., Belitz, K., Reddy, J.E., Johnson, T.D., 2018a. Elevated Manganese Concentrations in United States Groundwater, Role of Land Surface–Soil–Aquifer Connections. Environmental Science & Technology 53, 29–38.

Railsback, L.B., An earth scientist's periodic table of the elements and their ions. Geology 2003; 31 (9): 737–740. doi: https://doi.org/10.1130/G19542.1

Spangler and Reid, 2010, Biol. Trace El. Res., 133(2), 128-135.

Swain, L.A., Hollyday, E.F., Daniel, C.C., Zapecza., O.D., 1991, Plan of Study for the Regional Aquifer System Analysis of the Appalachian Valley and Ridge, Piedmont, and Blue Ridge Physiographic Provinces of the Eastern and Southeastern United States, With a Description of Study-Area Geology and Hydrogeology, Water-Resources Investigations Report 91-4066.

Tebo, B.M., Ghiorse, W.C., van Waasbergen, L.G., Siering, P.L., Caspi, R., 1997. Bacterially mediated mineral formation; insights into manganese (II) oxidation from molecular genetic and biochemical studies. Reviews in Mineralogy and Geochemistry 35, 225–266.

Tolman, C.F., 1937, Ground Water, McGraw Hill Book Company, 593p.

Torovisk, T.H., Cocks, L.R.M., 2017, Earth History and Palaeogeography: Cambridge University Press, 332 p.

Trapp, H., Horn, M.A., Ground Water Atlas of the United States Delaware, Maryland, New Jersey,

North Carolina, Pennsylvania, Virginia, West Virginia, https://pubs.usgs.gov/ha/ha730/ch_l/L-text5.html.